Ph.D. Program in Civil, Chemical and Environmental Engineering

Curriculum in Chemical, Materials and Process Engineering

Department of Civil, Chemical and Environmental Engineering

Polytechnic School, University of Genoa, Italy.

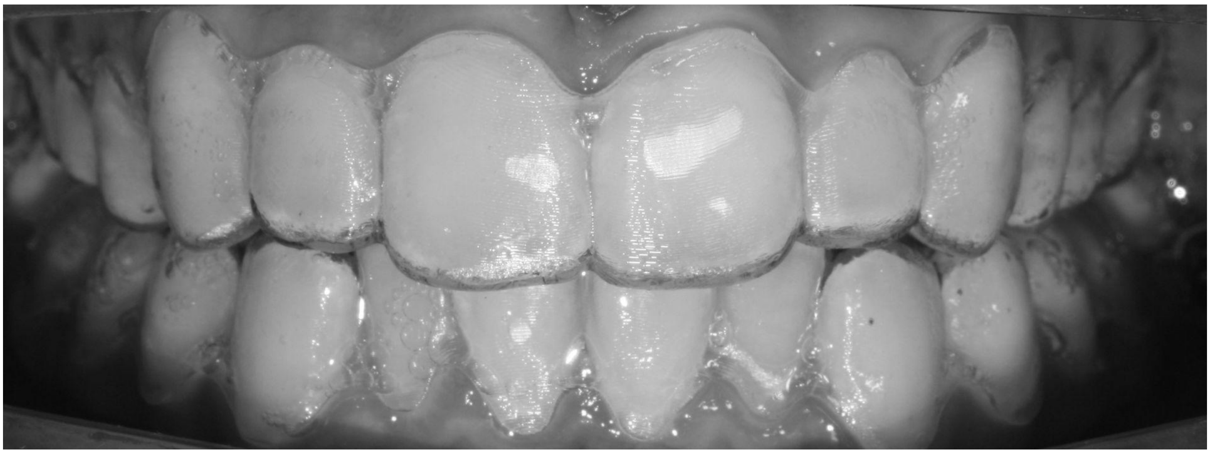

Thermo-mechanical and geometric properties of 3D printable shape memory resins for orthodontic aligners

Sara Drago

Thermo-Mechanical And Geometric Properties Of 3D Printable Shape Memory Resins For Orthodontic Aligners

By

Sara Drago

Dissertation discussed in partial fulfillment of
the requirements for the Degree of

DOCTOR OF PHILOSOPHY

Civil, Chemical and Environmental Engineering
Curriculum in Chemical, Materials and Process Engineering,
Department of Civil, Chemical and Environmental Engineering, University of Genoa, Italy

May, 2026

Advisers:
Prof. Alberto Lagazzo – Department of Civil, Chemical and Environmental Engineering, University of Genova
Prof. Marco Migliorati – Department of Surgical and Diagnostic Integrated Sciences, University of Genova

External Reviewers:
Prof. Juan Felipe Basbus –Institut Laue–Langevin, Grenoble, France
Prof. Domenico Dalessandri – Department of Medical and Surgical Specialties, Radiological Sciences, and Public Health, University of Brescia

Examination Committee:
Prof. Elisabetta Finocchio – Department of Civil, Chemical and Environmental Engineering, University of Genova
Prof. Amirreza Khataee –KTH Royal Institute of Technology, Sweden
Prof. Monica Puccini – Department of Civil and Industrial Engineering, University of Pisa
Prof. Ignacio Sirés Sadornil – Department of Materials Science and Physical Chemistry, University of Barcelona

Ph.D. program in Civil, Chemical and Environmental Engineering

Curriculum in Chemical, Materials and Process Engineering

Cycle XXXVIII

Acknowledgements

Acknowledgement for fellowship sponsored by Smiledge s.r.l.

ABSTRACT

In the last decade rapid prototyping technologies have radically transformed the approach to orthodontic treatments. This is particularly evident with clear aligners, an appliance to move the teeth without bands, brackets, or wires which is based on vacuum-formed dental contour devices.

Accordingly, several efforts have been made to develop advanced materials that are suitable for the CAD/CAM technology. Currently, various thermoplastic materials such as polyethylene terephthalate glycol (PETG), polypropylene, polycarbonate, thermoplastic polyurethanes (TPU), and copolyester, are being used by different actors to manufacture clear aligners. Furthermore, multi-hybrid materials have been developed to overcome the limitations of a single material by improving the physical properties of maximum tensile load-bearing capacity . The development of new materials and enhancement of the material properties have significantly improved the performance of the clear aligners. However, these aligners are still manufactured by the conventional method of vacuum thermoforming biocompatible thermoplastic transparent materials on a dental model, which is a complex manufacturing process requiring considerable time and effort. In addition, geometric inaccuracies are induced during the thermoforming process. The shrinkage and expansion of the material that occurs during the thermoforming process affects the orthodontic force and fit of the clear aligners to the dentition, in addition to the changes in various physical properties such as transparency, water absorption, surface hardness, and elastic modulus.

To overcome the limitations of the conventional manufacturing method, direct 3D printing of clear aligners with biocompatible materials has been recently attempted. This method requires less time and materials waste, and also results in fewer geometric inaccuracies. However, the mechanical properties and behavior of 3D printing materials composed of cross-linked polymers are expected to be different compared with conventional thermoplastic materials composed of non-cross-linked polymers used for thermoforming.

The purpose of the present project was to evaluate the thermo-mechanical, viscoelastic and geometric properties of the currently available orthodontic 3D direct printing materials, to test their biocompatibility and to implement a preliminary computational model for the assessment of the obtained orthodontic forces.

INDEX

ORTHODONTIC ALIGNERS DEVELOPMENT

1.1 INTRODUCTION

In the last decade, clear aligners treatments have been increasingly used in orthodontics as a potential alternative to the conventional bracket–archwire system, even though the efficiency of this system has to be evaluated under biomechanical considerations and is currently under discussion [1]. Since their introduction in orthodontics, clear aligners have been appreciated by patients, including adults, for their comfort and low aesthetic impact [2]. Many different cases are considered eligible for orthodontic therapy with these devices: moderate crowding, distalization, resolution of a deep overbite, narrow arches that can be expanded and major rotations [3]. Patients are advised to wear their aligners for a minimum of 22 h per day, with removal recommended only during meals and teeth brushing. The technique comprises a series of several aligners, each one being worn for one or two weeks, according to the producer's protocol, before being replaced with the next one.

Aligners are made of polymeric materials: they are lightweight, easy to process, cost-effective, and versatile. In dentistry, they are used for prostheses, implants, and orthodontic appliances. The term polymer derives from the Greek *poly* – many, and *meros* – unit: they are molecules consisting of repeating high-numbered units – monomers – which form long, intertwined chains. The properties of a polymer can vary significantly depending on the polymer chains of which it is composed: specifically, they depend directly on the molecular weight and the molecular chemical structure [4].

There are different ways to classify polymeric materials. The main classification is based on thermal properties, through which we can distinguish:

- **Elastomers**: rubbery-state polymers with high mechanical performance.
- **Thermosetting polymers**: materials that, when subjected to thermal stress, transform into rigid, insoluble, and infusible materials.
- **Thermoplastic polymers**: materials that undergo melting and reshaping following thermal stimulation.

Thermoplastic materials are, in turn, divided into two types: amorphous and semi-crystalline. Amorphous materials are characterized by an inherently irregular molecular structure. They appear soft, transparent, and possess high impact resistance.

Semi-crystalline materials, on the other hand, are characterized by a mixed structure, in which semi-crystalline areas, ordered regions, and amorphous regions alternate. These are more translucent and more rigid than the former. Indeed, the crystalline regions provide the material with greater hardness and stiffness [5].

An additional structural differentiation is between single-layer and multi-layer materials. In the clear aligner industry, there has been a gradual evolution from monophasic materials to multilayered materials. The latter alternate hard layers and softer layers: this results in an optimization of the material's properties, as the 'soft layers' improve the elastic deformation, resilience, and fit of the aligner, while the 'hard layers' ensure strength and resistance [4,5].

Due to their prolonged staying in the oral cavity, several studies have been conducted to summarize the biocompatibility and safety of vacuum thermoformed clear aligners, such as their BPA release, adverse effects, cytotoxicity, and estrogenic effects [6-9].

Novel resin materials for direct 3D printing of clear aligners have been recently introduced, and it has been noted that, compared to the thermoforming method, direct printing streamlines the workflow, decreases plastic waste, and results in aligners with better fit; in some cases the literature reports the results for cytotoxicity and estrogenicity tests [10-12]. Furthermore, under various environmental and mechanical factors these materials, which are classified as plastic photopolymers, with a polyester-urethane polymer structure, in the oral cavity can be broken down into smaller fragments (100–1000 nm), known as secondary microplastics, and factors such as fluctuations in oral temperature, exposure to numerous substances found in foods and beverages, and intraoral aging can convert microplastics into nanoplastics, which are smaller in size (1–100 nm) and can easily penetrate biological membranes, potentially entering cells and tissues [13].

Among the limited number of materials presently available on the market for the direct 3D printing of aligners, Tera Harz TC-85 (Graphy Inc., Seoul, Republic of Korea) received approval for biocompatibility from the Korean and United States Food and Drug Administration [14] and exhibited the capability of delivering light forces, with a reduced force decay [15]. CLEAR-A (Senertec, Karatas-Izmir, Turkey) is another resin designed for direct 3D printing of aligners which is already available on the market and, recently, LuxCreo DCA (LuxCreo, Chicago, IL, U.S.A) was introduced for the clinical use.

1.2 POLYMERS FOR CLEAR ALIGNERS: BEHAVIOR AND PROPERTIES

The physical behavior of these materials is distinctive: they exhibit characteristics intermediate between a solid and a fluid, reacting to stresses initially in an elastic manner and subsequently in a plastic manner.

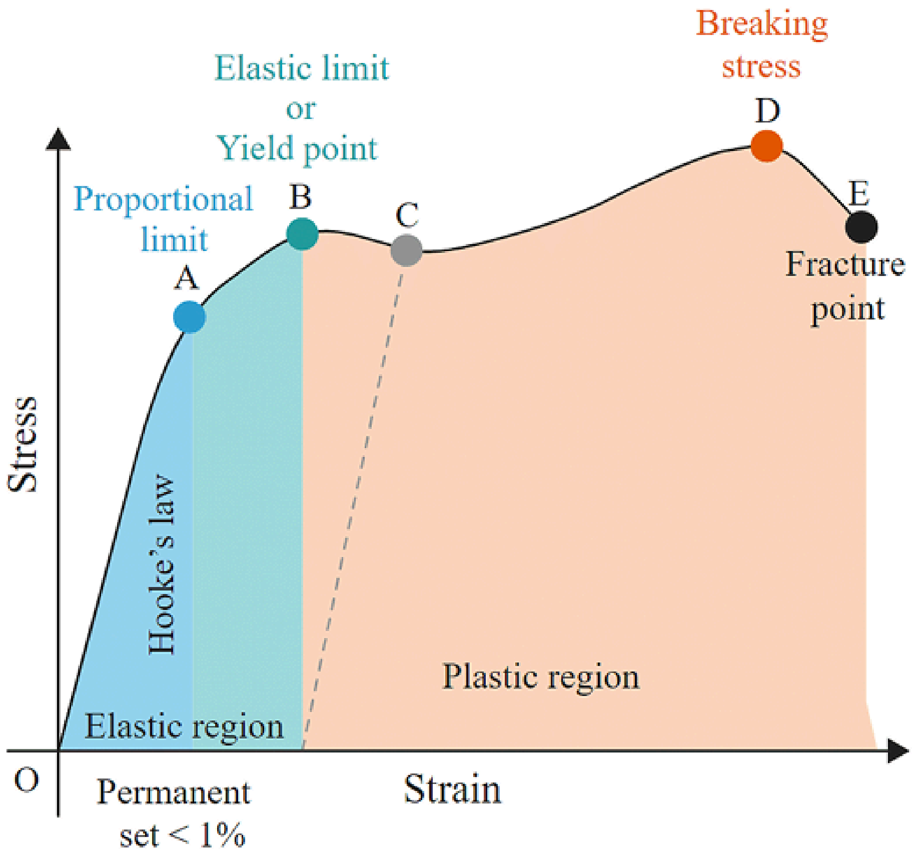

Figure 1-1: Stress-strain curve and characteristic points of a generic material

Clear aligners, within the oral cavity, are subject to both short-term forces and forces prolonged over time [4]. When the orthodontic device is inserted onto the dental arches, it undergoes a short-term load: it will experience a deformation, which can be quite severe; however, this will only be temporary, as the aligner will return to its original shape once the initial force is removed [16].

This phenomenon is justified by the fact that thermoplastic materials, when subjected to short-term forces, behave in an elastic manner, complying with the so-called Hooke's Law (Figure 1.1). Below the elastic limit, there is a proportionality between the applied stress and the resulting strain: the material undergoes a change in size and/or shape, but upon removal of the external agent, it is capable of reassuming its original characteristics. This is strictly related to the material's hardness, elasticity, and resilience.

When, on the other hand, polymers are subjected to forces for a longer period of time, their behavior is viscoelastic, resulting in a time-dependent relationship between load and deformation. Viscoelastic materials are capable of absorbing shocks, vibrations, and forces by deforming and stretching. Under prolonged constant loads, they exhibit increasing flexibility over time, which decreases as the intensity of the force is reduced. This leads to the phenomenon of stress relaxation, in which the applied stress decreases while the material is held at a constant strain [4].

Therefore, once worn for the first time, the aligner is kept in place by the patient for a significant period (at least 7–10 days and for approximately 22 hours per day) [17]. In response to these long-term forces, resulting from both the programmed tooth movement and the reaction forces of the musculoskeletal system, the device will undergo progressive 'relaxation'. This phenomenon is strictly related to the properties of the material itself, but not exclusively: it also depends on the magnitude of the forces, the thickness, and several intraoral factors, most notably temperature. Managing these factors is fundamental to maintaining the device's efficiency. In correlation with the above, polymeric materials for dental use must exhibit other key characteristics in addition to mechanical stability: resistance to chemical corrosion and tolerance to temperature variations.

The oral environment contains various substances, first and foremost saliva, which is composed of water, electrolytes, bacteria, and enzymes: a system that is already heterogeneous is made even more complex by the daily intake of food and beverages, which can lead to pH changes or corrosive effects.

Consequently, as polymers must be applied in the oral cavity for a prolonged period, they must exhibit high chemical stability. Furthermore, especially in relation to diet, the temperature of the oral cavity—which is generally around 37°C—can undergo significant thermal fluctuations: it can range from sub-zero temperatures to high peaks of up to 60°C. This demonstrates how the material must satisfy the requirement of dimensional stability across different temperatures; otherwise, phenomena of expansion and contraction would occur, leading to subsequent permanent deformation and a decrease in clinical efficacy [4].

Another relevant aspect is the tendency toward aging, which is strictly correlated to the molecular structure of the polymers. There are two types of aging—physical and chemical—which share common characteristics such as increased brittleness and stiffness of the polymer, along with a significant reduction in mechanical strength. These are caused by internal imbalances or interactions with the surrounding environment.

Furthermore, an additional adverse event may occur: material stretching. This occurs primarily due to external mechanical stress, such as a parafunction [4].

Summarizing the concepts just described, the properties generally sought after are:

a. Sufficient Elasticity. Every material exhibits a specific **elastic modulus** or **Young's modulus**: this is an indicator of the material's stiffness and is defined as the ratio between stress and the resulting strain. An increase in this index leads to a reduction in the material's elasticity, resulting in greater stiffness; in a clinical setting, this would lead to difficulty for the patient when inserting and removing the aligner. Likewise, should the index assume low values, the biomechanical efficacy would also be reduced. Thermoplastic materials for the fabrication of aligners must, therefore, possess an intermediate Young's modulus, such as to allow dental movements while maintaining a certain degree of elasticity, which enables a smooth fitting of the aligner [5].

b. High Resilience. This represents the capacity of a material to absorb energy when elastically deformed and to release it upon unloading, without resulting in permanent deformation. Although thermoplastic materials exhibit good resilience, it is lower when compared to that of conventional metal devices (Stainless Steel - SS): consequently, the loading capacity with CAT (Clear Aligner Therapy) is limited and fatigue is higher. This also explains the biomechanical differences between the two therapies, most notably the speed of tooth movement [4].

c. Low Hardness, which refers to the material's ability to resist plastic deformation.

d. High resistance to mechanical stress (bending, tension, fracture). In patients with parafunctions—such as grinding or clenching—occlusal forces are exerted for a much longer period than the normal range (9–12 minutes per day) and can reach high levels of intensity. Several studies have been conducted to evaluate the actual changes caused by these loads and, in general, by high-intensity stress: it has been demonstrated that these factors, especially in the posterior regions, are responsible for abrasion, delamination, and an increase in the material's stiffness [16,18]. However, it has also emerged that within the ideal period of aligner activity—which ranges between 7 and 14 days—such forces do not cause significant levels of wear or mechanical failure [4].

e. High resistance to thermal stress. Physical stability is strictly correlated to the polymer structure, which is in turn influenced by the temperature of the surrounding environment and the treatments the material has undergone. Polymers for orthodontic purposes are mainly in an amorphous, and therefore disorganized, form. Every polymer possesses a specific glass transition temperature (T_g): this is an indicator of the phenomenon in which an amorphous material, when subjected to gradual cooling, undergoes a (re)organization of the polymeric chains until it transitions into a crystalline, glassy form. The T_g is therefore the thermal range in which a polymer transitions from a fluid-like state into a solid-like state. In clinical terms, a glassy material—as previously mentioned—will possess properties that are not ideal for the fabrication of aligners: it will exhibit greater stiffness and hardness, as well as inferior optical properties. It follows that knowing the T_g for each individual material is crucial: the thermoforming process, for instance, must necessarily take place above this temperature to maintain the polymer in a primarily amorphous form that is mechanically stable within the oral environment, which typically presents temperatures lower than the T_g [4]. To ensure the maintenance of the amorphous structure and its primarily elastic properties, along with a significant delay in physical aging, it is also necessary to instruct the patient to remove the aligners when consuming hot food or beverages. Temperature variations could cause dimensional changes—resulting from the expansion and contraction of the material—which in turn are responsible for alterations in mechanical properties and the overall shape of the aligner, following a decrease in internal molecular cohesion.

f. **High Transparency.** Optical properties, especially transparency and chromatic stability, are fundamental to the aesthetic success of invisible aligners. These characteristics can be influenced by various intraoral factors: masticatory loads, contact with saliva, or staining agents found in food, mouthwashes, and beverages. Aligner materials must exhibit high light transmittance and should be capable of transmitting 80% of visible light. Indeed, the polymers primarily used are in an amorphous form: they typically display high translucency, in contrast to crystalline polymers, which are highly opaque and unappealing [19]. Lombardo et al. investigated, via spectrophotometry, the optical properties of different commercially available aligners (Invisalign, F22, and All-in), before and after immersion for 14 days in artificial saliva at 37°C, enriched with staining substances [20]. The samples consisted of aligners in which the lingual part was removed in order to analyze the buccal portion more accurately. In this way, the absorbance—the property that quantifies the absorption of light by a body—and the transmittance—the ability of a sample to allow an incident light beam to pass through it—were examined. The F22 aligners exhibited higher transmittance and lower absorbance values, both before and after the aging process [20]. It should be remembered, in fact, that these properties—and their variations—are strictly correlated to the components of the mixture used: other studies have demonstrated, for example, that TPU exhibits lower chromatic stability, thus influencing the optical behavior of aligners in which it is a major component, such as Invisalign [21]. For all samples, a susceptibility to deterioration with chromatic variation was observed; however, the differences found are not to be considered significant. In conclusion, optical properties should remain significantly constant during the aligners' period of activity, provided that the actual oral environment is inherently different from the one simulated in vitro.

g. High resistance to physico-chemical stress. Aligners are in constant contact with saliva, which is composed of 99% water. The absorption of water is responsible for both physical and chemical aging. From a physical standpoint, water molecules diffuse between the polymer chains, causing the breaking of chemical bonds between them, a subsequent decrease in internal cohesion, and an increase in molecular mobility. Clinically, this effect results in plasticization—a loss of the aligner's elasticity—which initially makes the material softer and progressively less effective, until it becomes stiff and particularly brittle, often exhibiting internal fracture lines. Physical aging is also evidenced by a typical discoloration of the device. The latter is also correlated to exposure to chromogenic agents, such as coffee, black tea, and red wine. The penetration of pigments is influenced not only by the type of material, its molecular density, or surface roughness, but also—and significantly—by the degree of water absorption [4].

h. Low cytotoxicity and high biocompatibility. Plastic materials placed within the oral environment may be exposed to thermal or humidity fluctuations, may interact with bacterial microorganisms or salivary enzymes, and finally, may be subject to masticatory or parafunctional trauma: it follows that, in addition to the properties mentioned in the previous sections, bioinertness and biocompatibility are equally fundamental. These environmental changes could lead to material aging, resulting in degradation and the subsequent release of biologically active substances—potentially cytotoxic—or molecules with estrogenic activity; that is, substances capable of inducing adverse reactions or modifications at the genetic level. An example is Bisphenol A (BPA), a compound typically found in certain polymeric materials, including polycarbonate and epoxy resins. Not only can it cause estrogenic interactions, but it can also induce intense proliferative cellular stimulation and various toxic effects. The United States Environmental Protection Agency (EPA), in agreement with the Food and Drug Administration (FDA), has identified a safe dosage of BPA at 50 μg/kg/bw per day. However, adverse events have been observed even at doses lower than this threshold, particularly affecting the prostate or the placenta.

The literature concerning the toxicity and the risk of BPA release from clear aligners, overall, is not particularly extensive and includes conflicting results: while some studies show no cytotoxic or estrogenic effects, others do. Consequently, a systematic review published in March 2023 aimed to summarize current information regarding biological safety. The evaluation of various *in vitro* tests supports the thesis that there is no significant estrogenic or cytotoxic capacity in either active clear aligners or retainers. However, it is well known that *in vitro* tests have significant limitations and thus cannot be fully indicative of real reactions, as the complex oral system—being highly dynamic and differentiated—cannot be perfectly reproduced, and the assessment methodologies themselves possess intrinsic limits. In fact, there is a clinical trial that refutes the results obtained from *in vitro* experiments, highlighting significant toxicity.

In conclusion, further experimental studies are necessary, which must be reproducible and combine multiple methodologies to increase their reliability; furthermore, it is imperative that clinical trials be proposed to evaluate the actual biological safety of aligners [22].

1.3 MATERIALS CURRENTLY IN USE

The materials currently most used for the fabrication of clear aligners are polyester, polyurethane, polycarbonate, polypropylene, ethylene-vinyl acetate (EVA), and polyvinyl chloride (PVC). Among these, the first three are amorphous polymers, while the remaining ones possess a semi-crystalline structure [16,19,20].

Polyester. In orthodontics, various polymers belonging to the polyester family are used, most notably PET (polyethylene terephthalate) and PETG (polyethylene terephthalate glycol-modified). Their widespread use in the fabrication of clear aligners is primarily related to their excellent mechanical and optical properties. PET is a material that exists in both amorphous and crystalline structures. While the former is transparent and characterized by better ductility, the latter is opaque and possesses greater hardness and robustness. However, PET crystallizes in response to deformation and high temperatures—phenomena encountered during the manufacturing process. It is precisely this crystallization that imparts a particularly high rigidity to the material.

PETG is a non-crystalline co-polyester consisting of two repeating units: polyethylene terephthalate and glycol. The latter prevents the crystallization of the material upon heating, thereby enhancing its resistance to mechanical stress [4]. Specifically, this co-polymer is essentially the transformation of PET from a semi-crystalline state to a completely **amorphous structure**, allowing for a more transparent and aesthetic result with superior handling properties. Indeed, it possesses optimal physico-chemical properties, making it suitable for various manufacturing methods, including **3D printing**, milling, and thermoforming [4].

Polyurethane. TPU is a thermoplastic polyurethane—a polymer composed of urethane monomers—that melts when heated, becoming moldable. Generally, it is a transparent, ductile, and impact-resistant material. It can exist in both flexible and rigid forms. The positive properties of this material are manifold, making it extremely versatile and stable: it exhibits excellent mechanical and elastomeric characteristics, along with ease of processing. It is characterized by outstanding flexibility and resilience: when subjected to a load, it deforms, but once the stimulus is removed, it is capable of regaining its original shape. These elastic properties appear to be optimized in multi-layer TPU, which is specifically used for clear aligners. Its application in orthodontics includes blending with other materials to enhance mechanical properties. It is also characterized by excellent printability, making it an ideal material for 3D printing. A single disadvantage of the material is its optical properties: polyurethane appears to be more susceptible to the adsorption of pigments and, according to the literature, does not offer sufficient color stability. Some authors have examined the color variations of TPU-based aligners, finding them to be higher than those of PETG-based ones: it follows that removing them before eating and drinking drastically influences their durability [19].

Polypropylene. Polypropylene is a robust and flexible material. It was among the first materials used for the fabrication of retainers: in 1993, Jack Sheridan utilized this polymer for the first 'Essix' appliance. Its characteristics make it the material of choice for the production of bite splints for bruxist patients, where greater resistance and flexibility are required to counteract occlusal forces [5, 19].

Polycarbonate. Polycarbonate is derived from the condensation of bisphenol A (BPA) and carbonyl chloride. It is an amorphous material characterized by excellent mechanical and optical properties: it possesses high hardness, fracture resistance, and transparency [23]. Its applications in dentistry are extensive and include the fabrication of brackets, prosthetic bases, and provisional crowns. However, its use is strictly limited by the potential release of BPA—a molecule with potential cytotoxicity—and by its susceptibility to irreversible hydrolysis, which can cause degradation of the polymer structure [19,24].

Polyvinyl Chloride. It is a polymer that finds limited use compared to the previously mentioned materials. Its advantages are primarily related to its excellent optical properties [19].

Polymer Blends. In most cases, aligner manufacturers utilize polymer blends to obtain materials that exhibit superior overall mechanical properties compared to their individual components. Polyesters, polyurethane, and polypropylene are commonly combined: the ratio between them plays a fundamental role in determining the final characteristics and the quality of the force exerted by the aligner [16].

1.4 THERMOFORMING

Thermoforming is the conventional manufacturing process for aligners. It utilizes pressure and vacuum to adapt a properly heated thermoplastic sheet to a mold of the dental arches. The models that serve as molds are primarily made of resin, obtained through 3D printing from dental impressions. The current workflow is predominantly digital and utilizes CAD/CAM technology (Computer-Aided Design / Computer-Aided Manufacturing): once the reproduction of the dental arches is obtained from intraoral or extraoral scans, a virtual model is created using dedicated software.Treatment planning begins on the virtual model through the creation of 'setups': specific algorithms segment individual teeth, whose positions are sequentially modified toward the desired final alignment [5]. For each stage of these movements, a corresponding physical model is generated; the actual thermoforming of a transparent sheet takes place on these models, followed by finishing and polishing. Thermoforming is performed using a machine equipped with holes through which air from the external environment is pumped. This facilitates, via negative vacuum pressure, the intimate adaptation of the sheet to the mold.

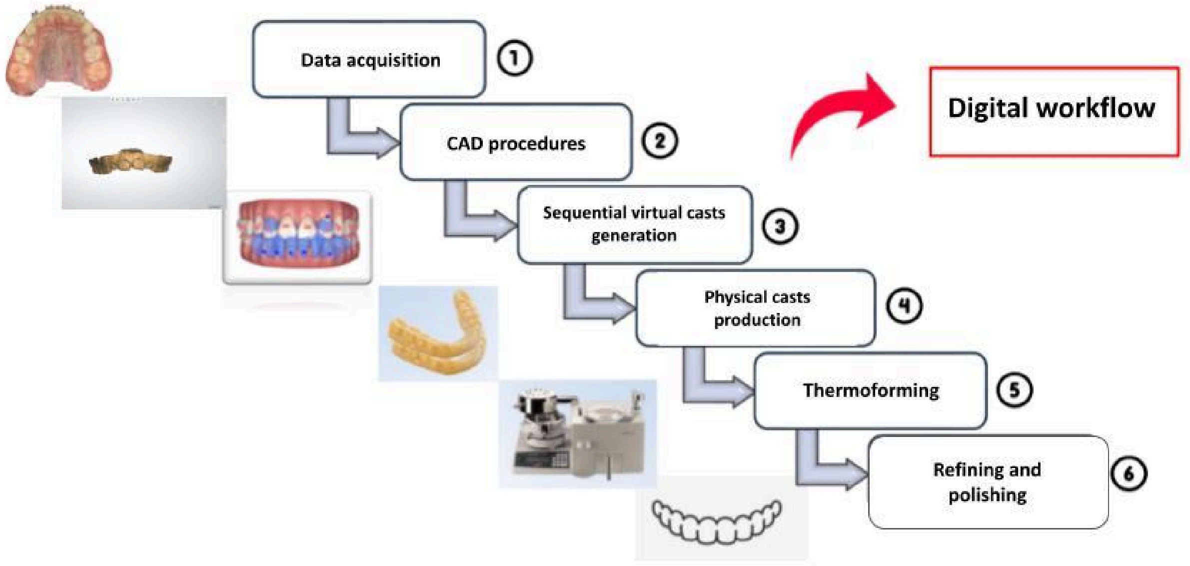

Figure 1-2: Conventional thermoforming workflow

This production technique is, however, laborious, expensive, and highly labor-intensive [25]. Another limitation concerns the sustainability of the process: there is a high amount of waste, significant energy consumption, and finally, the environmental impact of the printable resins used for the 3D models of the arches has not yet been accurately documented [26]. Furthermore, as some studies demonstrate, thermoforming is a process capable of causing variations—sometimes significant—in the mechanical, physical, and optical properties of the aligners, presumably due to the high temperatures and pressures involved. Specifically, there is a decrease in transparency and thickness, along with an increase in the material's solubility. This can result in lower tensile and flexural strength [27]. This has prompted researchers and clinicians to seek an alternative that could offer biomechanical and optical advantages while simultaneously having a lower environmental impact: this alternative is represented by in-office aligners, produced via direct 3D printing.

References

1. Castroflorio T, Sedran A, Parrini S, Garino F, Reverdito M, Capuozzo R, et al. (2023) Predictability of orthodontic tooth movement with aligners: effect of treatment design. Prog Orthod 24(1), 2. Erratum in: Prog Orthod 24(1), 47. doi: 10.1186/s40510-023-00499-8.
2. Bilello G, Fazio M, Amato E, Crivello L, Galvano A, Currò G (2022) Accuracy evaluation of orthodontic movements with aligners: a prospective observational study. Prog Orthod 23(1), 12. doi: 10.1186/s40510-022-00406-7.

3. Papadimitriou A, Mousoulea S, Gkantidis N, Kloukos D (2018) Clinical effectiveness of Invisalign® orthodontic treatment: a systematic review. Prog Orthod 19(1), 37. doi: 10.1186/s40510-018-0235.
4. Nanda R., Castroflorio T., Garino F., Ojima K. Principi di biomeccanica del trattamento con allineatori. Edizioni Martina, 2023.
5. Bichu YM, Alwafi A, Liu X, Andrews J, Ludwig B, Bichu AY, Zou B. Advances in orthodontic clear aligner materials. Bioact Mater. 2022 Oct 20;22:384-403.
6. Yazdi M, Daryanavard H, Ashtiani AH, Moradinejad M, Rakhshan V (2023) A systematic review of biocompatibility and safety of orthodontic clear aligners and transparent vacuum-formed thermoplastic retainers: Bisphenol-A release, adverse effects, cytotoxicity, and estrogenic effects. Dent Res J 20, 41.
7. Iliadi A, Koletsi D, Papageorgiou SN, Eliades T (2020) Safety Considerations for Thermoplastic-Type Appliances Used as Orthodontic Aligners or Retainers. A Systematic Review and Meta-Analysis of Clinical and In-Vitro Research. Materials 13, 1843.
8. Eliades T, Pratsinis H, Athanasiou AE, Eliades G, Kletsas D (2009) Cytotoxicity and estrogenicity of Invisalign appliances. Am J Orthod Dentofac Orthop, 136, 100–103.
9. Schuster S, Eliades G, Zinelis S, Eliades T, Bradley TG (2004) Structural conformation and leaching from in vitro aged and retrieved Invisalign appliances. Am J Orthod Dentofacial Orthop, 126, 725-728.
10. Nakano H, Kato R, Kakami C, Okamoto H, Mamada K, Maki, K (2019) Development of biocompatible resins for 3D printing of direct aligners. J Photopolym Sci Technol 32, 209–216.
11. Pratsinis H, Papageorgiou SN, Panayi N, Iliadi A, Eliades T, Kletsas, D (2022) Cytotoxicity and estrogenicity of a novel 3-dimensional printed orthodontic aligner. Am J Orthod Dentofac Orthop 162, e116–e122.
12. Campobasso A, Ariano A, Battista G, Posa F, Migliorati M, Drago S et al. (2023) Comparison of the cytotoxicity of 3D-printed aligners using different post-curing procedures: An in vitro study. Austral Orthod J 39, 49–56.
13. Zecca PA, Borgese M, Raspanti M, Zara F, Fastuca R, Serafin M, Caprioglio A. Comparative microscopic analysis of plastic dispersion from 3D-printed and thermoformed orthodontic aligners. Eur J Orthod. 2025 Apr 8;47(3):cjaf014. doi: 10.1093/ejo/cjaf014.
14. Rajasekaran A, Chaudhari PK (2023) Integrated manufacturing of direct 3D-printed clear aligners. Front Dental Med 3, 1089627.
15. Lee SY, Kim H, Kim, HJ, Chung CJ, Choi YJ, Kim SJ, et al. (2022) Termo-mechanical properties of 3D printed photocurable shape memory resin for clear aligners. Sci Rep, 12, 6246.

16. Zhang N, Bai Y, Ding X, Zhang Y. Preparation and characterization of thermoplastic materials for invisible orthodontics. Dent Mater J. 2011;30(6):954-9.
17. Boyd RI., Miller RJ, Vlaskalic V. The Invisalign system in adult orthodontics: mild crowding and space closure cases. J Clin Orthod. 2000; 34: 203-212.
18. Eliades T., Bourauel C. Intraoral aging of orthodontic materials: the picture we miss and its clinical relevance. Am. J. Orthod. Dentofacial Orthop. 2005;127(4):403–412.
19. Gold B.P., Siva S., Duraisamy S., Idaayath A., Kannan R. Properties of orthodontic clear aligner materials - a review. J. Evolution Med. Dent. Sci. 2021;10(37):3288–3294.
20. Lombardo L., Arreghini A., Maccarrone R., Bianchi A., Scalia S., Siciliani G. Optical properties of orthodontic aligners--spectrophotometry analysis of three types before and after aging. Prog. Orthod. 2015;16(1):41.
21. Frick, Achim e Rochman, Characterization of TPU-elastomers by thermal analysis (DSC). Arif. Issue 4, 2004, Polymer Testing, Vol. 23, p. 413-417.
22. Yazdi, Marzie, Daryanavard, Hanie; Ashtiani, Alireza Hashemi; Moradinejad, Mehrnaz; Rakhshan, Vahid. A systematic review of biocompatibility and safety of orthodontic clear aligners and transparent vacuum-formed thermoplastic retainers: Bisphenol-A release, adverse effects, cytotoxicity, and estrogenic effects. Dental Research Journal 20(1):41
23. Macrì M. G. Murmura, G. Varvara, T. Traini e F. Festa. Clinical performances and biological features of clear aligners materials in Orthodontics. 2022, Front. Mater 9:819121.
24. Khorsandi, Danial, et al. 3D and 4D printing in dentistry and maxillofacial surgery: Printing techniques, materials, and applications. 2021, Acta Biomaterialia, Vol. 122, p. 26-49.
25. Leite, W.D.O.; Campos Rubio, J.C.; Mata Cabrera, F.; Carrasco, A.; Hanafi, I. Vacuum Thermoforming Process: An Approach to Modeling and Optimization Using Artificial Neural Networks. Polymers 2018, 10, 143.
26. Tartaglia GM, Mapelli A, Maspero C, Santaniello T, Serafin M, Farronato M, Caprioglio A. Direct 3D Printing of Clear Orthodontic Aligners: Current State and Future Possibilities. Materials (Basel). 2021 Apr 5;14(7):1799.
27. Ryu, JH, et al. Effects of thermoforming on the physical and mechanical properties of thermoplastic materials for transparent orthodontic aligners. 2018, Korean J Orthod., Vol. 48, p. 316-325.

3D PRINTING OF ORTHODONTIC ALIGNERS

2.1 INTRODUCTION

By 3D printing, we mean a set of digitally-assisted manufacturing techniques that allow for the creation of three-dimensional objects through subtractive or additive processes. The general advantages of these techniques vary: foremost among them are high precision, speed of execution, and the possibility of customization. The birth of this technology dates back to the second half of the last century: the first patents trace back to the late 1970s, even though the capabilities and machinery were still at a rudimentary stage.

In 1984, Charles 'Chuck' Hull patented the first printing technique, known as stereolithography (SLA); only six years later, in 1990, Scott Crump introduced a second one: fused deposition modeling (FDM). Over the last 40 years, we have witnessed a rapid evolution in manufacturing technology, characterized by significant progress in machinery and the introduction of new techniques and materials. This resulted in an expansion of its applications, including the medical and dental sectors [1].

Focusing on the dental world, this technology is frequently used for prosthetic reconstructions and orthodontic or surgical devices, even complex ones. Subtractive processes are commonly used in the prosthetic field, where the milling of zirconia or lithium disilicate blocks via milling machines is a prime example. Additive processes, on the other hand, are more closely associated with the orthodontic or implant fields. This latter process is based on layer-by-layer manufacturing, meaning through the gradual overlapping of layers. The materials currently used are: resins, plastic polymers, nylon, wax, and titanium. Associated with these is a new specific property defined as 'printability', which refers not only to the physical possibility of extruding or solidifying the material, but also to its ability to maintain dimensional accuracy during cooling or polymerization [2].

In the medical field, this must necessarily be combined with biocompatibility, which is why materials must be biodegradable, possess low porosity, and exhibit limited cell adhesion levels.

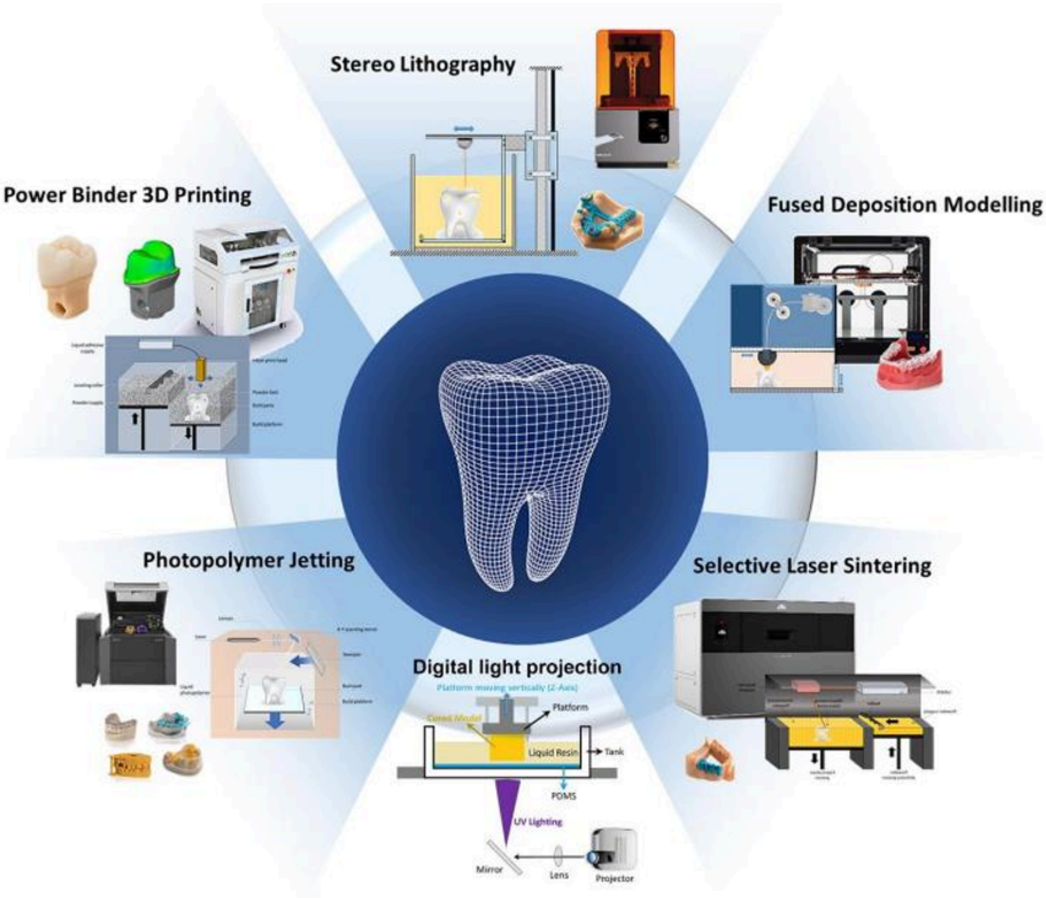

Figure 2-1 Printing Technologies

2.2 PRINTING TECHNOLOGIES

2.2.1. Stereolithography, or SLA

Stereolithography was the first additive printing technique introduced to the market, based on the photopolymerization of a liquid, photosensitive resinous material. We can distinguish between different stereolithographic strategies based on the movement of the build plate or the movement of the laser beam.

The process can be broadly divided into three phases: light laser exposure, platform movement, and resin refilling. Initially, the first layer of material is deposited and polymerized by a UV source; subsequently, once the exposure is complete, the build plate moves by a distance equal to the planned layer thickness, and the process continues to build the next layer until the complete 3D object is finalized. The discontinuity of this method can be overcome by combining SLA with Continuous

Liquid Interface Production (CLIP). Furthermore, parameters such as the intensity of the light source, the scanning speed, or the concentration of monomers and photoinitiators within the resin allow for control over the kinetics and properties of the final product. Currently, stereolithography is used for the fabrication of temporary or permanent crowns and bridges, surgical guides, and dental models. The main advantages of this technique include accuracy, high resolution, and geometric flexibility, which translate into significant potential for customization.

Conversely, there are some risks primarily related to the photopolymerization process: these include over-curing or under-curing, which could affect properties such as mechanical strength, surface smoothness, or, even more importantly, biocompatibility. In fact, the persistence of residual monomers could trigger actual inflammatory or irritant reactions, also compromising the longevity of the devices [1].

2.2.2 Digital Light Processing, or DLP

DLP is an additive printing technology similar to SLA. The materials used are liquid photosensitive resins that undergo a photopolymerization process, which causes them to harden layer by layer. The first layer is built directly onto the build plate. In this technique, light is reflected via a digital device based on micro-mirrors (DMD). This consists of a matrix of microscopic mirrors that direct the light from the projector to the projection lens. After the polymerization of each layer, the plate moves up or down (depending on the position of the light source) by a distance equal to the preset thickness, until the entire object is completed.

Although SLA and DLP are remarkably similar, they differ in several ways. First and foremost, the two techniques utilize different light sources: while the former relies on a direct UV laser beam, the latter uses a reflected UV source. Consequently, in stereolithography, the beam moves point-by-point, resulting in a corresponding polymerization; in digital light processing, the source is fixed and polymerizes the entire layer at once. This translates into higher accuracy and print quality with SLA compared to DLP, which is, however, faster. Furthermore, the intensity of the light source is adjustable in DLP, whereas it is not in SLA. Overall, DLP is advantageous for the rapid printing of large objects with lower definition, while SLA is preferable when high precision and resolution of intricate details are required [1].

2.2.3 Masked Stereolitography, or MSLA

MSLA represents an innovative technique similar to traditional SLA and DLP. This methodology is based on a liquid crystal display (LCD) that masks a UV light source: the panel, consisting of tiny pixels, serves to mask portions of the UV light to create a specific pattern for each layer. A 2021 study aimed to evaluate the printing accuracy of two different LCD printers in comparison to a traditional SLA printer, which is considered the gold standard. The conclusions state that these newly introduced printers have lower precision than conventional ones; however, the level of inaccuracy falls within the clinically acceptable limits for orthodontics, justifying their use in this field. Furthermore, it has been demonstrated that the layer thickness does not affect the precision or accuracy of the printed models.

One advantage of this technique is the higher printing speed, due to the fact that it depends solely on the number of planned layers—and therefore on the build height—rather than the amount of material in each individual layer. The print resolution in these devices can be improved by the choice of the LCD screen, and consequently, by the pixel size [1,3,4].

2.2.4 Fused Deposition Modeling, or FDM

FDM, also known as Fused Filament Fabrication (FFF), is the commercial name for a process used for polymers, composite materials, or metals, invented about 20 years ago. It is the second most widely used technique, following SLA. It is a more cost-effective methodology compared to the others. The technique is based on the extrusion of thermoplastic material filaments. These filaments are first softened and made malleable, and subsequently, via an extruder, they are deposited onto the build plate to form models layer-by-layer, always managed by a digital design. The filaments used are primarily thermoplastic polymers, composite materials (such as ABS or PC), and low-melting-point metal alloys.

Polymers can be combined with metallic nanoparticles, which reinforce the filament and improve certain thermal and mechanical characteristics. Mechanical properties, specifically, are heavily influenced by the material, structural parameters (infill density, print orientation, layup sequence), and manufacturing parameters (extrusion temperature, layer print time, build plate temperature). In general, however, these properties tend to be particularly unfavorable: their use is mainly limited to temporary crowns and bridges or simple anatomical models; the final result will be brittle and highly porous.

2.2.5 Selective Laser Sintering, or SLS

SLS is a system based on the use of a high-energy laser beam to fuse materials provided in powder form, creating solid layers. The platform then lowers to create space for the laser to sinter the next layer of powder. Specifically, the laser increases the temperature of the powder until it reaches or approaches the sintering point, where the solid particles are converted into a semi-liquid state. At the end of the additive process, the object is cooled and returns to a solid form. Through this technique, study models, guides, or metal frameworks can be produced. The advantages include the use of autoclavable materials, excellent mechanical characteristics, low costs, and the potential for high-volume production. Another positive factor of SLS is that the printed object is ready to use, unlike other printing methods that require sanding or finishing before the products can be utilized.

Furthermore, since SLS printers do not require structural supports during printing, the processing times are significantly faster compared to SLA and FDM. The disadvantages are related to the risk of material inhalation, the initial cost, and the need for additional equipment, such as compressed air for handling the powders.

2.2.6 Photopolymer Jetting

This method involves the combination of two techniques, utilizing a dynamic print head and a photocurable polymer. The photosensitive polymer is projected by an inkjet print head onto a platform and cured layer-by-layer on a descending build plate using a UV source. A support structure is also printed using a relatively brittle material to facilitate its removal. With this technique, crowns, anatomical study models, or implant preparation guides can be produced. The advantages include high production speed, cost-effectiveness, and excellent print quality in terms of both resolution and surface finish. Furthermore, in order to cover the entire width of the build platform, inkjet 3D printers can be equipped with multiple print heads. The disadvantages, however, include the difficulty of completely removing material due to the rigid support, the risk of skin irritation upon contact, the inability to undergo heat sterilization, and, finally, the high cost of materials.

2.2.7 Powder Binding Jetting

This additive process utilizes a liquid adhesive, contained within a modified inkjet print head, which is released in droplets to infiltrate a layer of powder underneath. Since it is a low-cost technology, it is used in applications that do not require sterilization, such as the printing of study models or prototypes. However, the printed objects are brittle and lack precision.

2.2.8 Computed Axial Lithography (CAL)

Computed Axial Lithography is a volumetric AM (Additive Manufacturing) printing technique. It bears a certain resemblance to the DLP method, as both systems employ a projector as a light source to photopolymerize the resin. The difference between Computed Axial Lithography and other conventional printing techniques is that light polymerization is applied from various angles of the material. In other words, Computed Axial Lithography can produce the entire object at once, rather than layer-by-layer. The concept of Axial Lithography is inspired by Computed Tomography (CT) scanners, where X-ray scans are performed from multiple angles: the object is fabricated by projecting light (at a specific wavelength) containing numerous 2D images—representing different perspectives of the object—into a rotating container of photocurable resin.

This technique allows for the fabrication of highly complex products, achieving an excellent surface finish in shorter timeframes compared to other AM methods. Currently, high-viscosity resins or solid materials are predominantly used for this technique. However, further in vivo studies are necessary to investigate the mechanical and chemical properties, tolerability, and biocompatibility of the photopolymerized resin products to ensure greater clinical safety.

2.3 IN-OFFICE PRINTING OF ALIGNERS

The direct printing of clear aligners was introduced thanks to the development of the first photocurable resin, TC-85DAC, by the South Korean manufacturer Graphy [3,4,5]. Consequently, the available literature is somewhat limited but currently expanding. Documentation is available presenting the most commonly used protocols, as well as experiments—including in vivo studies—that compare this methodology to the more traditional thermoforming process. The advantages of this protocol have already been identified and primarily concern the simplification of the workflow and the greater overall sustainability of the process. Furthermore, this methodology grants a primary role to the orthodontist, who will be fully responsible for the design and fabrication of the aligners, without delegating these processes to outsourced laboratories. This allows the clinician to control every stage of the treatment: from movement staging to mid-treatment modifications, including variations or additional refinements [5]. The main benefit of 3D printing is the ability to directly transfer STL files, derived from the setups, from the planning software to the printing software. Furthermore, post-printing treatments are limited to centrifugation, removal of printing supports (if present), and UV curing; the trimming, finishing, and polishing phases—which are necessary for thermoformed aligners—can be avoided. This contributes to a reduction in production times and decreases the risk of occupational irritation for the operator caused by contact with unpolymerized residues or dust [3,4,5]. A further advantage lies in the fact that, despite having shorter production chains, the manufacturing accuracy remains undiminished.

This is likely due to the reduction in cumulative errors resulting from analog impression-taking or subsequent thermoplastic treatment. The precision of in-office aligners concerns their fitting, specifically their adaptation to dental surfaces [3,4]. Koenig et al. focused their study on this topic, utilizing micro-CT for microscopic evaluation. They compared the accuracy of 3D-printed aligners with that of two commercially available thermoformed aligners. The gap measured 76–63 μm in the anterior and posterior sectors of the printed aligners, and 69–73 μm in the thermoformed ones. Consequently, no significant difference was observed between the samples, suggesting the reliability of the direct printing process [6]. Furthermore, the physical properties resulting from the printing process were investigated: these included lower values for elastic modulus, yield stress, and stress relaxation when the material was subjected to repeated loading. These mechanical properties were also evaluated after one week of use and were found to remain unchanged [5,6]. Regarding this last observation, a further study by Eliades et al. reported that after 7 days of application, there was a degradation of mechanical properties by approximately 10%; this stands in contrast to thermoformed aligners, which showed values reaching nearly 50% [7].

The thickness of an aligner can influence the intensity of the forces exerted to achieve controlled movements. In thermoformed aligners, the thickness tends to decrease following the thermoforming process and based on dental morphology: for instance, teeth with greater height or proinclined teeth can cause a reduction in thickness.

In aligners produced using additive methods, however, thickness can be more easily managed. Generally, aligner thickness varies between 0.25 and 1–2 mm. Today, it has been concluded that the ideal values are 0.5 mm for aligners worn for 7 days and 0.7 mm for aligners changed every 14 days. However, these guidelines do not necessarily have to be applied uniformly across the dental arches: with direct printing, thickness can be modified in specific areas where a change in force is required. If it is necessary to move an incisor more palatally, the thickness at the buccal level can be increased; alternatively, if the prescription includes the derotation of a tooth, the thickness can be increased at its mesial or distal aspects. This topic requires further investigation through more experimental and clinical studies to confirm its accuracy and efficacy. For instance, Edelmann et al. demonstrated that 3D printing can cause risky and unwanted increases in thickness, affecting the predictability of the manufacturing process [8].

Printing accuracy is determined by two fundamental factors: trueness and precision. The former indicates the ability of a printer to reproduce an object as faithfully as possible to its digital design; the latter represents the degree of reproducibility under identical conditions. Overall, accuracy is influenced by the printer's properties, most notably both XY and Z resolution.

2.3.1 Resolution

Horizontal resolution, or XY resolution, is an effective indicator of printing precision, as it represents the minimum feature size that a printer can reproduce horizontally within a single layer. In SLA printers, this depends on the laser beam diameter, whereas in LCD or DMD printers, it is correlated to the pixels of the screen or the projector, respectively. Conversely, Z-resolution represents the thickness of individual layers and depends on both the material and the printer: resolution values of 25 µm, 50 µm, or 100 µm are commonly available. Thinner layers lead to a higher number of repetitions, resulting in longer production times and an increased risk of artifacts or errors [9-11]. The layer height also affects the surface quality of the model: smaller heights yield smoother surfaces; however, this does not always guarantee greater dimensional accuracy [11-13]. Consequently, choosing the print resolution requires considering several factors, including the requirements for accuracy and surface smoothness of the model for clear aligner fabrication, as well as the efficiency of the office workflow.

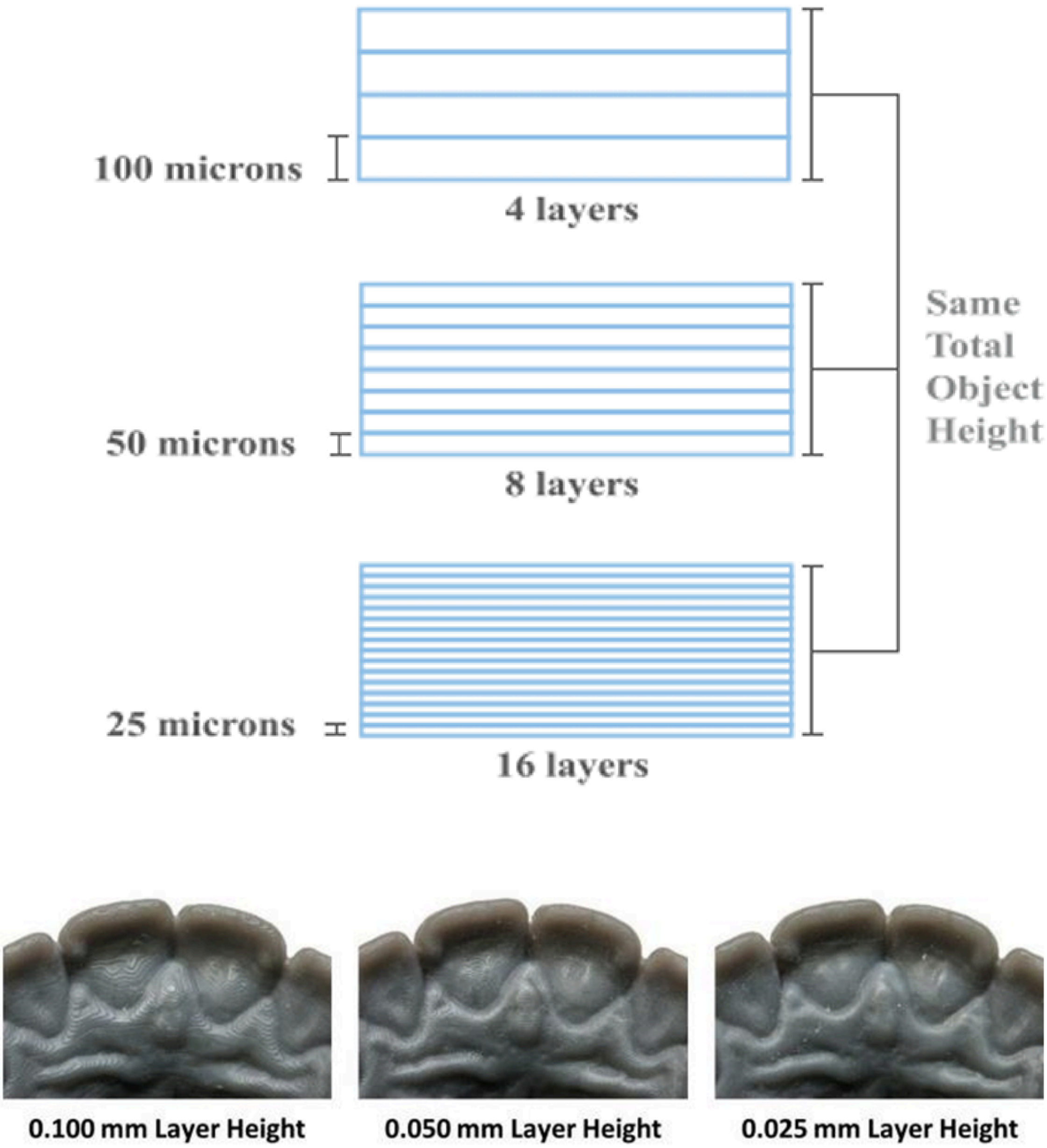

Figure 2-2 Printing Resolution concept and result

Although current 3D printers require the selection of a single layer height, the future development of printers capable of supporting multiple layer heights within a single print could enable the application of adaptive slicing approaches. In such cases, larger layer heights would be applied to less critical areas, such as the model base, while smaller layer heights would be applied to critical areas, such as the dentition, in order to balance efficiency and dimensional fidelity (or accuracy) [14]. Even at a fixed layer height, the accuracy of the same printed part can differ among various SLA printers [11].Other factors that can influence print quality include the print orientation and the polymerization (or curing) process.

2.3.2 Print Orientation and Support Structures

Preparing digital model files for printing also requires selecting an appropriate orientation for the part relative to the build platform and designing support structures, if necessary, to enable the realization of the virtual design. Since 3D printers build parts layer-by-layer, the part should be oriented in such a way that the regions of each layer connect with the previously printed layer; otherwise, unsupported regions may fail to be incorporated into the model [4,14,15]. Printer-specific software packages generally facilitate these stages. The inclusion of support structures in contact with critical regions of the model, such as the dentition, should be avoided, as the removal of these supports can cause dimensional deviations in these areas. The presence of supports requires additional material for model production and may increase the time needed for both printing and post-processing [14,15].

- Horizontal orientation consists of positioning the model in contact with the build plate, with the occlusal surfaces parallel to it. This results in a fewer number of layers and a consequently higher printing speed; however, fewer aligners can be printed simultaneously, and a greater number of supports is required to ensure printing accuracy.
- Vertical orientation involves positioning the occlusal surfaces approximately perpendicular to the platform, with the posterior region of the model in contact with it. This arrangement decreases printing speed because the number of layers increases; consequently, the risk of printing errors may also rise. With this parameter, however, although the required supports decrease, the number of aligners that can be printed simultaneously increases [14,15].

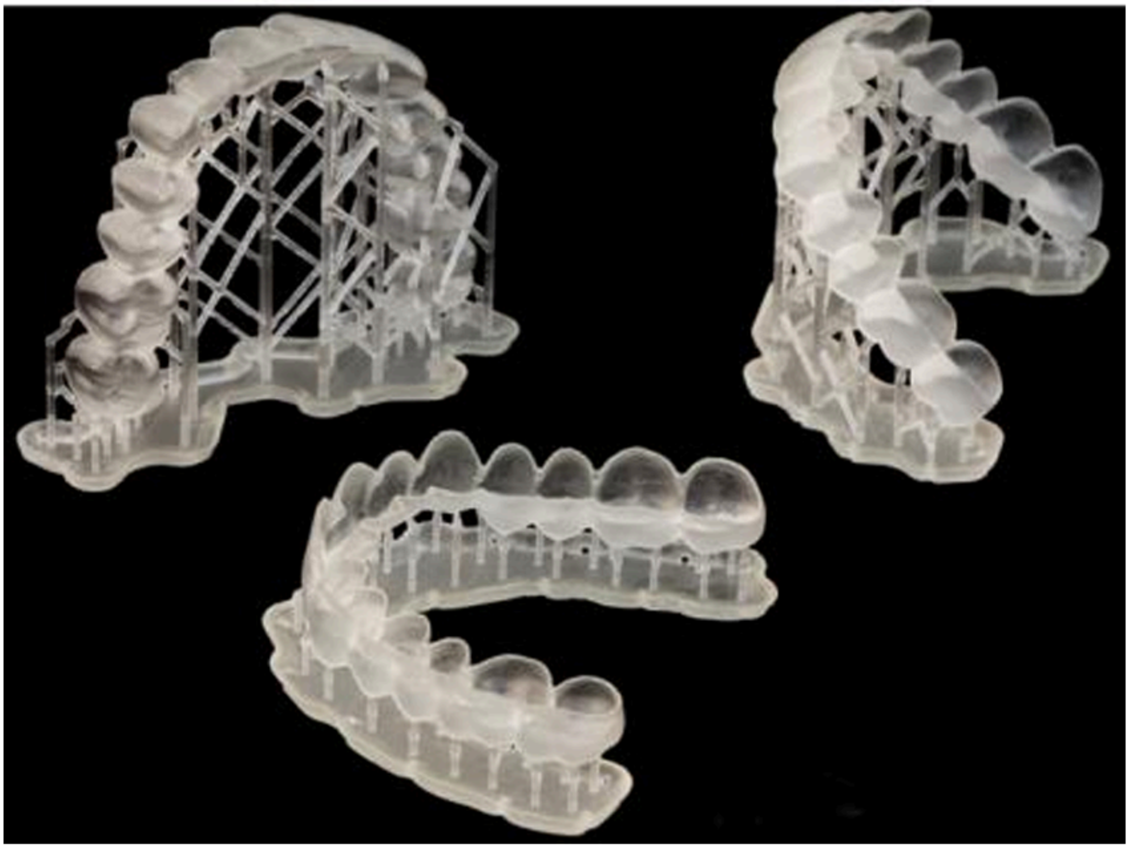

Figure 2-3 Aligners printed according to different printing orientations

- Oblique orientation represents an intermediate solution between the two aforementioned methods, both in terms of the number of required supports and printing speed. McCarty et al. investigated the effect of different print orientations on the dimensional accuracy of the samples: the research group observed that a 45° orientation was associated with the highest dimensional accuracy. This can hypothetically be attributed to a reduction in the cupping effect observed in the other two groups: the gingival, posterior, and anterior openings face the resin vat, forming a cup-like shape that traps air and resin during printing movements, consequently leading to precision defects [4].

To conclude, a further positive factor of this strategy is sustainability. Environmental pollution is a severe global issue today; therefore, the choice of a protocol that ensures a lower environmental impact by drastically reducing waste and carbon emissions is highly preferable. Direct printing eliminates the need for intermediate physical models—which are commonly made of non-recyclable resins—and produces aligners with a shape already defined during the CAD phase, requiring no trimming from an initial thermoplastic sheet [16].

2.4 DIRECT PRINTING MATERIALS

Evolution in materials science is the rationale upon which progress in various disciplines is founded, including orthodontics. Specifically, a significant innovation has been the introduction of 'smart materials,' also defined as stimuli-responsive materials. Among these, we identify Shape Memory Polymers (SMPs), which find specific indications within the dental field. In general, this category includes materials characterized by remarkable transparency, significant elastic deformation, and high chemical stability. What differentiates them is their property of reacting to various external stimuli—such as physical, thermal, or magnetic triggers—generating predictable and repeatable responses. More specifically, when subjected to a certain impulse, shape memory materials can exhibit an alteration in their macroscopic shape, reaching a transient shape that remains stable for a certain period of time; upon the application of another stimulus, they regain their original shape.

This mechanism is based on two crucial points: the presence of a stable polymer network, which determines the initial shape of the material, and its reversibility, which allows the material to transform into an altered, temporary shape [16,21-23].

Shape memory is therefore based on a two-domain system featuring two different glass transition temperatures: the polymer chains consist of a transition segment, whose stiffness varies depending on the stimulus, and an elastic segment. Upon reaching the transition temperature, the deformed shape-memory material exhibits elastic behavior and, by recovering its original shape, generates forces capable of producing orthodontic tooth movements [16,23]. The shape memory effect therefore refers to the phenomenon in which a material, after being deformed, is capable of recovering its original shape [23].

SMPs can exhibit more than one temporary shape, owing to a particularly wide temperature range for shape recovery and a much higher level of recoverable deformation. Some studies have postulated that these polymeric materials could constitute a viable option for the fabrication of clear aligners, as they are particularly adaptable to the oral environment, which is continuously subjected to thermal and humidity changes. Shape memory could allow a single aligner produced with these materials to replace up to three conventional aligners to achieve the same result. Consequently, the treatment could have a significantly reduced duration and lower costs [16,27]. Shape-memory polyurethane-based resins, for example, include microdomains of hard and soft segments; this combination allows the material to achieve both high strength and high toughness, optimizing the durability and biomechanical efficacy of oral devices [16]. This has progressively led to the introduction of various polymers developed for this purpose: each new material must, therefore, be adequately tested to demonstrate clinical efficacy and biocompatibility. However, the approval and commercialization of these innovative materials will require a significant amount of time, as they must be tested for their aesthetic, mechanical, and, most importantly, biological properties.

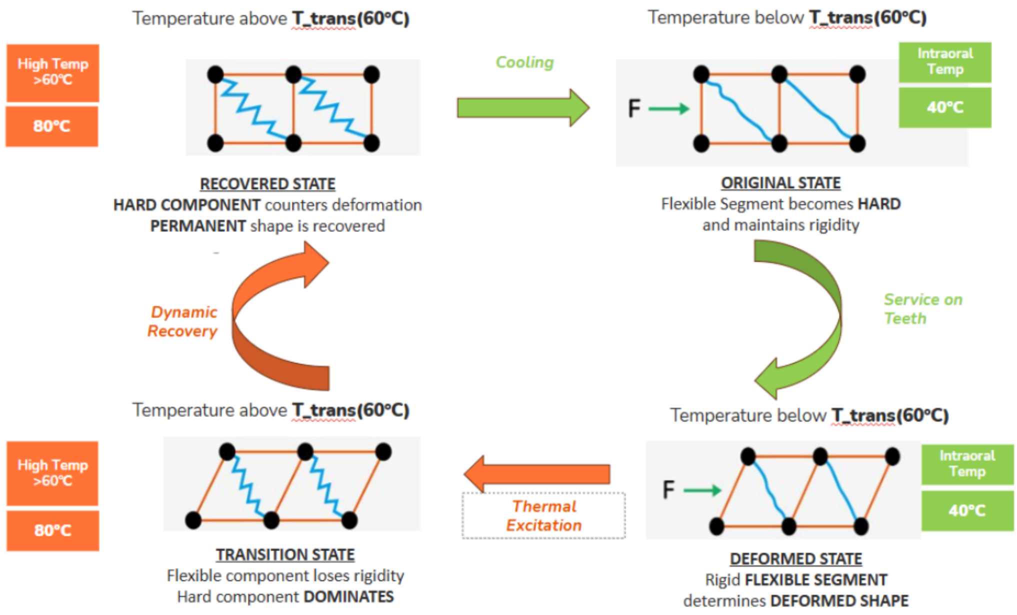

Figure 2-4 Shape memory polymers can be thought of as a cross linked structure made of polymer chains. The interaction between the polymer chains is described as a flexible segment in the net and changes with the temperature (the reported example refers to the transition temperature of the LuxCreo DCA resin)

Shape-memory polyurethane-based resins, for example, include microdomains of hard and soft segments; this combination allows the material to achieve both high strength and high toughness, optimizing the durability and biomechanical efficacy of oral devices [16]. This has progressively led to the introduction of various polymers developed for this purpose: each new material must, therefore, be adequately tested to demonstrate clinical efficacy and biocompatibility. However, the approval and commercialization of these innovative materials will require a significant amount of time, as they must be tested for their aesthetic, mechanical, and, most importantly, biological properties.

The first resin that has received approval for commercial use is Tera Harz TC-85 by the South Korean company Graphy. As of today, it has received clearance from the Korean FDA (Food and Drug Administration), the European Commission (CE marking), and more recently, the American FDA [3,14,16]. It is a biocompatible resin ideal for direct printing. The tests conducted highlight excellent physical properties, including strength, elasticity, and shape memory [14,16]. The manufacturer itself states that the resin exhibits high elongation, flexibility, and precision [24]. Due to patent-related issues, it is not possible to determine the material's chemical structure with precision; however, results from Fourier-transform infrared (FTIR) spectroscopy have indicated that the material is an aliphatic vinyl ester-urethane polymer, likely cross-linked with a methacrylate functionalization [22]. According to the study conducted by Se-Yeon Lee et al., TC-85 samples recovered their shape over time at 37°C after being bent at 80°C (a temperature above its T_g) [22]. This shape-memory behavior allows dentists to immerse the aligner in hot water before the patient wears it for the first time, making the procedure more comfortable without significantly altering its shape. In 2024, a new resin formula for DPAs, known as TA-28, was introduced. According to the manufacturer, this resin generates 30% more force than its predecessor, TC-85, and offers enhanced mechanical properties, including increased stiffness.

In the same year, another product, with a higher T_g, appeared: LuxCreo DCA (LuxCreo, Chicago, IL, U.S.A).

Other materials for direct printed aligners that were found in the literature include Dental LT clear resin (Formlabs, Somerville,MA, USA), Material X (Envisiontec, Inc.; Dearborn, MI, USA) and OD-Clear TF (3DResyns, Barcelona, Spain) [28]. Finally, Senertek Clear-A (Senertek, Izmir, Turkey) and ODS Clear (ODS, Yeonsu-gu, Korea) are emerging as potential alternatives for the fabrication of clear aligners, although they have not yet been approved or introduced to the market.

2.5 PRINTING PROTOCOL

In its initial stages, the direct printing protocol does not differ significantly from the typical workflow of traditional aligner fabrication: what distinguishes them is the phase following treatment planning and the creation of the working models. We can, therefore, define in-office production through its various sequential stages:

1. Dental arch scanning. As previously presented in the preceding chapters, this can be either direct or indirect, depending on whether it is performed using intraoral scanners or follows a traditional impression-taking method.

2. Import of digital scans and their subsequent processing. Specific CAD software provides tools for orienting models in space and for alignment with the occlusal plane, which is defined using three points identified on each arch.

3. Numbering and segmentation. The dental elements are defined, individually sectioned, and separated from the gingiva, allowing for the planning of movements during the setup. This phase is performed in an automatic or semi-automatic manner by the software, which approximates the landmarks (or reference points) of the elements; in case of error, the operator can manually correct the issue [17].

4. Definition of dental reference axes. Through specific tools, the center point of the teeth is identified; this serves as the reference used to measure all rotations and translations, or to reposition the axis passing through the roots. The software itself uses algorithms to attempt to define the approximate position of each tooth's root; however, as studies most often demonstrate, these results are not accurate [18]. A further innovation can be applied at this stage: the importation of the patient's CBCT data to be combined with the scans. This could be useful for visualizing the exact position and root inclination, thereby facilitating the identification of the correct dental axes. The limiting factor for this integration is the radiation exposure of the radiographic image, which must, therefore, necessarily present a medical justification for its indication.

5. Virtual Setup. All software programs feature tools for moving the dental elements, which is performed either via a slider or by numerically defining the amount of movement or the change in angulation. Should this displacement occur in an area lacking sufficient space, the need for IPR (Interproximal Reduction) can be planned and quantified [17]. Attachments are added at this stage, where necessary; the software includes libraries containing the most conventional shapes, but alternatively, it is possible to create customized attachments individualized to the specific movement. Subsequently, the different models can be numbered or labeled to facilitate tracking, thereby allowing for the monitoring of movements throughout the course of treatment.

6. File Export. Once the design of the aligners is complete, they are exported from the software in STL, OBJ, or PLY format, which can be read by a 3D printer. The models can then be virtually positioned on the printer's build plate.

7. Slicing. A fundamental step prior to printing is the use of a slicer, a program that sections the model into layers and allows for the management of various printing parameters: orientation, positioning on the build plate, layer height, exposure time, and polymerization time. During this phase, any necessary support structures are also designed.

8. Printing is performed using VAT polymerization technology, an additive manufacturing technique in which a liquid, photosensitive resin material undergoes hardening through UV polymerization. The preferred printing strategies are based on stereolithography in its main forms: SLA, DLP (e.g. iLux Pro Dental 3D printer, LuxCreo, Chicago, IL, U.S.A), and MSLA (i.e. Phrozen Sonic XL 4K 2022 printer, Phrozen Technology, Hsinchu, Taiwan; Accufab L4D printer Shining 3D, Hangzhou, China, NBee Unix printers). These methods allow for products with high resolution, smooth surfaces, and high precision.

9. **Removal of excess resin.** The removal of excess unpolymerized resin is performed via

- centrifugation in the Graphy workflow: the aligners are positioned with their internal surface facing outward and centrifuged for 5–6 minutes at a speed of 500–600 rpm (revolutions per minute). This process is essential for ensuring an adequate fit to the dental structures.
- double Automatic 99% Isopropanol Wash in the LuxCreo DCA workflow

- 10 min 130°C drying and heating in the LuxCreo DCA workflow (thermosetting phase)

10. Removal of support structures. In the Graphy workflow, supports are removed before UV post-curing; however, doing so may affect the final shape of the aligner [14]. For this reason, in the LuxCreo workflow they are removed after the UV polymerization process is complete.

11. UV Curing. UV curing is the key process for imparting the final properties to the aligner. Curing units can now be found in various designs, capacities, light intensities, etc. The first unit introduced specifically for this purpose was the Cure M. Although this unit achieved excellent performance—at least for printed aligners—compared to other units, the company Graphy has modified the polymerization protocol several times in an attempt to idealize the printing result. This led to the introduction of the Tera Harz Cure, a newly conceived curing unit which, unlike its predecessor, allows for a treatment (20 minutes) in the absence of oxygen, a known polymerization inhibitor. This is made possible by the integration of a nitrogen generator within the machine, which disperses oxygen to create an anoxic environment." It has been demonstrated that complete polymerization is associated with greater biocompatibility of the material: resins are toxic, irritating, and allergenic if they remain unpolymerized [3,14,20]. Curing temperature and time are extremely important for the compressive strength, overall strength, and biocompatibility of the printed resin; this is because they allow for the formation of a greater number of cross-linked bonds, enhance the mechanical properties of the material, and reduce residual stress [16].

12. 2 min ultrasonic bath at 80°C and a double sequence of 10 min heating and washing in running water for the Graphy workflow, which ends by 1 min bath in boiling water.

13. Polishing. Polishing is performed using rotating brushes, especially at the points where the support structures were positioned. During this phase, the surface can also be further smoothed by applying a thin layer of resin, which is then polymerized for 2–3 minutes. However, this process can be skipped. At the end of this procedure, the aligner is immersed in hot water for a few seconds to remove any residual substances that could cause adverse reactions to the patient [14,19].

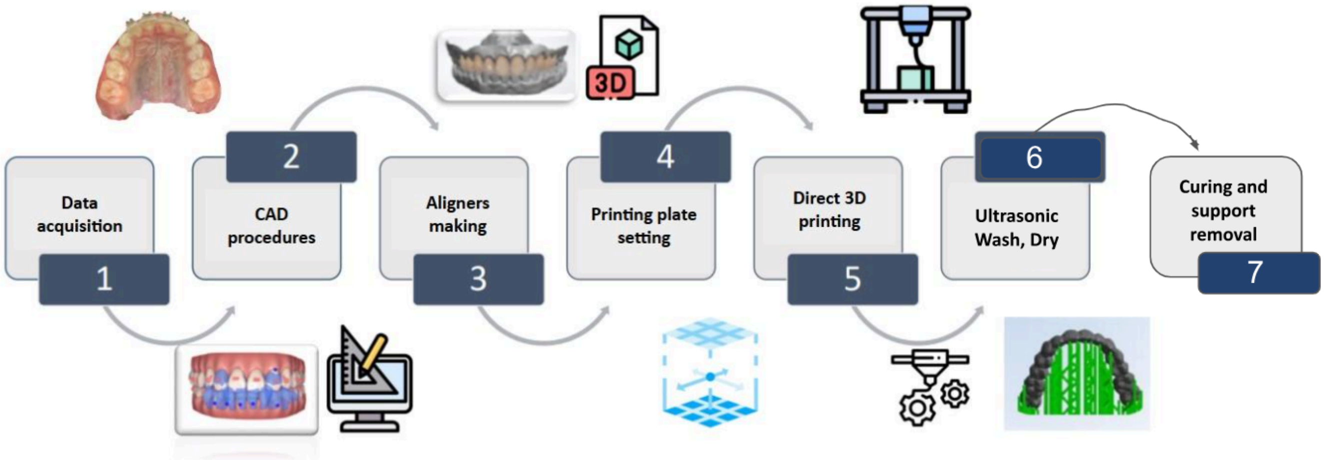

Figure 2-5 3D printed aligners workflow (the reported example refers to the DCA LuxCreo resin)

2.6 OBJECTIVES OF THE THESIS PROJECT

The introductory part of this thesis has demonstrated that the use of 3D-printed clear aligners in clinical practice represents, to date, a viable alternative to the use of traditional thermoformed aligners. However, although the advantages have already been identified, further investigation into material properties and fabrication processes is required to ensure greater efficacy and safety of the aforementioned CAT (Clear Aligner Treatment). Indeed, the final properties of the aligners can be heavily influenced by these two factors: to analyze the variability of mechanical properties as these factors change, specific in vitro tests were performed on samples differentiated by:

- Printing device
- Printer Z-axis resolution
- Thickness
- Curing process
- Printing material

Furthermore, due to the presence of different glass transition temperatures (T_g) in these polymers, the mechanical properties were investigated at the operating temperature as well (37°C) and over the time of use.

Since no direct measure of the stresses on the periodontal ligament, clear aligner and dentition is available at present, a preliminary finite elements model was developed where the collected mechanical parameters can serve for assessing the delivered forces and simulate the result of different resins and different movements.

Another issue concerning 3D printing materials is biocompatibility**.** Specifically, prior to the fabrication and polymerization processes, these materials are highly toxic. Various studies have demonstrated that thermoformed aligners exhibit lower cytotoxicity compared to direct-printed aligners. Particularly, the cytotoxicity of the latter appears to be at its peak on the first day of use and then gradually decreases [16].

Another study compared the roughness of printed aligners and Invisalign: surface roughness was higher in the printed aligner group compared to Invisalign. This results in greater exposure to risks related to the intraoral environment, most notably plaque accumulation, inflammation, reduced transparency, and the release of substances.

Roughness can be reduced by managing the printing phase—specifically the design and configuration—as well as the post-printing stages, namely polymerization and cleaning.

Finally, research concerning the possible degradation of TC-85 resin from the company Graphy demonstrated the absence of BPA release during one week of immersion in water. However, UDMA (urethane dimethacrylate) was detected, which raises concerns regarding potential health risks, as aligners are the only appliances that are renewed every 1–2 weeks, allowing for a fresh release of urethane [14,29].

Then to address these issues, tests on the following behaviours were carried on:

- Degradation
- Wettability
- Biocompatibility
- Capability of recovering the original geometry.

References

1. Khorsandi, Danial, et al. 3D and 4D printing in dentistry and maxillofacial surgery: Printing techniques, materials, and applications. 2021, Acta Biomaterialia, Vol. 122, p. 26-49.
2. Naghieh S, Chen X. Printability-A key issue in extrusion-based bioprinting. J Pharm Anal. 2021 Oct;11(5):564-579.

3. Tartaglia GM, Mapelli A, Maspero C, Santaniello T, Serafin M, Farronato M, Caprioglio A. Direct 3D Printing of Clear Orthodontic Aligners: Current State and Future Possibilities. Materials (Basel). 2021 Apr 5;14(7):1799
4. Marian C. McCarty, Stephen J. Chen, Jeryl D. English, and F. Kasper Effect of print orientation and duration of ultraviolet curing on the dimensional accuracy of a 3-dimensionally printed orthodontic clear aligner design
5. Koenig N, Choi JY, McCray J, Hayes A, Schneider P, Kim KB. Comparison of dimensional accuracy between direct-printed and thermoformed aligners. Korean J Orthod 2022;52(4):249-257.
6. Hertan, E., McCray, J., Bankhead, B. et al. Force profile assessment of direct printed aligners versus thermoformed aligners and the effects of non-engaged surface patterns. Prog Orthod. 23, 49 (2022).
7. Can E, Panayi N, Polychronis G, Papageorgiou SN, Zinelis S, Eliades G, Eliades T In-house 3D-printed aligners: effect of in vivo ageing on mechanical properties. Eur J Orthod. 2022 Jan 25;44(1):51-55
8. Edelmann, A.; English, J.D.; Chen, S.J.; Kasper, F.K. Analysis of the thickness of 3-dimensional-printed orthodontic aligners. Am. J. Orthod. Dentofac. Orthop. 2020, 158.
9. Tsolakis IA, Papaioannou W, Papadopoulou E, Dalampira M, Tsolakis AI. Comparison in Terms of Accuracy between DLP and LCD Printing Technology for Dental Model Printing. Dent J (Basel). 2022 Sep 28;10(10):181.
10. https://formlabs.com/it/blog/risoluzione-stampa-3d/
11. Favero CS, English JD, Cozad BE, Wirthlin JO, Short MM, Kasper FK. Effect of print layer height and printer type on the accuracy of 3-dimensional printed orthodontic models. Am J Orthod Dentofacial Orthop. 2017 Oct;152(4):557 565.
12. Loflin WA, English JD, Borders CL, Harris LM, Moon AL, Holland JN, et al. Effect of print layer height on the assessment of 3D-printed models. Am J Orthod Dentofacial Orthop 2019;156(2):283-289.
13. Zhang ZC, Li PL, Chu FT, Shen G. Influence of the three-dimensional printing technique and printing layer thickness on model accuracy. J Orofac Orthop 2019;80(4):194-204.
14. Nearchos Panayi, Jung-Yeol Cha, Ki Beom Kim 3D Printed Aligners: Material Science, Workflow and Clinical Applications, Seminars in Orthodontics, Volume 29, Issue 1, 2023, 25-33
15. Short MM, Favero CS, English JD, Kasper FK. Impact of orientation on dimensional accuracy of 3D-printed orthodontic models. J Clin Orthod 2018;52(1):13-20.
16. Bichu YM, Alwafi A, Liu X, Andrews J, Ludwig B, Bichu AY, Zou B. Advances in orthodontic clear aligner materials. Bioact Mater. 2022 Oct 20;22:384-403.

17. Shah MJ, Kubavat AK, Patel KV, Prajapati NH. Fabrication of in-house aligner- A review. J Contemp Orthod 2022;6(3):120-124.
18. Trikka PM, Halazonetis D, Athanasiou A. Estimation of root inclination of anterior teeth from virtual study models: Accuracy of a commercial software. Prog Orthod. 2019;20(1):43.
19. Panayi NC. Directly Printed Aligner: Aligning with the Future. Turk J Orthod. 2023 Mar 21;36(1):62-69.
20. Migliorati, M.; Drago, S.; Lagazzo, A.; Campobasso, A.; Battista, G.; Kerberger, R.; Drescher, D.; Becker, K. Effect of Curing Time and Nitrogen Generator Usage on Direct 3D-Printed Aligners Thicknesses—An In Vitro Micro-CT Study. Appl. Sci. 2023, 13, 11952.
21. L. Sun, W. M. Huang, Z. Ding, Y. Zhao, C. C. Wang, H. Purnawali e C. Tang, «Stimulus-responsive shape memory materials: A review,» Materials & Design, vol. 33, pp. 577-640, 2012.
22. S. Y. Lee, H. Kim, H. J. Kim, C. J. Chung, Y. J. Choi, S. J. Kim e J. Y. Cha, «Thermo-mechanical properties of 3D printed photocurable shape memory resin for clear aligners,» Scientific Reports, vol. 12, n. 6246, 2022.
23. X. Wu, W. M. Huang, Y. Zhao, Z. Ding, C. Tang e J. Zhang, «Mechanisms of the Shape Memory Effect in Polymeric Materials,» Polymers, vol. 5, n. 1169 1202, 2013.
24. scheda-tecnica-TeraHertz-TC-85 DAC-REV 02.pdf (yenco.it)
25. Selvaraj M, Mohaideen K, Sennimalai K, Gothankar GS, Arora G. Effect of oral environment on contemporary orthodontic materials and its clinical implications. J Orthodont Sci 2023;12:1.
26. Koletsi D, Panayi N, Laspos C, Athanasiou AE, Zinelis S, Eliades T. In vivo aging induced surface roughness alterations of invisalign® and 3D-printed aligners. Journal of Orthodontics. 2022;146531252211459.
27. Tigmeanu, C.V.; Ardelean, L.C.; Rusu, L.-C.; Negrutiu, M.-L. Additive Manufactured Polymers in Dentistry, Current State-of-the-Art and Future Perspectives-A Review. Polymers 2022, 14, 3658.
28. Jungbauer, R.; Sabbagh, H.; Janjic Rankovic, M.; Becker, K. 3D Printed Orthodontic Aligners—A Scoping Review. Appl. Sci. 2024, 14, 10084. https://doi.org/10.3390/app142210084.
29. Selvaraj M, Mohaideen K, Sennimalai K, Gothankar GS, Arora G. Effect of oral environment on contemporary orthodontic materials and its clinical implications. J Orthodont Sci 2023;12:1.

MECHANICAL PROPERTIES AT ROOM TEMPERATURE

3.1 INTRODUCTION

The choice of resin, printing resolution, and sample thickness are among the factors that mostly impact the mechanical and functional properties of the printed aligners. Understanding how these variables influence the aligner's performance is crucial for optimizing the material properties and achieving the desired clinical outcomes. For example, Zinelis et al. recently compared the mechanical properties of orthodontic aligners produced by five commercially available 3D printers using Tera Harz TC-85 as the resin, with significant differences observed across the printers in the mechanical assets. In particular, aligners from LCD printers showed superior mechanical properties compared to those from DLP printers [1].

It is known that each printer has a specific resolution, including an XY resolution and a Z resolution, which are crucial aspects for achieving dimensional accuracy. In particular, the horizontal resolution is correlated to the devices' UV sources, while the Z-axis resolution determines the layer thickness, which can be adjusted depending on the chosen material and printer: the recommended thicknesses are 25 μm, 50 μm and 100 μm [2,3]. It has to be noted that a higher resolution does not necessarily coincide with increased accuracy: it requires longer printing sessions and a greater number of layers, which in turn enhances the risk of errors or failure [2].

It has been poorly investigated in the literature how different resins perform under varying conditions, such as differences in printing resolutions, sample thickness, and the specific 3D printing technologies employed. It is essential to assess how these factors affect the mechanical behavior of the printed materials, particularly their tensile strength, bending resistance, and overall structural integrity. In addition to mechanical properties, biocompatibility is a vital parameter in the selection of materials for medical applications [4,5].

The aim of this study was to compare the mechanical properties and biocompatibility of Tera Harz TC-85 and Clear A resins, considering different 3D printing resolutions, sample thicknesses, and printing technologies. By conducting tensile and bending tests, the strength, flexibility, and resilience of samples were assessed.

3.2 MATERIALS AND METHODS

3.2.1 Sample Design and Fabrication

Samples were designed using UltiMaker Cura CAD modeling software based on STL files. Two geometries were employed, tailored to the specific mechanical tests to be performed: dog-bone and parallelepiped shapes. The dog-bone samples were designed with an overall width of 20 mm, a gauge width of 10 mm, an overall length of 90 mm, and thicknesses of 2 mm, 1 mm, or 0.5 mm, depending on the experimental group (Figure 3.1 (a)). The parallelepiped samples were designed with a width of 12 mm, a length of 80.5 mm, and thicknesses of 2 mm or 1 mm (Figure 3.1 (b)). Thickness and width measurements were conducted to address potential inhomogeneities in the samples. Measurements were performed at multiple sections of each specimen using a digital caliber, and average values were calculated for both thickness and width.

Two photopolymer resins were utilized for sample production: Tera Harz TC-85 resin (Graphy Inc., Seoul, Korea) and Clear A resin (Senertek, Karatas, Izmir, Turkey). Samples were fabricated through direct 3D printing using a Phrozen Sonic XL 4K 2022 printer (Phrozen Technology, Hsinchu, Taiwan) or the Accufab L4D printer (Shining 3D, Hangzhou, China), with the resolution set at 50 or 100 µm. Support structures, required to ensure the precise positioning of the samples on the build plate, were designed using the Uniz software (Uniz, San Diego, CA, USA). Upon completion of the printing process, the samples were manually detached from the build plate, and the support structures were carefully removed.

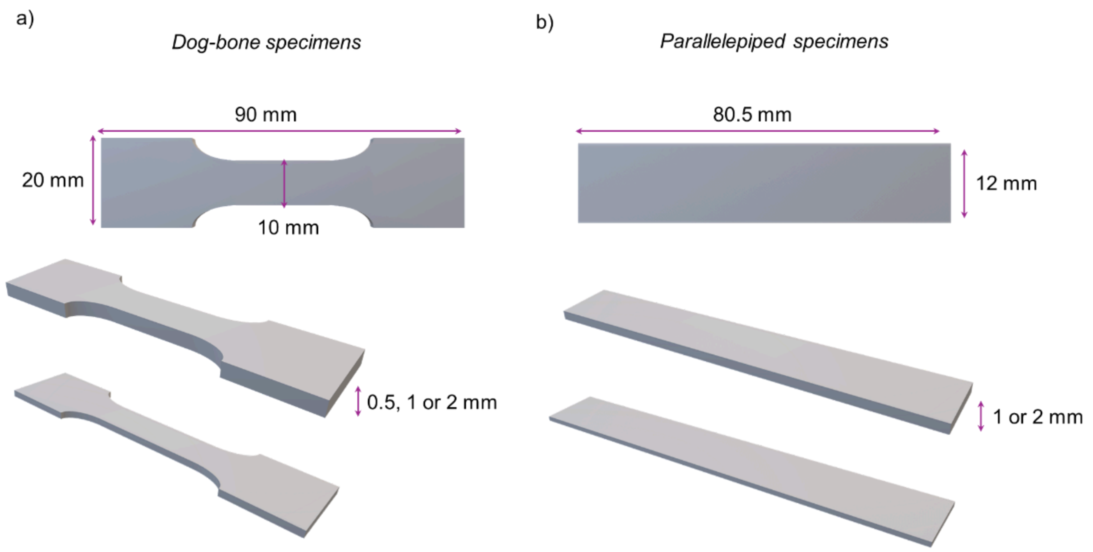

Figure 3-1 Dimensions of a) dog-bone and b) parallelepiped test specimens

Table 3-1 Experimental variables tested for 3D printing, including printer model, printing resolution, resin type, and sample thickness

Variables tested			
Printer	Phrozen Sonic XL 4K	Accufab L4D	
Printing resolution (μm)	50	100	
Resin	Tera Harz TC-85	Clear-A	
Sample thickness (mm)	0.5	1	2

3.2.2 Post-processing

Following printing, residual resin was removed by centrifugation at 1000 rpm for two cycles of 5 minutes each. Post-curing was performed under controlled conditions. In particular, samples fabricated with Tera Harz TC-85 resin were post-cured for 20 minutes using the Tera Harz Cure unit (Graphy Inc., Seoul, Korea). This compact curing system is equipped with UV LED light sources operating at a wavelength of 405 nm and delivers a UV energy density of 280,000 mJ/cm^2 within 5 minutes, with a UV irradiance of 1,000 mW/cm^2. An integrated nitrogen generator provides an inert environment, preventing oxygen inhibition and ensuring optimal polymerization. In contrast, samples fabricated with Clear A resin were post-cured for 20 minutes without the use of nitrogen.

3.2.3 Mechanical Testing

The mechanical performance of the samples was evaluated using a Zwick/Roell Z0.5 testing machine (Zwick Roell Group, Ulm, Germany), equipped with a full-scale range of 500 N. Tensile tests were performed on the dog-bone samples at room temperature (18°C) and continued until rupture. Bending tests were conducted on the parallelepiped samples under the same environmental conditions. The mechanical test parameters were set as follows: a preload of 1 N, with a preload speed of 1 mm/min, modulus speed of 1 mm/min, and test speed of 10 mm/min.

3.2.4 Statistical analysis

Results are expressed as the means ± S.D. of at least three independent experiments for each experimental condition. Statistical analysis was assessed using a Student's paired t-test using GraphPad Prism 8.0 (GraphPad Software v8.0, San Diego, CA, USA). Asterisks or other indicators (see Figure captions) indicate the following p-value ranges: $p > 0.05$ no symbols, * = $p < 0.05$, ** = $p < 0.01$, *** = $p < 0.001$.

3.3 RESULTS

3.3.1 Tensile tests

The results from the tensile tests are summarized in Figure 3.2 and in Tables 3.2 and 3.3. Additionally, Table 3.4 compares the intended and actual measured thicknesses and widths to evaluate the precision and consistency of the 3D printing process.

Samples printed with the Phrozen Sonic XL 4K and Accufab L4D printers showed slight differences in mechanical properties. In particular, the Phrozen printer yielded a higher Young's modulus (1131.30 ± 63.99 MPa), while the Accufab printer achieved marginally better maximum load (23.99 ± 1.16 MPa) and elongation at break (75.76 ± 27.86%) (Figure 3.2 (a) and Table 3.2). However, these differences were not statistically significant, indicating similar performance between the two printers.

Samples printed at a finer resolution of 50 µm demonstrated a higher maximum load (23.99 ± 1.16 MPa, $^{**}p < 0.01$) compared to those at 100 µm (21.81 ± 0.29 MPa). However, the elongation at break was higher for samples printed at 100 µm (90.09 ± 13.05%) compared to 50 µm (75.76 ± 27.86%) (Figure 3.2 (b) and Table 3.2). It has to be noted that printing resolution had minimal impact on thickness consistency, though the 50 µm resolution showed marginally closer adherence to the intended thickness compared to 100 µm (Table 3.4).

Importantly, the type of resin emerged as the factor showing the most statistically significant differences between the two groups (Figure 3.2 (c) and Table 3.2). Clear A resin demonstrated markedly superior tensile properties, with a significantly higher Young's modulus (2088.28 ± 99.31 MPa, $^{***}p < 0.001$) and maximum load (41.06 ± 2.14 MPa, $^{***}p < 0.001$). Conversely, TC-85 exhibited a much higher elongation at break (66.45 ± 20.54%) compared to Clear A (16.48 ± 4.97%, $^{***}p < 0.001$).

Analyzing the data in Figure 3.2 (d), Table 3.3 reveals a strong influence of sample thickness on mechanical properties. In particular, the 2 mm samples could withstand the highest maximum load (41.46 ± 1.89 MPa), significantly higher than the 1 mm (26.62 ± 1.36 MPa) and 0.5 mm samples (25.22 ± 6.43 MPa). Thicker samples exhibited better ductility, meaning they could endure more deformation before failure.

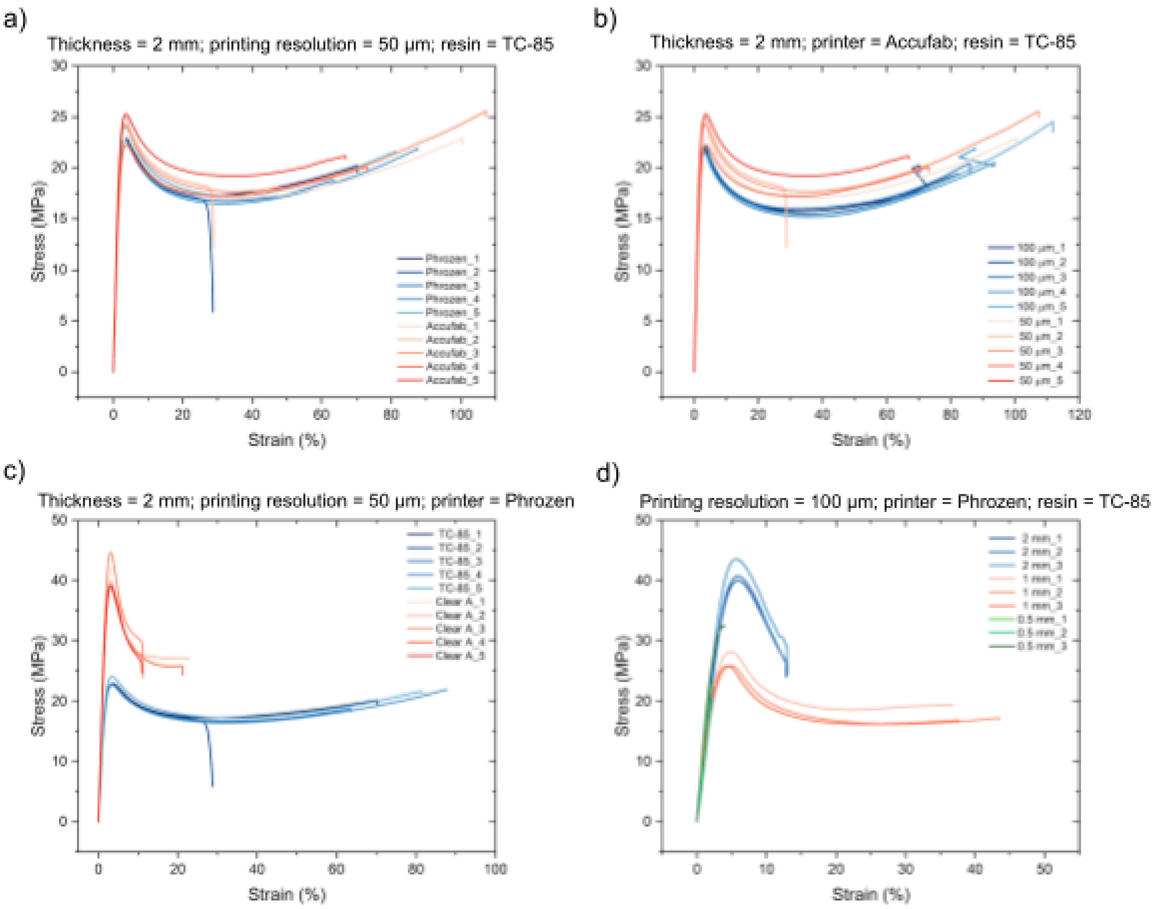

Figure 3-2 Tensile stress-strain curves of samples fabricated with a) two types of printers, b) two printing resolutions, c) two types of resins, and d) three values of thickness. Five samples (n=5) for each type were tested

Table 3-2 Young's modulus, maximum load, and elongation at break values of the tested samples fabricated with different printers, printing resolutions, and resin types

		Young's modulus (MPa)	***Maximum load (MPa)***	***Elongation at break (%)***
Printer	*Phrozen*	1131.30 ± 63.99	23.03 ± 0.52	66.45 ± 20.54
	Accufab	1055.95 ± 154.58	23.99 ± 1.16	75.76 ± 27.86
Printing resolution	*100 µm*	1051.51 ± 38.89	21.81 ± 0.29	90.09 ± 13.05
	50 µm	1055.95 ± 154.58	23.99 ± 1.16 **	75.76 ± 27.86

Resin	*TC-85*	1131.30 ± 63.99	23.03 ± 0.52	66.45 ± 20.54
	Clear A	2088.28 ± 99.31 ***	41.06 ± 2.14 ***	16.48 ± 4.97 ***

** $p < 0.01$, *** $p < 0.001$.

Table 3-3 Measured thickness, Young's modulus, maximum load, and elongation at break values of the tested samples fabricated with different thickness values

		Measured thickness (mm)	***Young's modulus (MPa)***	***Maximum load (MPa)***	***Elongation at break (%)***
Sample thickness	*2 mm*	2.35 ± 0.08	960.45 ± 36.20	41.46 ± 1.89	12.95 ± 0.08
	1 mm	1.27 ± 0.15	907.08 ± 44.14	26.62 ± 1.36	39.22 ± 3.70
	0.5 mm	0.60 ± 0.05	1050.10 ± 252.57	25.22 ± 6.43	2.77 ± 1.05
				***$p < 0.001$ (2 mm vs 1 mm) *$p < 0.05$ (2 mm vs 0.5 mm)	***$p < 0.001$ (2 mm vs 1 mm) ***$p < 0.001$ (2 mm vs 0.5 mm) ***$p < 0.001$ (0.5 mm vs 1 mm)

3.3.2 Bending tests

The bending test results (Figure 3.3 and Table 3.4) demonstrate the influence of printing resolution, resin type, and printer model on the mechanical properties of 3D-printed materials.

During the bending tests, the material did not reach breaking point, but a maximum deflection of 7 mm was applied. Regarding printing resolution, the flexural elastic modulus slightly decreases from 651.98 at 100 µm resolution to 644.31 MPa at 50 µm resolution. Similarly, the maximum flexural stress decreases from 8.80 MPa at 100 µm to 8.27 MPa at 50 µm. These differences are minimal and indicate a negligible effect of printing resolution on material properties. In contrast, resin type has a significant impact. In particular, Clear A resin shows a much higher flexural elastic modulus (1358.55 ± 177.82 MPa) and maximum flexural stress (16.44 ± 1.69 MPa) compared to TC-85 resin, which exhibits a flexural elastic modulus of 448.63 ± 59.27 MPa and maximum flexural stress of 6.11 ± 0.64 MPa. Statistical analysis indicates that these differences are highly significant (***$p < 0.001$). Surprisingly, printer models also influence the results in a statistically significant way. In particular, the Accufab L4D printer yields a flexural elastic modulus of 644.31 ± 22.84 MPa and a maximum flexural stress of 8.27 ± 0.25 MPa, while the Phrozen Sonic XL 4K printer results in a modulus of 448.63 ± 59.27 MPa and stress of 6.11 ± 0.64 MPa. These latest observations are consistent with the conclusions reached by Zinelis et al., who, in 2021, through a comparative analysis, investigated the effect of using different 3D printers on the final properties of dental aligners. The research group had indeed highlighted that the choice of different printing devices actually led to variations in the mechanical characteristics of the obtained samples in terms of Martens-Hardness, indentation-modulus, and elastic-index [1].

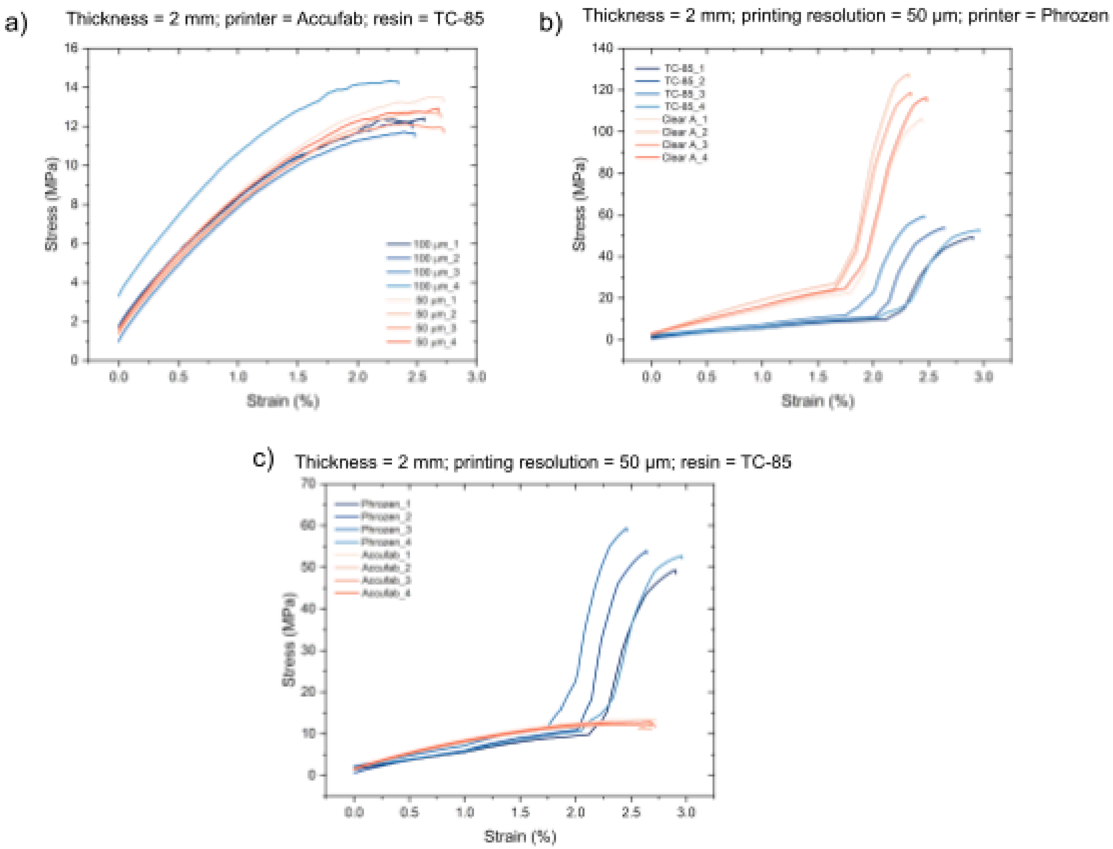

Figure 3-3 Bending stress-strain curves of samples fabricated with a) two printing resolutions, b) two types of resins, and c) two types of printers. Four samples (n=4) for each type were tested

Table 3-4 Flexural elastic modulus and maximum flexural stress of 3D-printed samples under different printing resolutions, resin types, and printer models

		Flexural elastic modulus (MPa)	***Maximum flexural stress (MPa)***
Printing resolution	100 µm	651.98 ± 34.10	8.80 ± 1.25
	50 µm	644.31 ± 22.84	8.27 ± 0.25
Resin	TC-85	448.63 ± 59.27	6.11 ± 0.64
	Clear A	1358.55 ± 177.82 ***	16.44 ± 1.69 ***
Printer	Phrozen	448.63 ± 59.27	6.11 ± 0.64
	Accufab	644.31 ± 22.84 ***	8.27 ± 0.25 ***

*** $p < 0.001$.

3.4 DISCUSSION

The results obtained from both mechanical testing and biocompatibility assessments highlight the important relationship between 3D printing settings and the properties of polymeric materials used in the production of orthodontic aligners. From the tensile tests, the comparison of 3D printing processes revealed that both the two printing resolutions and the two printers provided similar performance, with no statistically significant differences in mechanical properties. On the other hand, the type of resin used showed the most pronounced differences in tensile and bending properties. The differences were significant for all parameters considered. By observing Figure 2 and the respective values in Table 2, it is possible to compare the tensile mechanical properties of TC-85 and Clear-A resins at the same printing resolution (50 µm). The former has a stress-strain curve typical of a ductile material; Clear A, on the other hand, has a higher elastic modulus, higher maximum load, and a very reduced plastic plateau, at the end of which the fracture strain is only 16%. Clear A resin's superior stiffness and strength make it suitable for aligners requiring rigidity and durability. In contrast, the higher ductility of TC-85 resin suggests its potential for applications prioritizing flexibility and adaptability, which could enhance patient comfort and improve performance in scenarios involving complex dental geometries [6].

Sample thickness also played a critical role in determining mechanical properties. Thicker aligners (2 mm) demonstrated higher strength and ductility, making them appropriate for cases requiring significant force application. However, this comes at the potential cost of reduced patient comfort due to lower flexibility. Thinner aligners (0.5 mm), on the other hand, exhibited greater stiffness but reduced ductility, which may improve precision in tooth movement while potentially compromising durability and adaptability [6].

The choice of the Accufab printer with a layer thickness setting of 50 μm appears to be the one that minimizes oversizing of the samples, which however remains around 10%. Park et al. had already quantified this oversizing as approximately 12% of the designed volume. Edelmann et al. also investigated this aspect, demonstrating that clear aligners fabricated by 3D printing presented wall thicknesses greater than designed [7]. Moreover, the study by Favero et al. established a clinically acceptable threshold of 0.25 mm for dimensional accuracy, and their findings demonstrated that all treatment groups, irrespective of the print layer height or printer type, maintained mean average absolute deviations below this threshold, indicating that the printed models are likely suitable for clinical applications. Notably, the 100-μm layer height group exhibited the least average overall deviation, which not only enhances clinical and laboratory efficiency but also results in shorter print job times compared to the 50-μm layer heights [2]. It has to be noted that there is no perfect level of elasticity for dental aligners. If the material used to fabricate aligners has a very high elastic modulus (indicating significant stiffness), the aligner may become overly rigid, making it challenging for patients to insert and remove. Conversely, if the material is too flexible, it may lack the necessary stiffness to produce sufficient force for effective tooth movement.

The results of the bending tests confirm that while printing resolution has a minimal effect on the mechanical properties of 3D-printed materials, resin type but also printer model are critical factors influencing material performance. The decrease in bending modulus by about half compared to that of tensile strength could be due to the anisotropic properties of the material, typical of polymer resins. The statistical differences between the two printers were significant for all parameters: the samples obtained with Accufab L4D had higher values, indicating a greater stiffness of the material. Similarly to the findings of the tensile tests, significant differences also emerged from the bending tests when comparing the two resins, with relevant variations in bending elastic modulus, between the two groups. Interpreting the obtained curve, it can be concluded, in accordance with the results from the tensile tests, that the resin Clear A appears to be stiffer, hence more fragile, compared to the TC-85. However, the behavior of the Clear A resin has been poorly studied in the literature, emphasizing the importance of continuing these tests, expanding the number of samples, and varying the environmental conditions.

Overall, these findings emphasize the importance of selecting the right combination of resin and printer model for achieving optimal material properties in 3D printing applications and underscore the need to balance mechanical performance, material properties, and patient comfort in designing dental aligners, with considerations tailored to the specific clinical requirements of each case.

3.5 CONCLUSIONS

The choice of different printing resolutions on the Z-axis does not seem to influence the final properties of the Tera Herz TC-85DAC material. - The use of different 3D printers (Phrozen Sonic and Accufab L4D) can result in variations in the thickness of the TC-85DAC resin samples and in terms of material ductility. - The variation in printing thickness does not cause significant changes, except for the breaking load. - The choice of printing material significantly influences the final, geometric, and mechanical properties of the samples: the resin Senertek resulted in greater rigidity and less plastic behavior. Artificial intelligence is expected to be integral to this technological evolution, influencing both software development and the optimization of printing techniques while offering valuable feedback to orthodontists.

References

1. Zinelis S, Panayi N, Polychronis G, Papageorgiou SN, Eliades T. Comparative analysis of mechanical properties of orthodontic aligners produced by different contemporary 3D printers. vol. 25. Orthodontics & Craniofacial Research; 2022. p. 336–41.
2. Favero CS, English JD, Cozad BE, Wirthlin JO, Short MM, Kasper FK. Effect of print layer height and printer type on the accuracy of 3-dimensional printed orthodontic models. Am J Orthod Dentofacial Orthop 2017;152:557–65.
3. Piedra-Cascón W, Krishnamurthy VR, Att W, Revilla-León M. 3D printing parameters, supporting structures, slicing, and post-processing procedures of vat polymerization additive manufacturing technologies: a narrative review. J Dent 2021;109:103630.
4. Milovanović A, Sedmak A, Golubović Z, Mihajlović KZ, Žurkić A, Trajković I, Milošević M. The effect of time on mechanical properties of biocompatible photopolymer resins used for fabrication of clear dental aligners. J Mech Behav Biomed Mater 2021;119:104494
5. Nemec M, Bartholomaeus HM, H. Bertl M, Behm C, Ali Shokoohi-Tabrizi H, Jonke E, Andrukhov O, Rausch-Fan X. Behaviour of human oral epithelial cells grown on Invisalign® SmartTrack® material. Materials 2020;13.

6. Bichu AY, Zou B. Advances in orthodontic clear aligner materials. Bioact Mater 2023;22:384–403.
7. Edelmann A, English JD, Chen SJ, Kasper FK. Analysis of the thickness of 3 dimensional-printed orthodontic aligners. Am J Orthod Dentofacial Orthop 2020; 158:e91–8.

MECHANICAL PROPERTIES AT OPERATING TEMPERATURE

4.1 INTRODUCTION

A significant innovation introduced by these new resins is that they are stimuli-responsive materials, belonging to shape memory polymers (SMPs). In general, this category includes materials characterized by remarkable transparency, significant elastic deformation, and high chemical stability [1]. What sets them apart is their ability to respond to various external stimuli—such as physical, thermal, or magnetic—by producing predictable and repeatable reactions. More specifically, shape memory materials, when exposed to a certain stimulus, can undergo a change in their macroscopic shape, reaching a temporary form that they are able to maintain for a certain period of time; upon application of another stimulus, they return to their original shape [2].

This mechanism is based on two crucial aspects: the presence of a stable polymer network, which defines the initial shape of the material, and its reversibility, which allows the material to transform into an altered, temporary shape. For this reason, an experimental activity was conducted to determine the mechanical properties of several so-called shape-memory resins at operating temperature.

4.2 MATERIALS AND METHODS

4. 2.1 Sample Design and Fabrication

Samples were designed using UltiMaker Cura CAD modeling software based on STL files. Dog-bone samples were designed with an overall width of 20 mm, a gauge width of 10 mm, an overall length of 90 mm, and thicknesses of 1 mm. Thickness and width measurements were conducted to address potential inhomogeneities in the samples. Measurements were performed at multiple sections of each specimen using a digital caliber, and average values were calculated for both thickness and width.

Two photopolymer resins were utilized for sample production: Tera Harz TA-28 resin (Graphy Inc., Seoul, Korea) and DCA (LuxCreo, Chicago, IL, U.S.A). TA-28 samples were fabricated through direct 3D printing using a NBee printer (Uniz, San Diego, CA, USA) with the resolution set at 100 µm. DCA samples were fabricated through direct 3D printing using an iLux Pro Dental 3D printer (LuxCreo, Chicago, IL, U.S.A.).

4.2.2 Post-processing

Following printing, residual resin of TA-28 samples was removed by centrifugation at 1000 rpm for two cycles of 5 minutes each and supports were removed. Post-curing was performed under controlled conditions; in particular, the samples were post-cured for 20 minutes using the Tera Harz Cure unit (Graphy Inc., Seoul, Korea).

To remove any residual resin from the DCA samples after printing, a two-stage ultrasonic washing in IPA (>99%) was performed at room temperature (iLuxWash Dental) for 8 minutes (4 minutes for each stage). Post-curing was carried out using a iLuxCure Pro curing unit (LuxCreo, Chicago, IL, U.S.A.) for 20 minutes, no nitrogen, as per the manufacturer's instructions. The supports were subsequently manually eliminated.

4.2.3 Mechanical Testing

The mechanical performance of the samples was evaluated using a Zwick/Roell Z0.5 testing machine (Zwick Roell Group, Ulm, Germany), equipped with a full-scale range of 500 N. Tensile tests were performed on the dog-bone samples at 37° C in a climatic chamber (Figure 4.1) and continued until rupture. The mechanical test parameters were set as follows: a preload of 1 N, with a preload speed of 1 mm/min, modulus speed of 1 mm/min, and test speed of 10 mm/min.

4.2.4 Statistical analysis

Results are expressed as the means ± SD of at least three independent experiments for each experimental condition. Statistical analysis was assessed using a Student's paired t-test using the R v4.2.2 software environment. Asterisks or other indicators (see Figure captions) indicate the following p-value ranges: $p > 0.05$ no symbols, * = $p < 0.05$, ** = $p < 0.01$, *** = $p < 0.001$.

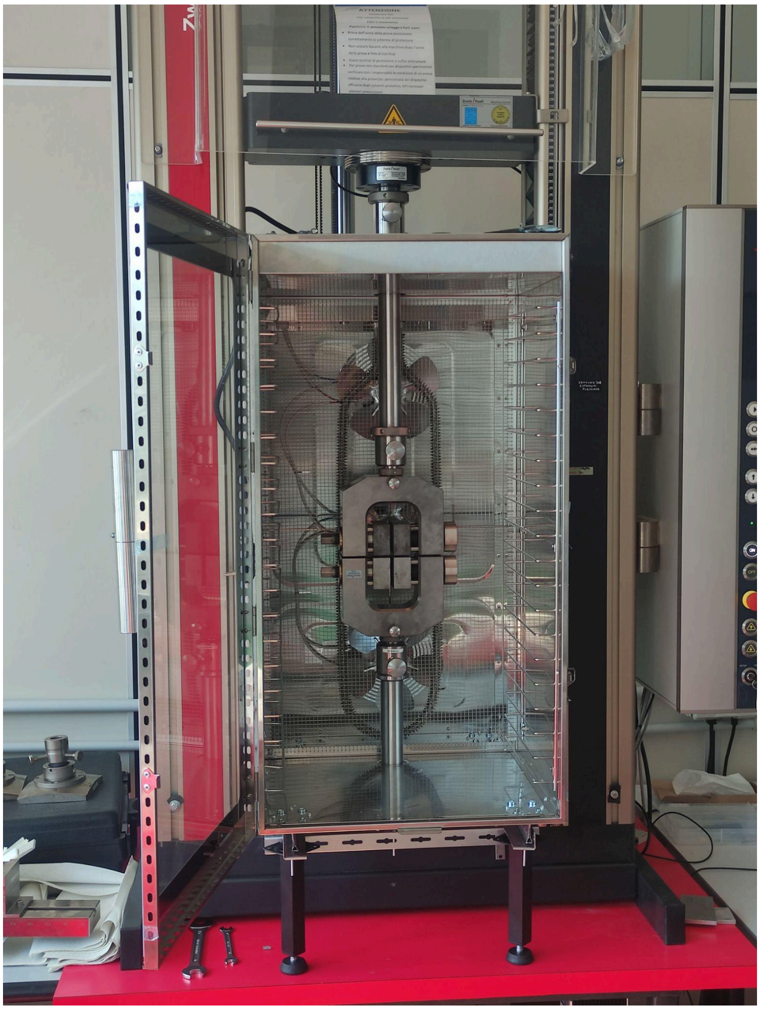

Figure 4-1 The Zwick-Roell machine, set with the climatic chamber

4.3 RESULTS

The results from the tensile tests are summarized in Figure 4.2 and 4.3 and in Tables 4.1.
Samples printed with both types of resin showed significant differences between temperature conditions in all the considered mechanical properties. In particular, at 37°C the DCA resin yielded a Young's modulus of 819.77 ± 73.51 MPa, while at 24°C it was 1067.26 ± 44.79 MPa. Both values are higher than those established by the TA-28 resin (431.65 ± 34.10 MPa and 762.69 ± 66.00 respectively). The DCA at 37°C achieved almost the same maximum load as TA-28 at 24°C (21.16 ± 0.83 MPa and 22.93 ± 2.55 MPa respectively), whose value dropped to 11.79 ± 6.47 MPa at 37°C. Elongation at break raised from 88.66 ± 9.82 MPa at 24°C to 108.90 ± 11.02 MPa at 37°C for DCA, and from 20.22 ± 6.68 MPa to 119.10 ± 7.00 MPa for TA-28; both differences were significant.

Table 4-1 Young's modulus, maximum load, and elongation at break values of the tested samples fabricated with different resin types and at different temperatures

		Young's modulus (MPa)	*Maximum load (MPa)*	*Elongation at break (%)*
DCA	*24°C*	1067.26 ± 44.79	30.00 ± 0.62	88.66 ± 9.82
	37°C	819.77 ± 73.51***	21.16 ± 0.83***	108.90 ± 11.02*
TA-28	*24°C*	762.69 ± 66.00	22.93 ± 2.55	20.22 ± 6.68
	37°C	431.65 ± 34.10**	11.79 ± 6.47 **	119.10 ± 7.00***

** $p < 0.01$, *** $p < 0.001$.

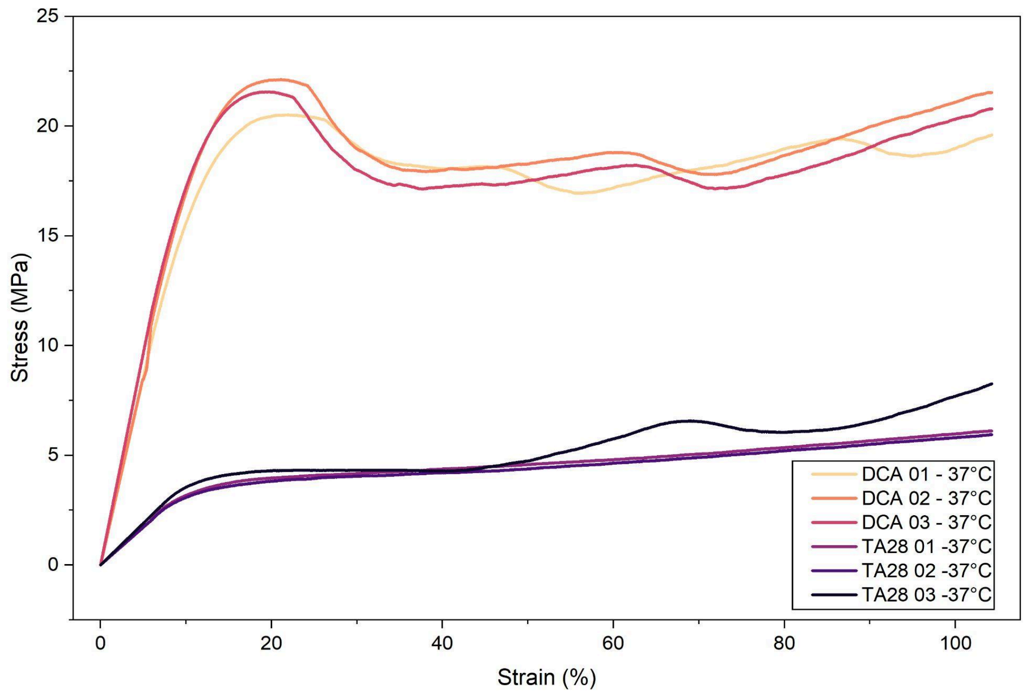

Figure 4-2 Tensile stress-strain curves of samples fabricated with the two types of resins. Three samples (n=3) for each type were tested

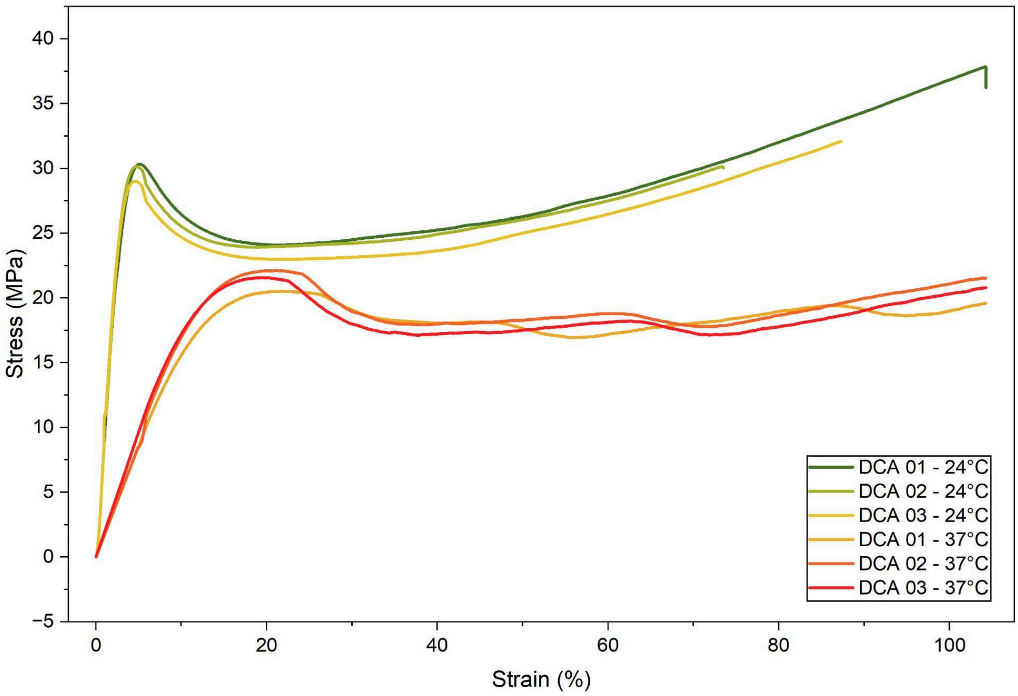

Figure 4-3 Tensile stress-strain curves of DCA samples at room temperature (24°C) and at operating temperature (37°C). Three samples (n=3) for each type were tested

4.4 DISCUSSION

The Phase Transition Temperature is critical to ensure intraoral temperature stiffness. It is important to first clarify a technical point: the glass transition T_g is not a thermodynamic 'first-order' phase transition (such as melting or boiling), but rather a second-order transition (or more precisely, a kinetic transition). While melting occurs at a sharp point, during the glass transition, the polymer shifts from a 'glassy' state (rigid and brittle) to a 'rubbery' state (flexible and elastic) through a temperature range. The temperature range in which this transformation occurs can vary considerably depending on the nature of the polymer. Generally, the transition occurs over an interval ranging from 10°C to 30°C. The polymer begins to show the first signs of softening as early as 5°C or 10°C before the nominal T_g value reported in technical data sheets and the material completes the shift to the rubbery state approximately 10°C or 20°C above the T_g. In this range, thermal energy becomes sufficient to allow the movement of polymer chain segments. Below the T_g the chains are 'frozen.'

Above the T_g the elastic modulus drops drastically (often by three orders of magnitude), and the behavior becomes markedly viscoelastic.

For the shape-memory polymers used in orthodontics, the T_g is designed to be close to or slightly higher than body temperature (37°C). Particularly, the reported TC-85 T_g is 69.45 °C [3]. This value was derived by DMA under the stress relaxation mode [3] and could not be confirmed by DSC (see Appendix, Figure A.1).

If the T_g range of the TC-85 (and maybe TA-28) is very wide and begins around 30°C–35°C, the material will start to 'creep' much faster once in the mouth, as it is already in the initial phase of the transition.

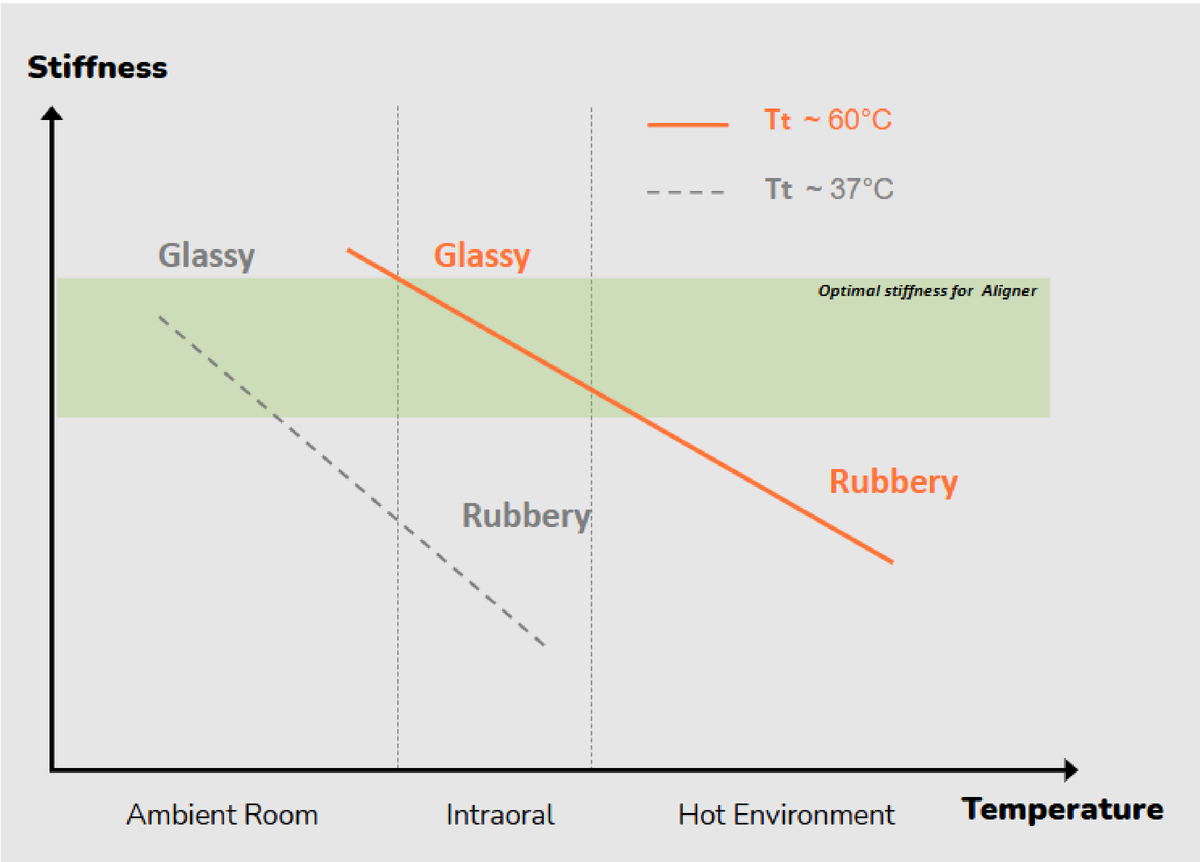

Figure 4-4 Sketch of stiffness variation according to the achieved and transition temperature

4.5 CONCLUSIONS

The tensile tests revealed that room or operating temperature significantly affects the performance of the resins used for the production of 3D printed orthodontic aligners for all the considered mechanical properties. On the other hand, the type of resin used showed big differences in tensile properties, which were significant for all parameters considered. The tensile mechanical properties of

DCA and TA-28 resins at the same printing resolution (100 μm) were compared. DCA has a higher elastic modulus, higher maximum load, with a similar plastic plateau. DCA resin's superior stiffness and strength at operating temperature show the same magnitude order of traditional thermoformed materials and are coherent with the producer's declaration of a higher T_g , therefore they could increase the mechanical reply of the aligners.

References

1. Bichu YM, Alwafi A, Liu X, Andrews J, Ludwig B, Bichu AY, Zou B. Advances in orthodontic clear aligner materials. Bioact Mater. 2022 Oct 20;22:384-403.
2. L. Sun, W. M. Huang, Z. Ding, Y. Zhao, C. C. Wang, H. Purnawali e C. Tang, «Stimulus-responsive shape memory materials: A review,» Materials & Design, vol. 33, pp. 577-640, 2012.
3. S. Y. Lee, H. Kim, H. J. Kim, C. J. Chung, Y. J. Choi, S. J. Kim e J. Y. Cha, «Thermo-mechanical properties of 3D printed photocurable shape memory resin for clear aligners,» Scientific Reports, vol. 12, n. 6246, 2022.

VISCOELASTIC PROPERTIES OF SHAPE-MEMORY POLYMERS FOR 3D DIRECT PRINTING OF ORTHODONTIC ALIGNERS: A CHARACTERIZATION OVER THE FIRST WEEK

5.1 INTRODUCTION

The effectiveness of the direct printing of dental aligners primarily depends on two factors: the characteristics of the printer and the materials used. This study focused on both variables, in order to identify the highest-performing materials and the better printing conditions for the direct printing of orthodontic aligners.

The resins compared in this study are TC-85 and TA-28, both manufactured by Graphy. These are shape-memory polymers (SMPs), categorized as 'smart' materials, which are particularly utilized in these contexts due to their ability to return to their original shape following an external stimulus capable of deforming them. In orthodontics, this characteristic is highly sought after as it ensures constant mechanical action and resistance, which is vital for the success of orthodontic treatments. In fact, clear aligners materials are subjected to stress relaxation, which refers to the gradual decrease in force exerted by the aligner on the teeth over time subjected to constant strain. Clinically, this means that the force levels may drop substantially within hours or days of insertion. Moreover, aligners are subjected to creep, which is the time-dependent increase in deformation (strain) of the aligner material under a constant applied load. As a consequence, the simple force may still be expressed but the moments (couples) generated may not be sufficient to produce the desired tooth movements.

To evaluate their viscoelastic properties, the two aforementioned resins were subjected to creep tests in a setup designed to replicate the conditions of the oral cavity—specifically, humidity and heat. These tests, repeated over one week, allow for an accurate analysis of the time-dependent behavior of the resins' viscoelastic properties while subjected to a constant load. The differences emerging from this direct comparison can thus prove useful in selecting increasingly sophisticated and high-performance materials.

The objective of this study is to evaluate the decline in mechanical properties over time of a polymer suitable for the direct 3D printing of orthodontic aligners currently on the market (Tera Harz

TC-85) and another material under preliminary investigation (Tera Harz TA-28). Moreover, TC-85 from two different printers, the Phrozen Sonic XL 4K 2022 printer (Phrozen Technology, Hsinchu, Taiwan) and the Accufab L4D printer (Shining 3D, Hangzhou, China), was tested.

5.2 MATERIALS AND METHODS

Ten samples per group (material and printer, 30 in total) were prepared in the form of parallelepipeds measuring 80 mm in length, 12 mm in width, and 1 mm in thickness, following the manufacturer's instructions (20 minutes of polymerization, print resolution of 100 microns). The specimens were measured with a digital caliper to verify uniformity, and each sample was immersed in water at 80°C for one minute. This facilitates the distribution of internal stresses within the material, thereby preventing possible cracks or fractures that could compromise the integrity of the samples and the success of the tests. Then the samples were transferred to a temperature-controlled bath at 37°C, containing saline solution, and subsequently fixed to a support by drilling two holes near the ends, securing them with a nut and a bolt. To prevent rust formation, it was essential to use stainless steel nuts and bolts for securing the specimens. Each sample was then placed inside the preheated tanks to ensure complete immersion throughout the duration of the measurements (Figure 5.1). The water level and the saline concentration of the solution were kept constant through the addition of distilled water during the week. Creep tests were conducted on each sample, with each test lasting one week. The creep tests recreated the model of a beam fixed at two points, where the sample placed on a support is constrained at both ends and subjected to a constant transverse load along the central axis.

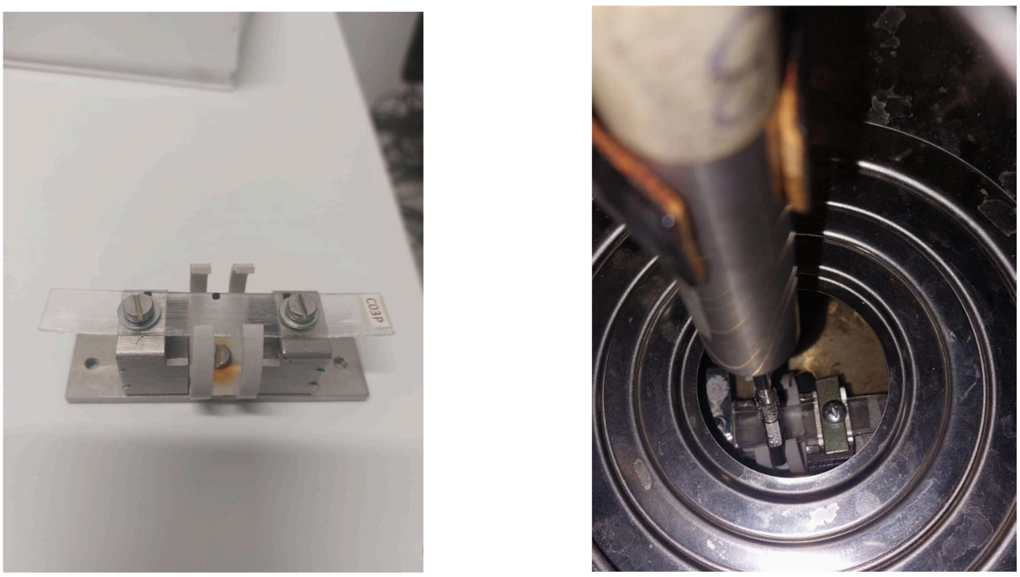

Figure 5-1 Sample setup and LVDT positioned on the specimen

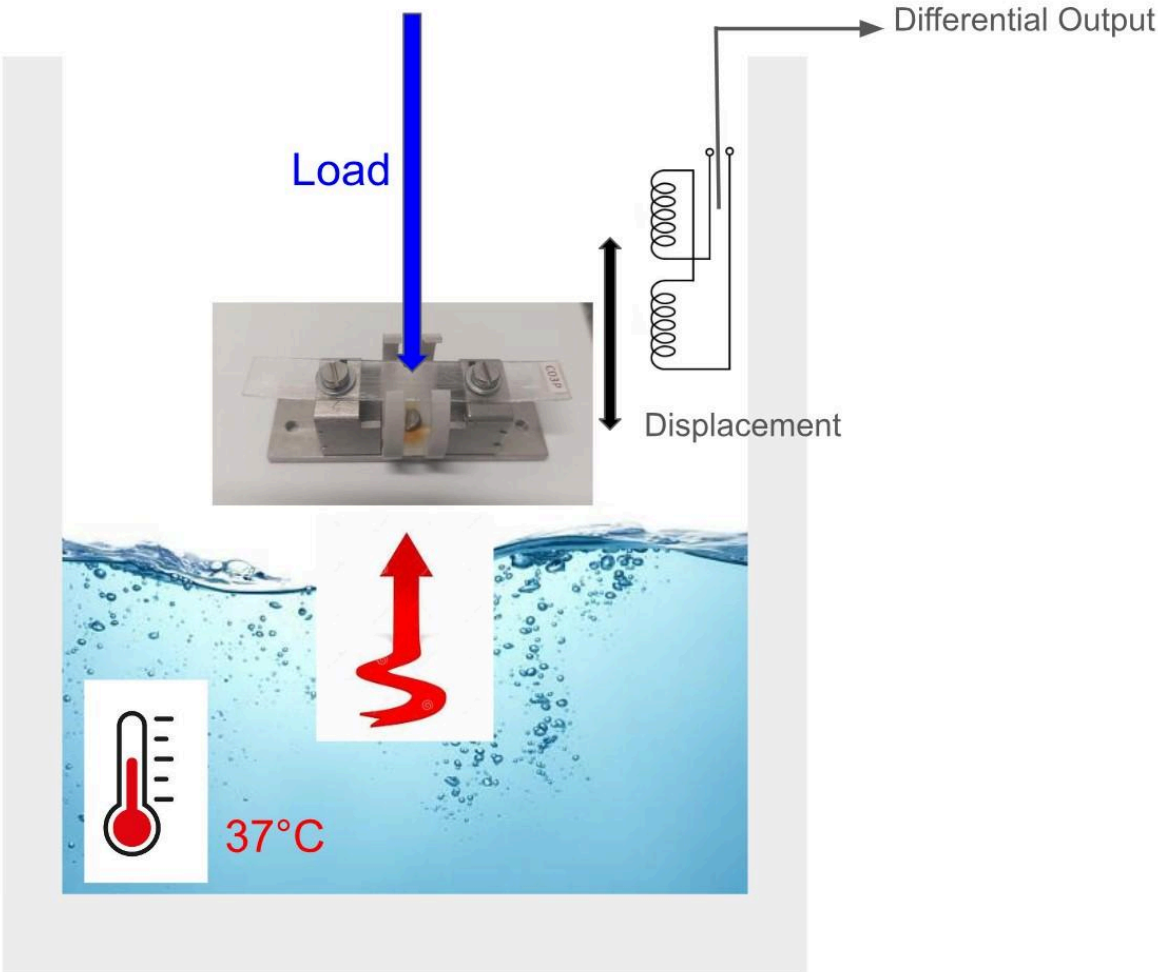

Figure 5-2 Scheme of the experimental setup

A load of 0.5 Newton was applied using an LVDT (Linear Variable Displacement Transducer) with an extendable external tip. This transducer provides a voltage value, expressed in volts (within a range of [-10.5V; +10.5V]), and converts the linear movements of the appendage into electrical signals (Figure 5.2). Each transducer was then connected to a single PC for signal recording via a data acquisition system (DAQ). For each sample, the week was divided into sequential periods of 600 seconds, during which the data was sampled every second, and the results were automatically saved at the end of each period. The temperature in each well was monitored using two thermocouples inserted into the tanks alongside the samples, in direct contact with the solution.

The data collected at the completion of each experimental cycle were transferred to Matlab and processed to obtain the time-dependent trend of the percentage strain. The formula used to convert the voltage values into percentage values of ε is as follows:

$$\varepsilon = \delta/L$$

Where δ represents the maximum deflection and L is the length of the specimen (80 mm). From this formula, the ε graphs were generated for each completed test, along with the average graph derived from the combination of all tests (Figures 5.3 and 5.4).

5.3 RESULTS

The graphs in Figures 5.3 and 5.4 illustrate the average behavior of the samples subjected to continuous mechanical stress for one week. The strain, on the y-axis, is expressed as a percentage, while time, on the x-axis, is shown in days. As expected, the curves show a rapid increase in ε at the start of the test, as soon as the load is applied to the specimen. During this phase, the deformation is elastic and its rate decreases over time until it stabilizes toward a plateau. This latter behavior is influenced by the viscoelastic properties of the polymers. Consequently, the first part of the graph provides information on the elastic properties of the polymer, while the second part allows us to understand the degree of viscosity of the tested materials.

Based on the analysis of the creep tests performed on the TC-85 samples produced with two different printers (Phrozen and Accufab), both samples exhibit a very similar time-dependent response. The graph represented in Figure 5.3, obtained by averaging the tests performed, shows—as expected—a rapid initial deformation followed by a gradual adjustment toward a plateau. This behavior is typical of polymers subjected to constant stress.

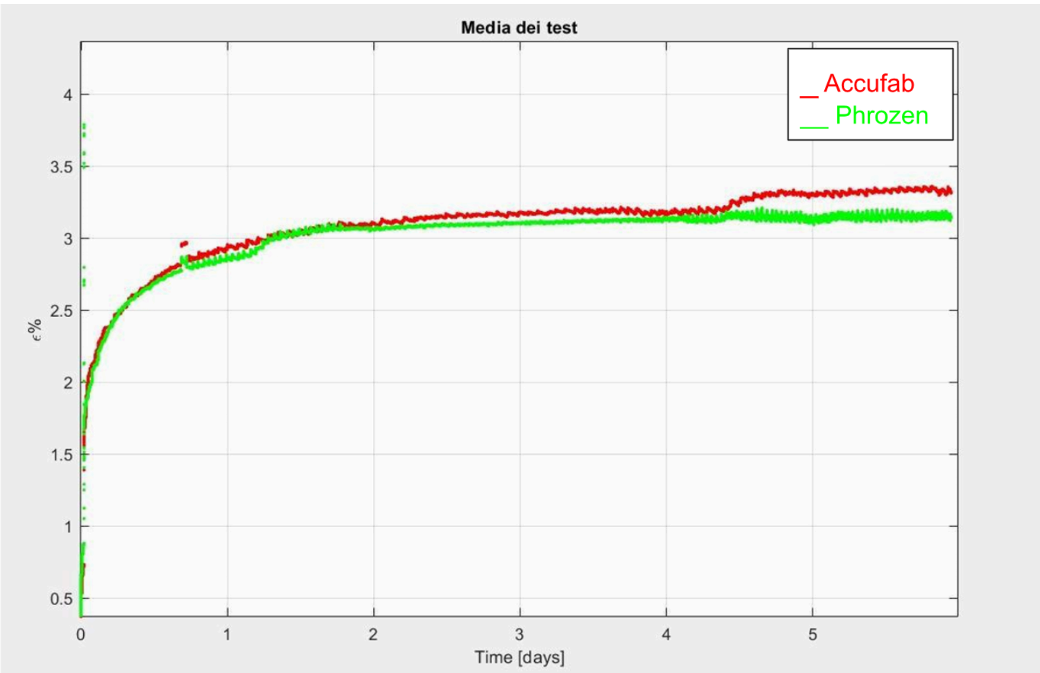

Figure 5-3 Time-dependent trend of the percentage strain for TC-85 samples printed by different printers

The Phrozen samples exhibited a slightly more stable response over time, with less fluctuation compared to the ones printed by Accufab. The elastic modulus and viscosity of the Phrozen samples are marginally higher, suggesting a greater resistance to deformation.

The Accufab samples exhibited greater variability in the collected data, with more evident fluctuations and a weaker response to the load. This could suggest a difference in the printing process that affects the mechanical properties of the sample.

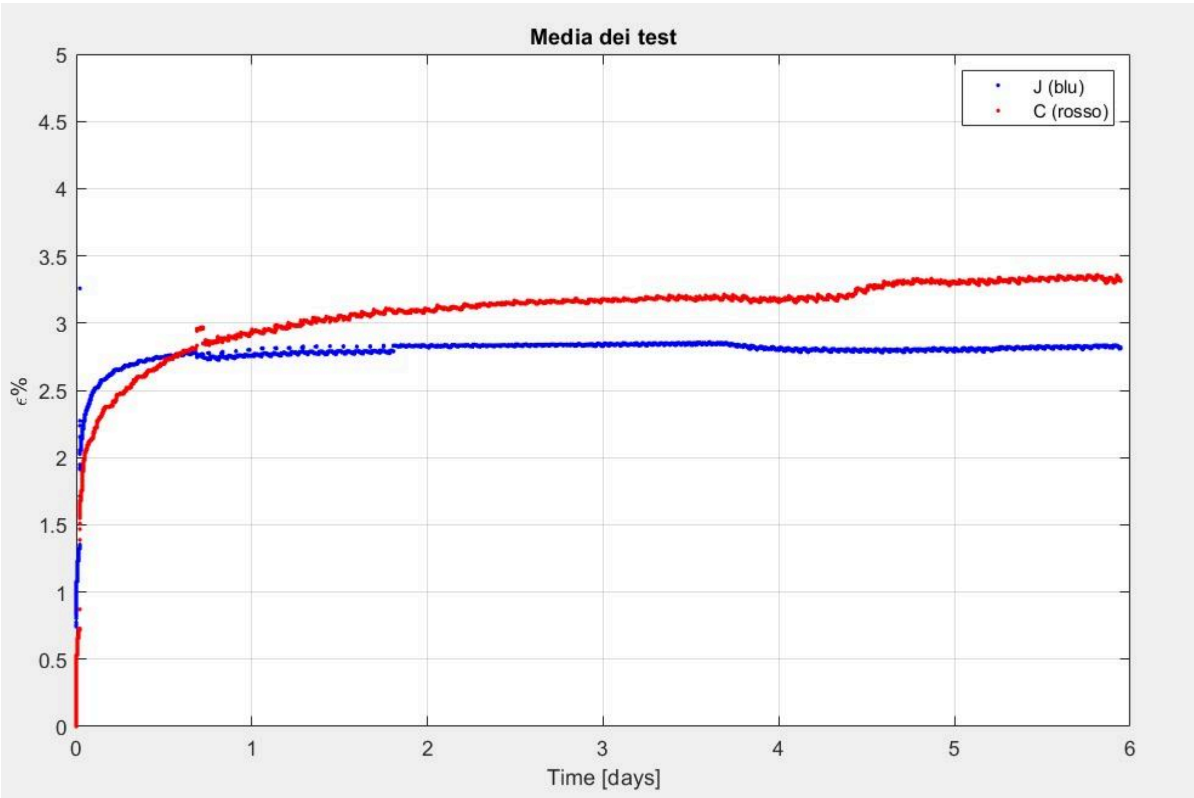

_ TA-28
_ TC-85

Figure 5-4 Time-dependent trend of the percentage strain for TC-85 and TA-28 samples

The time-dependent graph of the percentage strain for TC-85 and TA-28 is depicted in Figure 5.4. The results obtained highlight differences in both the elastic and viscoelastic behavior of the two resins. On average, the TC-85 samples (shown in red) underwent greater deformation compared to TA-28, exhibiting more pronounced fluctuations and a slightly steeper plateau. This implies a lower resistance to deformation, which becomes evident after the first day of testing—the point at which the two curves begin to deviate significantly. The TA-28 samples (shown in blue) present an elastic phase with a steeper slope compared to TC-85, followed by a slower and more stable deformation in the subsequent stages. Consequently, both the elastic modulus and the viscosity of TA-28 are higher than those of TC-85. Overall, although TA-28 exhibits lower resistance during the initial hours of the test, it appears to possess superior mechanical properties compared to TC-85, demonstrating better long-term performance.

5.4 DISCUSSION

Some of the tests performed were unusable due to malfunctions encountered in the experimental setup. This highlights the need to improve the instrumentation for future analyses: in this case, the precision of the LVDT must be enhanced to reduce fluctuations in the collected data. Specifically, severe interference during testing can lead to the rejection of entire weeks of work due to compromised values.

The setup used for the tests was rudimentary and experimental, which influenced the precision of the measurements. Future improvements could include better temperature stabilization, a more precise calibration of the LVDT, and a working environment less subject to external disturbances.

Both polymers produced with the two different printers possess mechanical characteristics that are sufficiently reliable over time to be proposed for clinical use as orthodontic aligners. However, the slight superiority of TA-28 in terms of stability may make it more suitable for applications requiring high precision and consistency of mechanical properties throughout the entire duration of the treatment.

Based on the results obtained from the tests, the TA-28 resin demonstrates superior performance in creep tests compared to the TC-85 resin. Consequently, it may be preferable to TC-85 as the material of choice for the direct 3D printing of orthodontic aligners. Indeed, a crucial factor to consider in the fabrication of these devices is the preservation of mechanical efficiency and structural resistance throughout their use, ensuring there is no decrease in the forces exerted on the dentition. Further investigations could focus on optimizing the printing process to reduce variability between samples and enhance the mechanical properties of the printed materials.

New shape-memory polymers could also be evaluated to determine if they offer better performance than TC-85, taking into account biocompatibility and long-term response within the oral environment. Ultimately, this study allows us to understand the importance of an in-depth and detailed comparison between different materials to identify the one that possesses the optimal characteristics for various clinical needs and demonstrates how crucial accuracy in an experimental setup is for gathering reliable data, thus paving the way for future analyses in this field. This is a necessary step that can provide a significant contribution to the research of innovative materials in the orthodontic and biomedical fields, placing the focus on everything that represents an advancement over previous models.

5.5 CONCLUSIONS

In conclusion, while both the Phrozen and Accufab printers produce TC-85 components with comparable viscoelastic profiles, the samples from the Phrozen process demonstrate a marginal advantage in mechanical consistency. The slightly higher elastic modulus and viscosity, paired with reduced fluctuations during creep, suggest that this printing setup may offer superior structural integrity and a more stable polymer network. However, given the proximity of the results, both systems prove highly effective for applications requiring standard TC-85 performance. Based on the results obtained from the tests on the materials, the TA-28 resin demonstrates superior performance in creep tests compared to the TC-85 resin. Consequently, it may be preferable to TC-85 as the material of choice for the direct 3D printing of orthodontic aligners.

References

1. Virginia Astio, “Caratterizzazione meccanica e microstrutturale di allineatori ortodontici innovativi ottenuti con stampa 3D di resine a memoria di forma foto-polimerizzabili”, tesi magistrale in bioingegneria, giugno 2023
2. Sun, Li, and Wei Min Huang. "Mechanisms of the multi-shape memory effect and temperature memory effect in shape memory polymers." Soft Matter 6.18 (2010): 4403-4406.
3. Lee, Se Yeon, et al. "Thermo-mechanical properties of 3D printed photocurable shape memory resin for clear aligners." Scientific reports 12.1 (2022): 6246. [4] Casini, Vasta - Scienza delle Costruzioni (4a Ed.) - Città Studi Edizioni (2019)

COMPUTATIONAL MAPPING OF THE FORCES APPLIED TO THE DENTAL ARCH BY 3D PRINTED ORTHODONTIC ALIGNERS OF DIFFERENT MATERIALS AND DESIGNS

6.1 INTRODUCTION

The selection of resin, printing resolution, and sample thickness are key factors that significantly affect the mechanical and functional characteristics of the printed aligners. It is essential to comprehend how these variables impact the performance of the aligners in order to optimize their material properties and attain the desired clinical results. The performance of different resins under varying conditions (differences in printing resolutions, sample thickness, specific 3D technology applied, etc.) has been-so far- somewhat investigated in laboratory tests where mechanical properties, such as Young modulus, ultimate tensile strength and elongation at break were measured [1]. Attempts were made to measure the force level exerted by aligners using strain gauges as well, for example recent studies have shown that varying DPA thickness can significantly impact the forces and moments applied to teeth, particularly in the upper incisor region [2].

Understanding how the stress distribution varies over time is a key factor to define the most suitable protocols and properly choose an adequate material, but no direct measure of the stresses on the periodontal ligament, clear aligner and dentition is available at present and this lack of data make it is difficult to quantitatively predict tooth displacement. Finite element models can be used to understand the biomechanics of different materials and different orthodontic treatment movements, by assessing the stresses generated within the teeth, periodontal ligament, and alveolar bone.

Particularly, the present project implemented the following phases:

- Construction of FEM model of teeth, periodontal ligament, and alveolar bone.
- Application of orthodontic loads and simulation of displacements and stresses.

Future work will be focused on

- Parametric analysis to investigate influence of material choice and device design.
- Comparison of simulation results with literature or available clinical data.
- Validation guidelines for the mechanical design of an orthodontic device.

The aim of this study is to elucidate the effects of the material, thickness, elastic modulus on residual stresses resulting from the interaction between an orthodontic aligner, the teeth, the periodontal ligament, and the alveolar bone using finite element methods (FEM) set up on two elementary movements: expansion of a posterior upper tooth and bodily movement of an upper incisor.

6.2 MATERIALS AND METHODS

The modeling of the system involved in the simulation is based on the data acquired by conducting a particular examination, which utilizes Cone-Beam Computed Tomography (CBCT), a radiological imaging technique. CBCT produces clear, detailed, and three-dimensional images of the oral cavity and it is particularly useful for accurately analyzing internal anatomical structures. Using the data obtained during the examination, and combining them with photographs or facial scanning, it is possible to gather all the necessary information to develop a personalized treatment plan for each individual patient.

During the examination, the equipment rotates around the patient's head, emitting a conical beam of X-rays that progressively passes through all the areas to be examined. Then, the acquired information is sent to dedicated software, which processes the data and reconstructs a three-dimensional model of the area of interest. The main advantages of this technique are that it minimizes the amount of radiation that the patient receives, and provides accurate diagnostic results. Furthermore, it allows for the subsequent treatment to be specifically adapted to the patient's needs based on the collected data.

For the purposes of this discussion, a sample patient's CBCT was analyzed to obtain a virtual reproduction of the dental arch, from which a tooth was selected for further investigation. It was also necessary to obtain a scan of the patient's mouth using a specific 3D intraoral scanner, a step crucial in the design of aligners as it replicates the initial condition of the dentition, allowing for work to be done on it in a virtual environment.

Once the scan was obtained, it was imported into the workspace of a software (DAD, Graphy, Seoul, South Korea) that allows for manipulation of the mesh. The first step involved performing a cleaning process. This phase is crucial as it allows for the removal of any artifacts caused by issues during the scanning process or other defects that could complicate file management by the program, thereby simplifying the entire workflow.

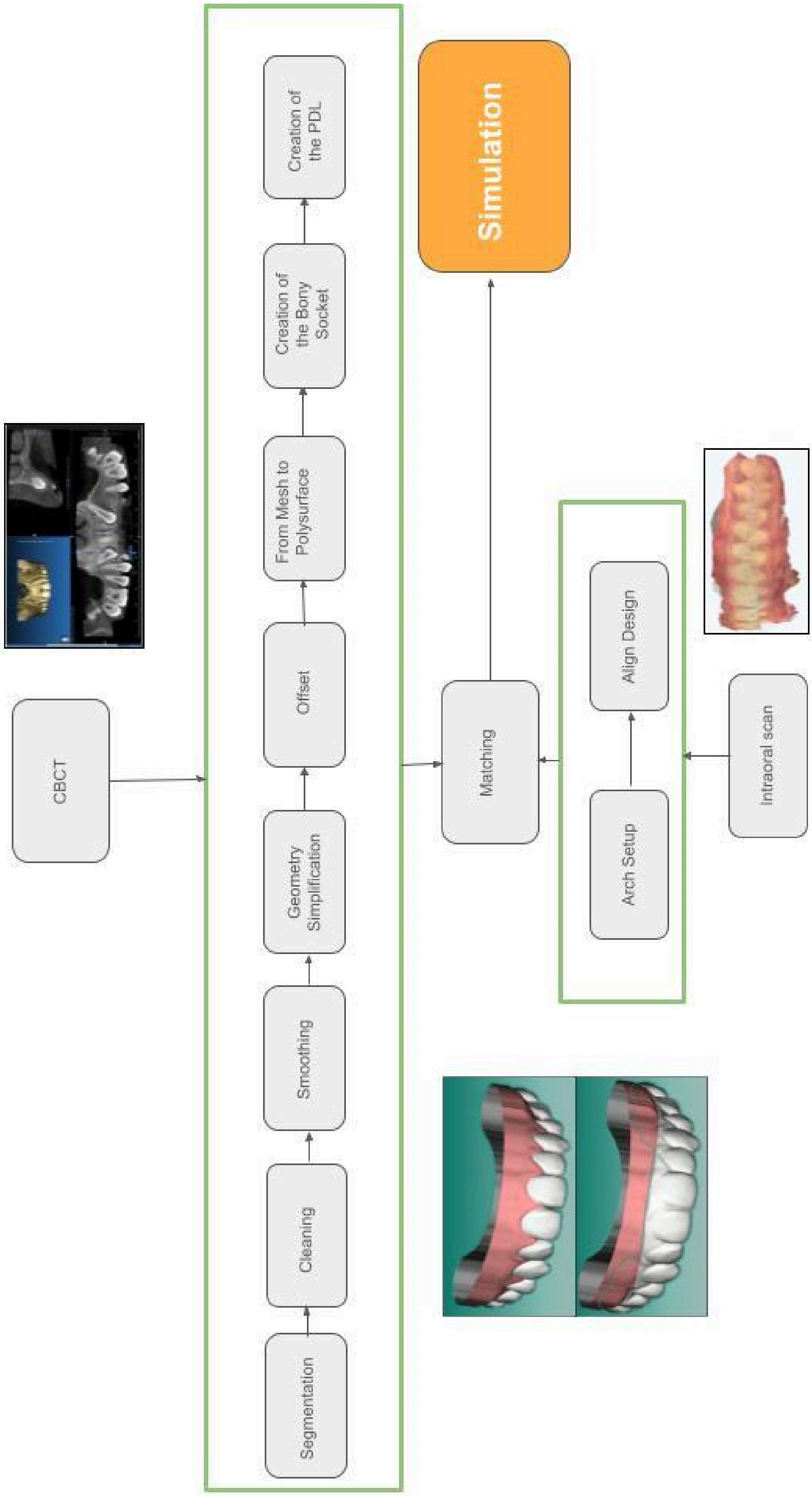
CBCT
Segmentation
Cleaning
Smoothing
Geometry Simplification
Offset
From Mesh to Polysurface
Creation of the Bony Socket
Creation of the PDL
Intraoral scan
Arch Setup
Align Design
Matching
Simulation

The mesh was then processed by indicating to the software the portion of the mesh corresponding to each of the crowns of the individual teeth. These portions were subsequently separated, transforming a single mesh into a collection of elements, each associated with a specific tooth, or more precisely, with each crown. From the scan, the program creates a virtual model of the patient's dentition, thus providing a faithful reproduction of it.

With the individual crowns as independent meshes, it is possible to manipulate the dental arch, searching for the optimal position for each tooth. The procedure is carried out manually using specific operations of rotation and translation. This arrangement represents the objective to be achieved by the end of the treatment.

Depending on the extent of the shifts of the various teeth, the complexity of the movements and the sequence in which adjustments are made, the reorganization of the dentition is tailored to the specific case by varying a series of parameters.

For the purpose of our study, a translation of the crown of the individual tooth 16 (the upper right first molar) was performed by 0.5 mm in the vestibular direction.

When satisfied with the new configuration and the gradual approach to achieve it, the automatic process of creating models begins, and the journey to the desired position of the teeth is replicated step by step. If proceeding with thermoforming, these models are sufficient. If direct 3D printing is desired, corresponding meshes for the aligners are generated based on each of these models.

Two aligners were created for the purposes of this study:

1. Passive Aligner. This aligner is passive, meaning it applies no forces and simply covers the dental arch in its initial shape. This step was useful for achieving correct alignment between the dentition and the aligner in the simulation software.
2. Active Aligner. This device is intended for the patient as the first active step in repositioning the teeth. It was generated for conducting actual tests, as its geometry differs from that of the untreated dentition, applying forces where needed.

The tooth selected for inclusion in the system to be studied was derived from the model obtained through CBCT. To obtain the tooth, complete with root, as a single body, work was done in a 3D modeling environment provided by Rhinoceros 8. After importing the model, several operations were carried out, which are listed below:

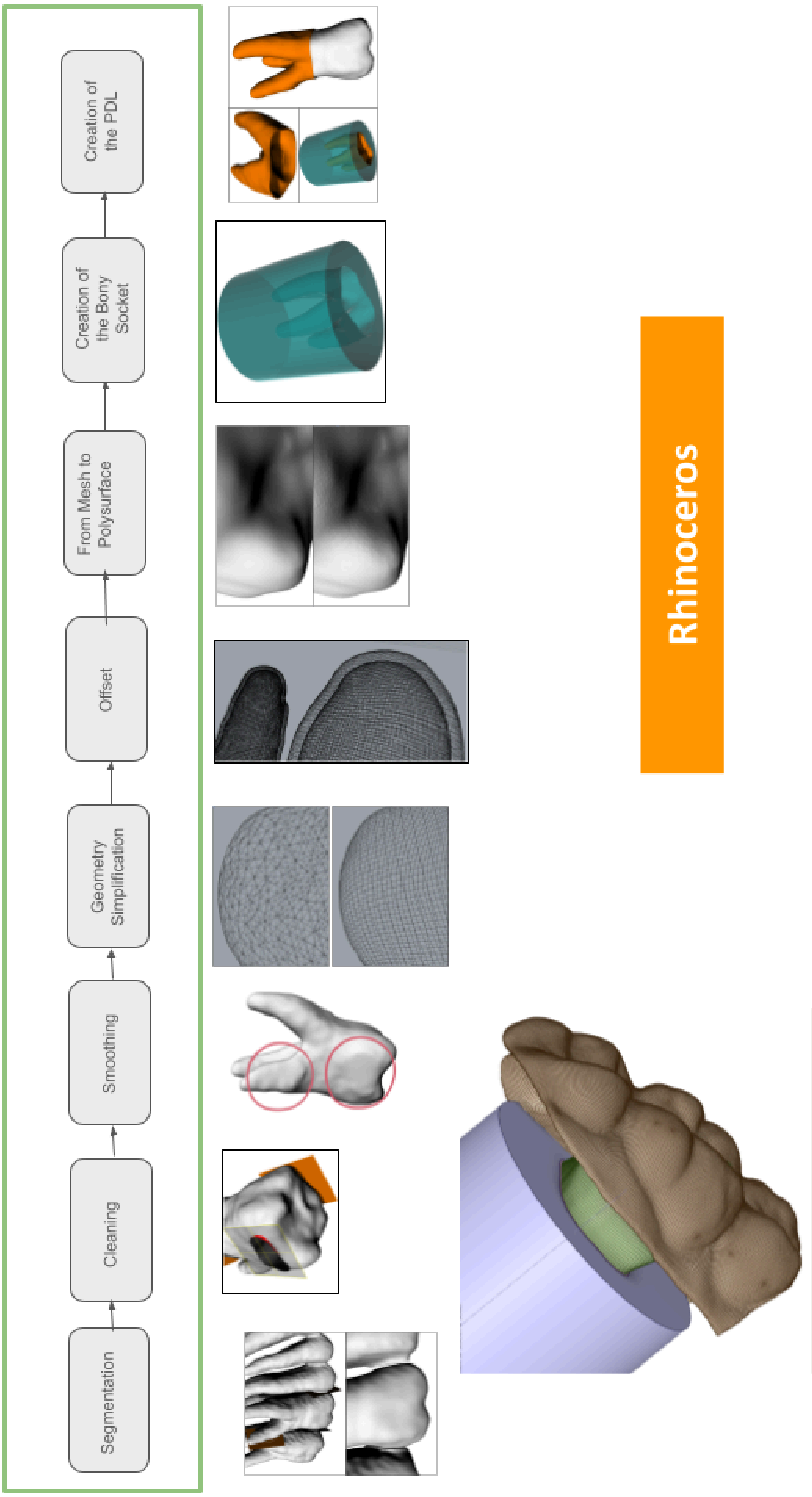
Segmentation
Cleaning
Smoothing
Geometry Simplification
Offset
From Mesh to Polysurface
Creation of the Bony Socket
Creation of the PDL
Rhinoceros

1. **Separation and Isolation.** Tooth 16 was separated from the mesh of the entire dentition using the command "MeshSplit". Strategically positioned planes were used as cutting objects between the crowns, specifically at the contact points between adjacent teeth. Planes were chosen as the cutting tool due to their simple geometry and ease of use.
2. **Cleaning the Mesh from Cutting and Scanning Artifacts.** The mesh of the dentition contained artificial necks between the teeth. These artifacts occur when two very close objects cannot be perfectly separated by the scanner. Therefore, they were removed as they would have caused disturbances in the simulation. In areas where cuts were made, holes formed due to the mesh being a hollow entity. This missing portion of the mesh needs to be restored as accurately as possible. A series of subsequent cuts were made using different planes after the initial roughing phase, gradually becoming more precise to smooth the surfaces at the edges of the necks. As in the previous phase, the "MeshSplit" command was used here as well. At this point, the holes in the contact areas between the teeth were closed using the command "FillMeshHoles".
3. **Smoothing process.** A smoothing process was performed using the "Smooth" command on the sharpest edges to reduce any remaining irregularities. Care was taken not to alter the overall shape of the object, as this would compromise the reliability of the simulations. This operation was complex because the mesh required multiple cycles of smoothing in specific areas, particularly at the edges formed by the cuts.
4. **Mesh Simplification.** The obtained mesh was processed to simplify its handling by the program. It was transformed from a triangular mesh to a quadrilateral mesh using the "QuadRemesh" command. This transformation resulted in approximately the same number of faces to maintain the resolution.
5. **Mesh Offset.** To replicate the periodontal ligament and the bony socket, it is necessary to create an offset of this mesh, 0.2 mm away from the base mesh in the outward direction using the "OffsetMesh" command. This operation generates an external shell that replicates the thicker shape of the tooth at the specified dimension. This component will be useful solely for the creation of the PDL (periodontal ligament) and the bony socket. The offset operation required special attention as initial attempts using a different type of geometry, a polysurface, yielded inconclusive results. Therefore, it was decided to circumvent the issue by first creating the offset of the desired surface in mesh form and subsequently transforming it into a polysurface as needed.
6. **From Mesh to Polysurface.** Meshes are geometries that do not allow for Boolean operations. Therefore, they were transformed into polysurfaces using the "ToNURBS" command, making them virtual objects capable of participating in such operations.

7. **Creation of the Bony Socket.** To create the bony socket, it was necessary to establish the starting zone of the periodontal ligament, located approximately 2.5 mm deep relative to the gingival surface in the root direction. A plane was carefully positioned at this "boundary," which provides a more or less approximate reference for the creation of the socket. The socket was generated by forming a cylinder, which was then modified. To make this cylinder the proper housing for the tooth and the periodontal ligament, a Boolean subtraction was performed using the “BooleanDifference” command. This command subtracted the volume associated with the previously offset polysurface of the tooth from the initial shape.
8. **Creation of the Periodontal Ligament (PDL).** The periodontal ligament was created from the portions covering the roots of the previously mentioned polysurfaces and by connecting them with a "crown"-shaped portion of the plane corresponding to the start of the PDL. This process creates a closed and well-defined volume suitable for Boolean operations. Before determining the best procedure to achieve a satisfactory result, various approaches were attempted, including creating it using a mesh and then transforming the mesh into a polysurface. However, this procedure did not yield the same results as the technique ultimately used.

After completing the previous steps, it was necessary to align the tooth-PDL-bony socket system with the passive aligner. In this phase of the work, several difficulties were encountered since the possibility of achieving a manual alignment is limited. In a new modeling environment using Rhinoceros 8, the passive aligner "0" was imported along with the tooth-PDL-bony socket system. The latter was moved and tilted to find its best positioning so that the tooth would be placed as if the device were being worn.

The aligner was kept in the same position in which the file was imported. Since the origin of the series of aligners is always the same, and modifications to the aligners only involve minimal and localized variations in their shape without shifting the inner device, the passive aligner can be utilized to find the correct reference for the study with the subsequent template.

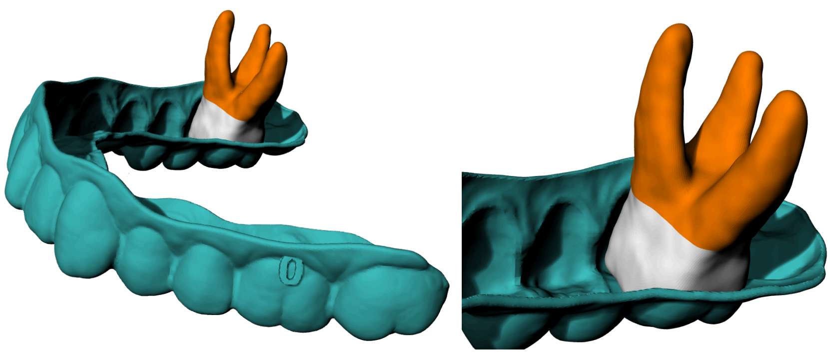

Figure 6-1 Dentition with segmented and modeled tooth, periodontal ligament, and fitted aligner

For the characterization of the materials treated in this study, tensile tests were chosen, conducted using the universal machine ZwickRoell Z050. The mechanical tests comprised two sessions of tensile testing, each with three dog bone specimens of specific dimensions.

First Series: Total Length: 90 mm (useful length approximately 45 mm), Width: 10 mm, Thickness: 1 mm

Second Series: Length: 40 mm (useful length approximately 20 mm), Width: 5 mm, Thickness: 1 mm

These measurements were taken with precision measuring instruments and recorded in the appropriate section of the testXpert III software, dedicated to the testing phase. The load application speed was set as constant at 5 mm/min. The specimens were secured to the machine's grips via manual tightening, while the measurements were conducted under ambient temperature conditions.

Once the preparation phase of the system is completed, the study of its actual behavior can begin. To investigate the local stresses that develop as a result of the interaction between the aligner and the tooth-PDL-bony socket system, it is necessary to use software capable of performing Finite Element Analyses (FEA). The software utilized for this purpose is “Ansys Workbench”, which is an engineering simulation environment for thermal, structural, fluid dynamic, and even multiphysics analyses. The type of analysis that was necessary to perform is structural, and Ansys provides all the necessary tools for this purpose.

To prepare a simulation of this type, it is necessary to provide the software with a set of information and set various parameters and conditions:

- Geometries: Geometries are necessary to define the system, volumes, and relative positions.
- Mesh: The resolution of the meshes establishes the definition of the geometries participating in the simulation, specifically how small the constituent elements of the volumes of the objects are.
- Materials: The definition of materials involves setting the type of response that a given geometry will have in response to a stimulus (mechanical, thermal, etc.). This depends, for example, on the mechanical properties of a material such as elastic modulus, Poisson's ratio, friction coefficient, bending strength, etc.
- Loads and Constraints: The settings for these parameters provide the necessary information for the software to correctly interpret the stresses to which the model will be subjected.
- Contacts: Contacts specify the type of interaction that occurs between the meshes in physical contact.
- Solution Parameters: The information entered in this context specifies what type of analysis should be performed and how the system of equations should be solved.

Finite Element analyses were performed based on the following structure. In the Ansys Workbench program, a Static Structural simulation was created, within which all necessary information was defined.

The first values defined were those related to the mechanical properties characterizing the system. For each material, a linear isotropic elastic modulus and a Poisson's ratio were set, with average values obtained from available literature. The next step was to import the geometries into the SpaceClaim program, a software interconnected with Workbench, where they were assembled with common origins and reference systems. An additional software, “Mechanical”, was used to associate the previously created materials with the different geometries. A mesh was then created to discretize the bodies.

The boundary conditions of the system were defined by constraining the sides of the aligner's geometry with “Fixed” and applying a pressure of 0.1 MPa on the cylinder that acts as the dental socket to prevent the tooth from slipping out of the aligner.

Afterward, the contacts between the elements were established by specifying the surfaces and defining their types. The contact between the dental socket and the PDL, as well as between the PDL and the tooth, was selected as “Bonded”. For the contact between the tooth and the aligner, the “Frictionless” option was chosen. The solutions requested from the software pertained to determining the reaction forces on the bony socket and assessing the displacements of the tooth.

6.3 RESULTS

Regarding the preparation of the simulations, the files were correctly imported into the simulation environment of Ansys Workbench with the proper orientation and relative positioning. The geometries are correctly separated and usable (only a portion of the aligner is depicted in the images for ease of processing). Materials have also been successfully prepared to be associated with each geometry, using the average values of parameters such as Young's modulus and Poisson's ratio obtained from the literature.

It can be stated that the pilot method developed in this work is functional, although it requires improvements that are practical and aimed at optimization. Most of the process, such as the preparation of the used files and the modeling of geometries via Rhinoceros software, is unfortunately still human-based, requiring almost total intervention from qualified personnel for its use. Future progress is expected to enable the complete automation of the process.

A starting point for this could be the combination of Rhinoceros with the Grasshopper plug-in, a visual editor for generative and parametric programming through algorithms in the form of networks and nodes. Further developments will make the application of the method more practical, allowing its use in the dental field and becoming a useful tool for improving treatment predictions.

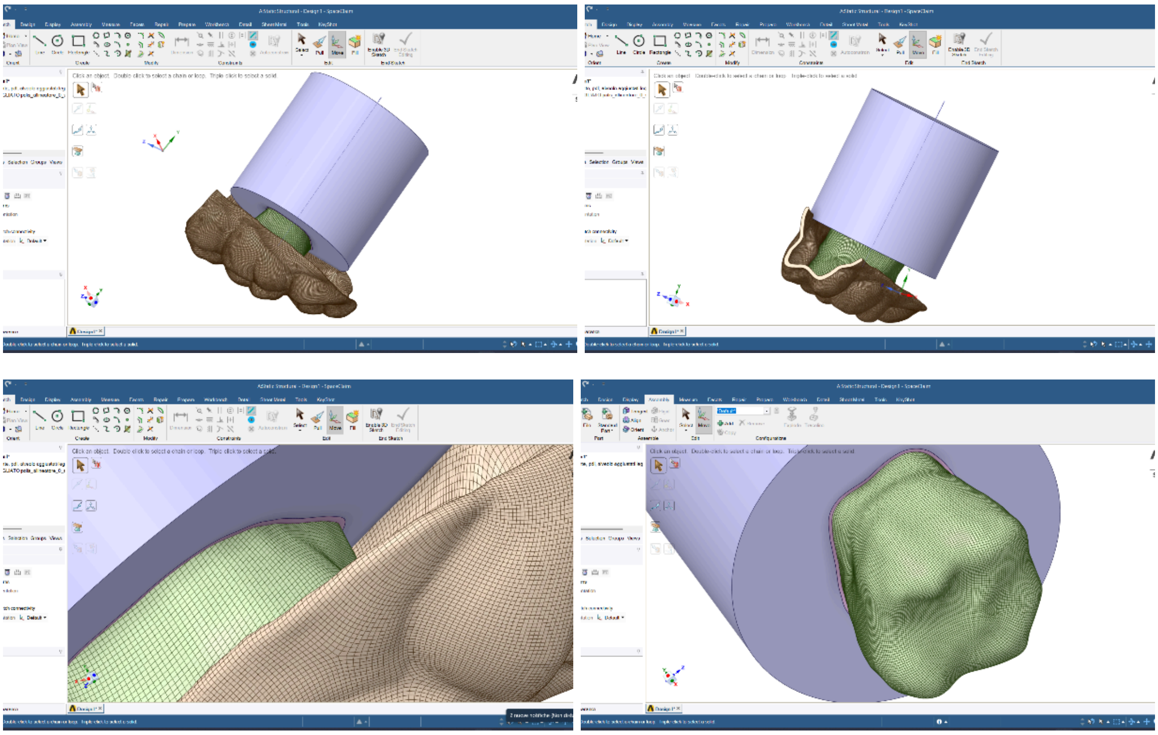

Figure 6-2 Finite Element analysis in the Ansys Workbench program

6.4 CONCLUSIONS

The present research represents the first step in developing a computational biomechanics tool to map and predict the forces applied to the dental arch by 3D printed orthodontic aligners of different materials, thicknesses and designs. The model aims to be a first step towards the construction of a fully automated and customizable tool that can help predict the dental movements of the virtual patient and select the most suitable designs and materials. Such a model can serve as a reference tool for materials developers and manufacturers and is intended to be reinforced by a clinical validation.

References

1. Migliorati M, Drago S, Lenzuni M, Marrella A, Giannoni P, Lagazzo A. Effect of 3D Printing Settings on the Mechanical Properties and Biocompatibility of Polymeric Materials Used for 3D Direct Printing of Orthodontic Aligners. Journal of Materials Research and Technology 2025;38:1724-1733.

2. Grant J, Foley P, Bankhead B, Miranda G, Adel SM, Kim KB. Forces and moments generated by 3D direct printed clear aligners of varying labial and lingual thicknesses during lingual movement of maxillary central incisor: an in vitro study. Prog Orthod. 2023 Jul 10;24(1):23.

EFFECT OF CURING TIME AND NITROGEN GENERATOR USAGE ON DIRECT 3D PRINTED ORTHODONTIC ALIGNERS THICKNESSES

7.1. INTRODUCTION

In order to maintain biocompatibility and to obtain an effective appliance, the production process of orthodontic aligners needs to carefully follow the processing protocol indicated by the manufacturing company, which disciplines not only the printing stage, but also the resin excess removal, the support removal, and the post-curing phase; each of these passages can have an impact on the surface characteristics and on the final mechanical properties of the product.

Since a standardised production workflow can avoid errors and lead to an efficient and time-saving in-office aligner production, several studies have been conducted to test the effect of different variables on the final product.

Boyer et al. concluded that the print orientation affected the dimensional accuracy of directly 3D-printed orthodontic aligners. Particularly, they recommended the three-dimensional printing of orthodontic aligners at a 90° angle owing to an improved dimensional accuracy of the intaglio surface, and also because a maximum number of aligners could be printed per job [1]. However, it has to be noted that this recommendation is not in line with the manufacturer‘s recommendations.

Another study took into consideration the fidelity of 3D printing technology and concluded that direct 3D printing was associated with an increased wall thickness of approximately 0.2 mm [2].
Cole et al. report that the dimensional accuracy of thermoformed and 3D-printed aligners ranged from 0.1 to 0.3 mm and from 0.1 to 0.4 mm, respectively [3]. Mc Carty and colleagues reported that 40 vs. 20 min of curing time had no impact on the dimensional accuracy of direct-printed passive clear aligners, as revealed by comparing surface distances among optical scans of the printed ones and the digital master [4].

However, difficulties were encountered in all studies involving optical scanning and superimposition techniques, because a spray application is required to collect the image of the transparent and reflective aligner surface, potentially leading to errors in the accuracy evaluation. On the other hand, a non-demolishing and precise method to assess thickness is available by means of micro-computed tomography, which has already been used to assess the aligner's geometrical characteristics [5–8]. To the best of our knowledge, no study has already used it to assess the impact of curing conditions on the final thickness of 3D-direct-printed aligners.

The aim of the present study was to investigate the effect of different curing times on the final thickness of direct 3D-printed aligners via micro-CT scanning. The null hypothesis was that different curing times have no impact on the final thicknesses of direct 3D-printed aligners. As secondary outcomes, the effect of nitrogen usage and variations in thicknesses among different tooth types and locations were evaluated.

7.2. MATERIALS AND METHODS

This study included in-office produced 3D-printed aligners of the upper jaw, and the printing and post-processing were performed by the same operator. No ethical approval was required for this in vitro experiment.

7.2.1. Virtual Setup

For the in-office aligners set up, the Aligner module from the OnyxCeph® (Onyxceph, Chemnitz, Germany) software was utilised. Starting from the 3D T0 digital model of a mild orthodontic case, the position of teeth was planned following aesthetic and functional principles. Aligning and levelling of dental arches were performed following orthodontic biomechanical principles. Every single aligner had a planned movement of 0.2 mm linear displacement, 2° long-axis rotation, and facial-lingual inclination of 2.5°. Then, a single step of the planned treatment was randomly selected and the same one was used for printing in all groups. In particular, neither cut outs for auxiliaries, such as elastics, temporary anchorage devices, or sectional vestibular appliances, nor attachments, power ridges, and bite ramps were included.

7.2.2. Aligner Production

The Tera Harz TC-85 (Graphy Inc., Seoul, Republic of Korea) was used for aligner production and aligners were directly 3D printed using the instructions provided by the manufacturer. Hereby, the Phrozen Sonic XL 4k 2022 printer (Phrozen Technology, Hsinchu, Taiwan) was employed for the printing. The aligners were designed with the thickness recommended by the producer (0.5 mm), and an offset of 0.05 mm was set between the aligner and the model. Printing was conducted in successive layers of 100 µm, with a down speed of 200 and a delay of 1000 ms. The first 6 layers were cured for 30 s. The height was 8 mm and the up speed was 100. The following layers were cured for 4 s with a 7 mm height and an up speed of 100. Supports were designed and planned using the Uniz software (Uniz, San Diego, CA, USA) to ensure the correct position with an angulation of 60° on the printer plate. When the printing process was terminated, aligners were removed from the plate and then the supports were manually removed.

The resin excesses were accurately removed from the intaglio surface using a centrifuge spinning at 1000× g revolutions per minute, which was used for 5 min two times. Thereafter, aligners were divided into 7 groups (Table 7.1). Each group consisted of 5 aligners and were post-cured according to a different curing time in a post-curing unit (Cure M, Graphy, Seoul, Republic of Korea). In total, 6 groups out of 7 were post-cured with a nitrogen generator, the 7th one was cured without a nitrogen generator. Curing times were the following: 15 min, 20 min, 25 min, 30 min, 40 min, and 50 min. The group without the nitrogen generator was cured for 30 min. After curing, aligners were put in boiling water at 100 °C for 2 min.

Table 7-1 Group production characteristics and composition

Printer Plate Angulation	Curing Time	Nitrogen Generator	N
60°	15 min	yes	5
60°	20 min	yes	5
60°	25 min	yes	5
60°	30 min	yes	5
60°	40 min	yes	5
60°	50 min	yes	5
60°	30 min	no	5

7. 2.3. Micro-Computed Tomography and Image Processing

Aligners underwent scanning using a micro-CT scanner (VivaCT 80, Scanco Medical AG, Wangen-Brüttisellen, Switzerland) at 45 kVp, 88 µA, with an integration time of 254 ms. The resultant scans were reconstructed to attain a nominal isotropic voxel size of 31.2 µm. Image processing was performed with an in-house developed script using the Image Processing Language (IPL) from Scanco Medical AG. This script executed a series of sequential steps.

Initially, a cylindrical volume of interest (VOI) was defined at the outer margin of the field of view. Thereafter, image filtering was accomplished through the application of a Gaussian filter with a sigma of 0.8 voxel and a support of 1 voxel. Subsequently, segmentation of the aligners was carried out utilising a threshold set at 4.2% of the maximum grey value. Aligner thickness was then calculated using the 3D Chamfer distance transform approach [9]. This approach calculates the outer contours of a segmented material and assigns the approximated Euclidean distance to its closest contour point as a grey value to every point within the segmented structure. Finally, for visualization purposes, the calculated aligner thickness values were displayed using a 3D rendering program (uct_3d, Scanco Medical AG, Wangen-Brüttisellen, Switzerland).

7. 2.4. Thickness Measurements

To assess local aligner thickness values, a total of n = 20 reference points were defined (Table 7.2). At each reference point, the respective local thickness was recorded.

Table 7-2 Reference points for assessment of local aligner material thickness values

Reference Point	Definition	Assessed at Teeth
MB	mesiobuccal cusp tip	16, 26
MP	mesiopalatal cusp tip	16, 26
DB	distobuccal cusp tip	16, 26
DP	distopalatal cusp tip	16, 26
FIS	mesiodistal centre of the central fissure	16, 15, 14, 24, 25, 26
V	central point of the facial surface	All teeth
B	buccal cusp tip	15, 14, 25, 24
P	palatal cusp tip	15, 14, 25, 24
I	most coronal, central point of the incisal edge	11, 21, 12, 22, 13, 23

7. 2.5. Statistical Analysis

To verify the normality of data, the Shapiro–Wilk test was used. Continuous variables are reported as means ± standard deviations (SD) or medians with interquartile range [IR] (whenever not normally distributed). Categorical variables are reported as a number and/or percentage. Additionally, when the data results were normally distributed, Levene's test for homogeneity of variances and the normality of residuals were validated.

The Spearman's rank correlation test was used to test for the association between the mean aligner thickness values and the respective curing time.

For each reference point, a comparison of local thickness values among groups (curing times: 15 min, 20 min, 25 min, 30 min, 40 min, and 50 min) was performed by ANOVA (if all assumptions could be validated) or the Kruskall–Wallis test, followed by the Mann–Whitney U-test with Bonferroni's correction for multiple comparisons when appropriate.

For the 30 min curing groups, comparisons between groups with and without nitrogen generator usage were carried out for each reference point using the Student's t-test (in case of normal distribution), or the Mann–Whitney U-test (if normality failed), adjusted by using Bonferroni's method.

The Kruskall–Wallis test was utilised to compare the standard deviations of aligner thicknesses (representing aligner thickness heterogeneity) among groups.

Comparison among tooth types and sites was performed using the Kruskall–Wallis test followed by the Mann–Whitney U-test with Bonferroni's correction for multiple comparisons.

Differences with a p-value <0.05 were selected as significant. Data were acquired and analysed in the R v4.2.2 software environment [10].

7.3. RESULTS

7. 3.1. Impact of Curing Time

The thickness values of 35 aligners (5 per curing time or conditions) at 40 different reference points entered the analysis. The maximal recorded thickness was 0.89 mm, and the minimum was 0.51 mm.

According to Spearman's rank correlation test, no significant association was found between thickness values and curing time ($p = 0.0617$). Despite this, when repeating the test for the individual reference points, at some locations there was a trend for reduced thickness at higher curing times, i.e., at 1.5 B ($\rho = 0.466$, $p = 0.009$), 1.5 p ($\rho = -0.451$, $p = 0.013$), and 1.6 MP ($\rho = 0.386$, $p = 0.039$).

When comparing the local thickness values at reference points among curing time groups, significant differences were found at 1.6 MP, 1.6 DB, 1.5 B, 1.5 P. 1.5 FIS, 1.4 FIS, 1.2 I, 1.2 V, 1.1 V, 2.6 MB, 2.6 DP, 2.6 V, 2.5 P, 2.4 B, 2.3 I, 2.2 I, 2.1 I, and 2.1 V (see Table 7.3 for details and p-values). The post hoc tests failed to reveal significant pairwise differences. However, it has to be noted that interquartile ranges varied across groups and locations, whereas within groups and locations, very small ranges were observed (the respective plots are provided in the Supplemental Material).

Table 7-3 Overall local thickness values at reference points and for the different curing time groups. Results are expressed in mm as Mean ± Standard Deviation or Median [Interquartile Range]. p-value: ANOVA or Kruskall–Wallis test p-value; MB: mesiobuccal cusp tip; MP: mesiopalatal cusp tip; DB: distobuccal cusp tip; DP: disto-palatal cusp tip; FIS: mesiodistal centre of the central fissure; V: central point of the facial surface; B: buccal cusp tip; P: palatal cusp tip; I: most coronal, central point of the incisal edge

1.6	**Overall**	**15 Min**	**20 Min**	**25 Min**	**30 Min**	**40 Min**	**50 Min**	***p*-Value**
MB	0.56 [0.51, 0.56]	0.58 [0.55, 0.62]	0.56 [0.56, 0.61]	0.56 [0.51, 0.61]	0.51 [0.51, 0.56]	0.56 [0.56, 0.56]	0.51 [0.51, 0.56]	0.359
MP	0.65 [0.61, 0.70]	0.68 [0.64, 0.70]	0.70 [0.70, 0.75]	0.61 [0.61, 0.66]	0.70 [0.66, 0.75]	0.66 [0.61, 0.66]	0.61 [0.61, 0.66]	0.010
DB	0.61 [0.56, 0.61]	0.63 [0.61, 0.66]	0.61 [0.61, 0.66]	0.56 [0.56, 0.61]	0.51 [0.51, 0.56]	0.56 [0.56, 0.61]	0.66 [0.61, 0.66]	0.010
DP	0.65 [0.65, 0.75]	0.73 [0.69, 0.76]	0.75 [0.70, 0.75]	0.70 [0.61, 0.75]	0.66 [0.66, 0.70]	0.66 [0.61, 0.66]	0.66 [0.66, 0.70]	0.453
FIS	0.75 [0.71, 0.80]	0.75 [0.73, 0.76]	0.75 [0.75, 0.84]	0.75 [0.66, 0.75]	0.80 [0.70, 0.84]	0.75 [0.75, 0.75]	0.80 [0.75, 0.84]	0.638
V	0.51 [0.51, 0.56]	0.54 [0.51, 0.57]	0.56 [0.51, 0.56]	0.51 [0.51, 0.56]	0.51 [0.51, 0.51]	0.56 [0.56, 0.56]	0.51 [0.51, 0.51]	0.456
1.5	Overall	15 Min	20 Min	25 Min	30 Min	40 Min	50 Min	*p*-Value
B	0.61 [0.61, 0.66]	0.66 [0.61, 0.70]	0.66 [0.66, 0.66]	0.61 [0.61, 0.61]	0.61 [0.56, 0.61]	0.61 [0.61, 0.61]	0.61 [0.61, 0.61]	0.032
P	0.61 [0.61, 0.66]	0.66 [0.66, 0.66]	0.70 [0.66, 0.70]	0.61 [0.61, 0.61]	0.61 [0.61, 0.61]	0.61 [0.56, 0.66]	0.61 [0.61, 0.66]	0.008
FIS	0.78 ± 0.06	0.85 ± 0.02	0.81 ± 0.08	0.77 ± 0.03	0.73 ± 0.04	0.73 ± 0.08	0.80 ± 0.07	0.018
V	0.51 [0.51, 0.51]	0.51 [0.51, 0.51]	0.51 [0.47, 0.56]	0.51 [0.51, 0.51]	0.51 [0.51, 0.56]	0.51 [0.51, 0.56]	0.51 [0.51, 0.51]	0.832
1.4	Overall	15 Min	20 Min	25 Min	30 Min	40 Min	50 Min	*p*-Value
B	0.56 [0.56, 0.61]	0.56 [0.56, 0.56]	0.61 [0.61, 0.61]	0.56 [0.56, 0.56]	0.61 [0.56, 0.61]	0.61 [0.56, 0.61]	0.56 [0.51, 0.56]	0.201
P	0.65 [0.61, 0.70]	0.70 [0.61, 0.70]	0.70 [0.70, 0.75]	0.66 [0.66, 0.70]	0.66 [0.66, 0.66]	0.70 [0.66, 0.70]	0.61 [0.61, 0.66]	0.084
FIS	0.84 [0.80, 0.89]	0.89 [0.80, 0.89]	0.89 [0.84, 0.89]	0.80 [0.80, 0.84]	0.80 [0.66, 0.80]	0.84 [0.70, 0.89]	0.84 [0.84, 0.89]	0.037
V	0.51 [0.51, 0.56]	0.56 [0.56, 0.56]	0.51 [0.51, 0.56]	0.51 [0.51, 0.51]	0.51 [0.51, 0.56]	0.56 [0.56, 0.56]	0.51 [0.51, 0.56]	0.337
1.3	Overall	15 Min	20 Min	25 Min	30 Min	40 Min	50 Min	*p*-Value
I	0.61 [0.56, 0.61]	0.61 [0.56, 0.61]	0.61 [0.56, 0.61]	0.56 [0.56, 0.56]	0.61 [0.61, 0.61]	0.61 [0.61, 0.61]	0.61 [0.61, 0.61]	0.076
V	0.56 [0.56, 0.56]	0.66 [0.61, 0.66]	0.51 [0.51, 0.56]	0.56 [0.56, 0.56]	0.56 [0.56, 0.56]	0.56 [0.56, 0.61]	0.56 [0.56, 0.56]	0.185
1.2	Overall	15 Min	20 Min	25 Min	30 Min	40 Min	50 Min	*p*-Value
I	0.61 [0.56, 0.66]	0.61 [0.61, 0.66]	0.66 [0.66, 0.70]	0.56 [0.56, 0.56]	0.66 [0.66, 0.66]	0.61 [0.61, 0.66]	0.61 [0.56, 0.61]	0.001
V	0.65 [0.61, 0.65	0.70 [0.66, 0.70]	0.66 [0.61, 0.66]	0.61 [0.61, 0.66]	0.56 [0.56, 0.61]	0.61 [0.61, 0.61]	0.66 [0.66, 0.66]	0.020

1.1	Overall	15 Min	20 Min	25 Min	30 Min	40 Min	50 Min	p-Value
I	0.65 [0.65, 0.70]	0.70 [0.66, 0.70]	0.66 [0.61, 0.75]	0.61 [0.61, 0.66]	0.70 [0.66, 0.75]	0.70 [0.66, 0.70]	0.66 [0.66, 0.66]	0.158
V	0.75 [0.75, 0.80]	0.84 [0.84, 0.89]	0.80 [0.80, 0.80]	0.70 [0.70, 0.70]	0.75 [0.70, 0.75]	0.80 [0.80, 0.80]	0.80 [0.75, 0.80]	0.001
2.1	Overall	15 Min	20 Min	25 Min	30 Min	40 Min	50 Min	p-Value
I	0.75 [0.70, 0.80]	0.75 [0.75, 0.80]	0.75 [0.75, 0.80]	0.70 [0.70, 0.70]	0.94 [0.84, 0.94]	0.84 [0.80, 0.98]	0.75 [0.70, 0.75]	0.009
V	0.80 [0.75, 0.80]	0.84 [0.80, 0.84]	0.80 [0.75, 0.80]	0.70 [0.70, 0.70]	0.75 [0.75, 0.80]	0.80 [0.80, 0.80]	0.80 [0.80, 0.80]	0.004
2.2	Overall	15 Min	20 Min	25 Min	30 Min	40 Min	50 Min	p-Value
I	0.61 [0.58, 0.66]	0.66 [0.66, 0.66]	0.66 [0.61, 0.66]	0.56 [0.56, 0.56]	0.66 [0.61, 0.70]	0.66 [0.61, 0.66]	0.61 [0.61, 0.61]	0.020
V	0.65 [0.61, 0.70]	0.70 [0.66, 0.70]	0.66 [0.61, 0.66]	0.66 [0.61, 0.70]	0.66 [0.61, 0.66]	0.70 [0.66, 0.70]	0.66 [0.66, 0.66]	0.360
2.3	Overall	15 Min	20 Min	25 Min	30 Min	40 Min	50 Min	p-Value
I	0.61 [0.61, 0.66]	0.61 [0.61, 0.61]	0.61 [0.61, 0.66]	0.56 [0.56, 0.61]	0.61 [0.61, 0.66]	0.66 [0.66, 0.66]	0.61 [0.61, 0.61]	0.009
V	0.56 [0.56, 0.56]	0.56 [0.56, 0.56]	0.56 [0.56, 0.61]	0.56 [0.51, 0.56]	0.56 [0.51, 0.56]	0.56 [0.56, 0.61]	0.56 [0.56, 0.56]	0.263
2.4	Overall	15 Min	20 Min	25 Min	30 Min	40 Min	50 Min	p-Value
B	0.61 [0.61, 0.66]	0.61 [0.61, 0.66]	0.66 [0.66, 0.66]	0.61 [0.56, 0.61]	0.61 [0.61, 0.61]	0.61 [0.61, 0.66]	0.61 [0.61, 0.61]	0.014
P	0.65 [0.63, 0.70]	0.70 [0.66, 0.70]	0.70 [0.70, 0.75]	0.66 [0.61, 0.66]	0.66 [0.66, 0.66]	0.70 [0.66, 0.75]	0.66 [0.66, 0.70]	0.072
FIS	0.75 [0.70, 0.80]	0.75 [0.75, 0.84]	0.80 [0.75, 0.80]	0.75 [0.70, 0.80]	0.70 [0.66, 0.80]	0.70 [0.51, 0.75]	0.84 [0.80, 0.84]	0.158
V	0.51 [0.51, 0.56]	0.56 [0.56, 0.56]	0.56 [0.51, 0.56]	0.51 [0.51, 0.51]	0.51 [0.51, 0.51]	0.56 [0.56, 0.56]	0.51 [0.51, 0.56]	0.102
2.5	Overall	15 Min	20 Min	25 Min	30 Min	40 Min	50 Min	p-Value
B	0.61 [0.61, 0.66]	0.66 [0.66, 0.70]	0.66 [0.61, 0.66]	0.61 [0.61, 0.61]	0.61 [0.61, 0.66]	0.66 [0.61, 0.66]	0.66 [0.61, 0.66]	0.206
P	0.66 [0.61, 0.70	0.70 [0.70, 0.70]	0.70 [0.70, 0.75]	0.66 [0.61, 0.66]	0.66 [0.61, 0.66]	0.61 [0.56, 0.66]	0.66 [0.66, 0.70]	0.015
FIS	0.75 ± 0.10	0.81 ± 0.10	0.80 ± 0.07	0.77 ± 0.06	0.74 ± 0.10	0.66 ± 0.12	0.80 ± 0.08	0.110
V	0.51 [0.51, 0.56]	0.56 [0.51, 0.56]	0.51 [0.51, 0.56]	0.51 [0.51, 0.51]	0.51 [0.51, 0.51]	0.56 [0.56, 0.56]	0.56 [0.51, 0.56]	0.267
2.6	Overall	15 Min	20 Min	25 Min	30 Min	40 Min	50 Min	p-Value
MB	0.66 [0.61, 0.66]	0.66 [0.66, 0.66]	0.66 [0.66, 0.70]	0.61 [0.61, 0.66]	0.70 [0.70, 0.70]	0.61 [0.61, 0.61]	0.66 [0.61, 0.66]	0.014
MP	0.66 [0.61, 0.72]	0.66 [0.61, 0.75]	0.70 [0.70, 0.75]	0.61 [0.61, 0.66]	0.70 [0.66, 0.80]	0.80 [0.66, 0.94]	0.66 [0.61, 0.66]	0.157
DB	0.66 [0.66, 0.70]	0.70 [0.70, 0.75]	0.70 [0.66, 0.70]	0.66 [0.66, 0.66]	0.70 [0.66, 0.70]	0.66 [0.61, 0.70]	0.70 [0.66, 0.70]	0.168
DP	0.66 [0.61, 0.68]	0.66 [0.66, 0.70]	0.70 [0.66, 0.70]	0.61 [0.56, 0.61]	0.66 [0.66, 0.70]	0.61 [0.61, 0.66]	0.66 [0.66, 0.66]	0.038
FIS	0.71 ± 0.08	0.69 ± 0.02	0.76 ± 0.04	0.69 ± 0.06	0.78 ± 0.10	0.62 ± 0.13	0.69 ± 0.07	0.050
V	0.56 [0.51, 0.56]	0.56 [0.56, 0.56]	0.51 [0.51, 0.56]	0.51 [0.51, 0.51]	0.56 [0.56, 0.56]	0.56 [0.56, 0.61]	0.56 [0.51, 0.56]	0.010

7. 3.2. Impact of Nitrogen Generator

A significant difference between the group with a 30 min curing time with a nitrogen generator and the same curing time group without a nitrogen generator was found (median value 0.66 mm IR [0.42, 0.94] and 0.61 mm IR [0.47, 0.89], respectively, Mann–Whitney U-test p-value = 0.004). Particularly, significant differences were found at the following reference points: 1.6 MP, 1.5 FIS, 1.3 I, 1.2 V, 1.2 I, 2.6 MB, 2.6 MP, 2.6 DB, 2.3 I, 2.2 I, and 2.1 I (see Table 7.4).

Table 7-4 Local thickness values at reference points for the different curing conditions (30 min curing time with and without nitrogen generator). Results are expressed in mm as Mean ± Standard Deviation or Median [Interquartile Range]. p-value: Student's t-test, or Mann–Whitney U test, p-value; MB: mesiobuccal cusp tip; MP: mesiopalatal cusp tip; DB: distobuccal cusp tip; DP: disto-palatal cusp tip; FIS: mesiodistal centre of the central fissure; V: central point of the facial surface; B: buccal cusp tip; P: palatal cusp tip; I: most coronal, central point of the incisal edge

1.6	**Without N2**	**With N2**	***p*-Value**
MB	0.51 [0.51, 0.56]	0.51 [0.51, 0.56]	0.910
MP	0.61 [0.61, 0.61]	0.70 [0.66, 0.75]	0.007
DB	0.56 [0.56, 0.61]	0.51 [0.51, 0.56]	0.125
DP	0.66 [0.61, 0.66]	0.66 [0.66, 0.70]	0.515
FIS	0.75 [0.75, 0.75]	0.80 [0.70, 0.84]	0.443
V	0.56 [0.51, 0.56]	0.51 [0.51, 0.51]	0.221
1.5	Without N2	With N2	*p*-Value
B	0.56 [0.56, 0.56]	0.61 [0.56, 0.61]	0.324
P	0.61 [0.61, 0.61]	0.61 [0.61, 0.61]	0.317
FIS	0.79 ± 0.02	0.73 ± 0.04	0.028
V	0.51 [0.51, 0.51]	0.51 [0.51, 0.56]	0.519
1.4	Without N2	With N2	*p*-Value
B	0.56 [0.51, 0.56]	0.61 [0.56, 0.61]	0.100
P	0.56 [0.56, 0.61]	0.66 [0.66, 0.66]	0.081
FIS	0.80 [0.75, 0.80]	0.80 [0.66, 0.80]	0.435
V	0.51 [0.51, 0.51]	0.51 [0.51, 0.56]	0.288
1.3	Without N2	With N2	*p*-Value
I	0.56 [0.51, 0.56]	0.61 [0.61, 0.61]	0.014
V	0.56 [0.56, 0.56]	0.56 [0.56, 0.56]	0.606
1.2	Without N2	With N2	*p*-Value
I	0.56 [0.56, 0.61]	0.66 [0.66, 0.66]	0.011
V	0.66 [0.66, 0.66]	0.56 [0.56, 0.61]	0.037
1.1	Without N2	With N2	*p*-Value
I	0.66 [0.66, 0.70]	0.70 [0.66, 0.75]	0.230
V	0.75 [0.75, 0.75]	0.75 [0.70, 0.75]	0.093
2.1	Without N2	With N2	*p*-Value
I	0.75 [0.70, 0.75]	0.94 [0.84, 0.94]	0.010
V	0.75 [0.70, 0.75]	0.75 [0.75, 0.80]	0.059
2.2	Without N2	With N2	*p*-Value
I	0.61 [0.56, 0.61]	0.66 [0.61, 0.70]	0.033
V	0.61 [0.61, 0.66]	0.66 [0.61, 0.66]	0.316
2.3	Without N2	With N2	*p*-Value
I	0.56 [0.56, 0.56]	0.61 [0.61, 0.66]	0.014
V	0.56 [0.56, 0.56]	0.56 [0.51, 0.56]	0.093

2.4	Without N2	With N2	*p*-Value
B	0.61 [0.56, 0.61]	0.61 [0.61, 0.61]	0.345
P	0.61 [0.61, 0.66]	0.66 [0.66, 0.66]	0.429
FIS	0.75 [0.70, 0.80]	0.70 [0.66, 0.80]	0.915
V	0.51 [0.51, 0.56]	0.51 [0.51, 0.51]	0.134
2.5	Without N2	With N2	*p*-Value
B	0.61 [0.56, 0.61]	0.61 [0.61, 0.66]	0.212
P	0.61 [0.61, 0.61]	0.66 [0.61, 0.66]	0.262
FIS	0.72 ± 0.09	0.74 ± 0.10	0.767
V	0.51 [0.51, 0.51]	0.51 [0.51, 0.51]	1.000
2.6	Without N2	With N2	*p*-Value
MB	0.61 [0.61, 0.61]	0.70 [0.70, 0.70]	0.005
MP	0.61 [0.61, 0.61]	0.70 [0.66, 0.80]	0.019
DB	0.61 [0.61, 0.61]	0.70 [0.66, 0.70]	0.037
DP	0.66 [0.66, 0.66]	0.66 [0.66, 0.70]	0.736
FIS	0.71 ± 0.06	0.78 ± 0.10	0.237
V	0.56 [0.51, 0.56]	0.56 [0.56, 0.56]	0.343

7. 3.3. Impact of Tooth Type and Site

When considering the different tooth types, the Kruskal–Wallis test revealed significance ($p < 0.001$), and the post hoc test confirmed significant differences among the majority of teeth (Table 7.5). When grouping the tooth types, significantly higher thickness values at the central incisors were noted ($p < 0.001$, Figure 7.1).

Table 7-5 Comparison of local thickness values (mm) aggregated for tooth type. p-value: Kruskall–Wallis test p-value. Pairwise comparisons were achieved using the Mann–Whitney U-test with Bonferroni's method for p-value adjustment. Ce: Centrals; L: Laterals; Ca: Canines; 1P: First Premolars; 2P: Second Premolars; M: Molars

	Thickness	*p*-Value	Ce	L	Ca	1P	2P	M
Ce	0.75 [0.70, 0.80]		-					
L	0.63 [0.61, 0.66]		<0.001	-				
Ca	0.58 [0.56, 0.60]	<0.001	<0.001	<0.001	-			
1P	0.64 [0.62, 0.67]		<0.001	0.45	<0.001	-		
2P	0.63 [0.62, 0.67]		<0.001	1.00	<0.001	1.00	-	
M	0.64 [0.61, 0.67]		<0.001	1.00	<0.001	1.00	1.00	-

When grouping data for the type of reference point, significant differences in thickness values were also detected ($p < 0.001$). Particularly, at the mesiodistal centre of the central fissure (FIS), the thickness values were significantly higher than in all the other locations, whereas at the central point of the facial surface (V) thickness values were significantly lower than in all the other locations except the mesiobuccal cusp tip (MB) (Figure 7.2 and Table 7.6).

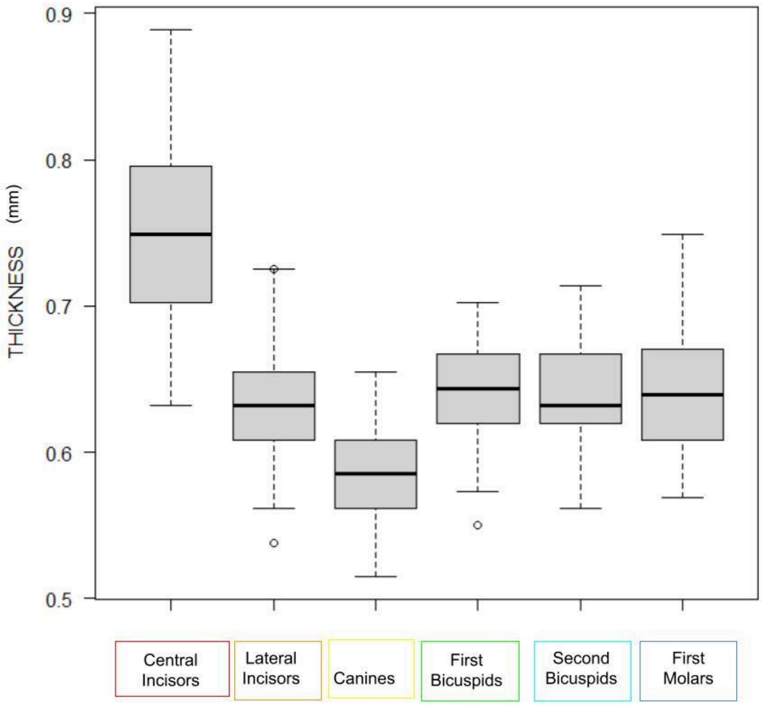

Figure 7-1 Boxplot showing the local thickness values at reference points. The thickness values at the reference points were aggregated by tooth type

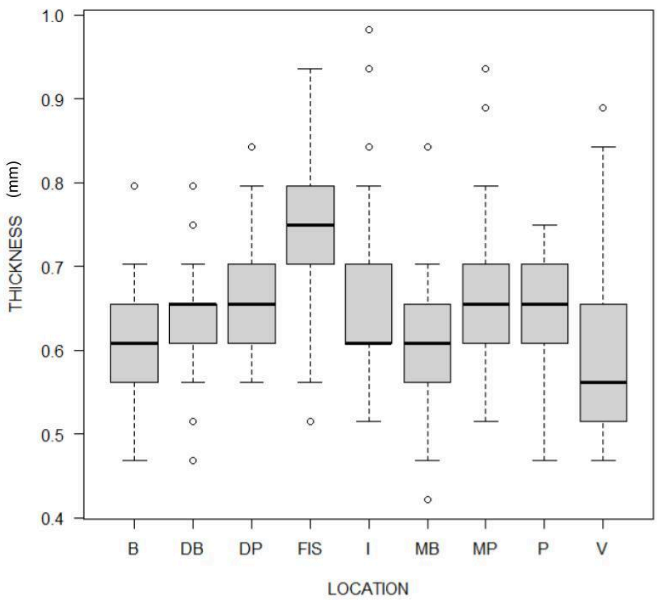

Figure 7-2 Boxplot showing the local thickness values at reference points. The thickness values at the reference points were aggregated by location

Table 7-6 Comparison of local thickness values (mm) aggregated for measurement location. p-value: Kruskall–Wallis test p-value. Pairwise comparisons were achieved using the Mann–Whitney U-test with Bonferroni's method for p-value adjustment. MB: mesiobuccal cusp tip; MP: mesiopalatal cusp tip; DB: distobuccal cusp tip; DP: distopalatal cusp tip; FIS: mesiodistal center of the central fissure; V: central point of the facial surface; B: buccal cusp tip; P: palatal cusp tip; I: most coronal, central point of the incisal edge.

Location	Thickness	*p*-Value	B	DB	DP	FIS	I	MB	MP	P	V
B	0.61 [0.56, 0.66]	<0.001	-								
DB	0.66 [0.61, 0.66]		0.051	-							
DP	0.66 [0.61, 0.70]		<0.001	0.058	-						
FIS	0.75 [0.70, 0.80]		<0.001	<0.001	<0.001	-					
I	0.61 [0.61, 0.70]		<0.001	1.000	0.033	<0.001	-				
MB	0.61 [0.56, 0.66]		1.0000	0.142	<0.001	<0.001	0.006	-			
MP	0.66 [0.61, 0.70]		<0.001	0.590	1.000	<0.001	0.378	<0.001	-		
P	0.66 [0.61, 0.70]		<0.001	1.000	1.000	<0.001	1.000	<0.001	1.000	-	
V	0.56 [0.51, 0.66]		0.002	<0.001	<0.001	<0.001	<0.001	1.000	<0.001	<0.001	-

7. 3.4. Heterogeneity

When comparing the standard deviation of aligner thicknesses, which corresponds to within-aligner heterogeneity, the Kruskal–Wallis test returned no significant differences among the groups (p = 0.0802, Figure 7.3), thus revealing that material heterogeneity was comparable among groups.

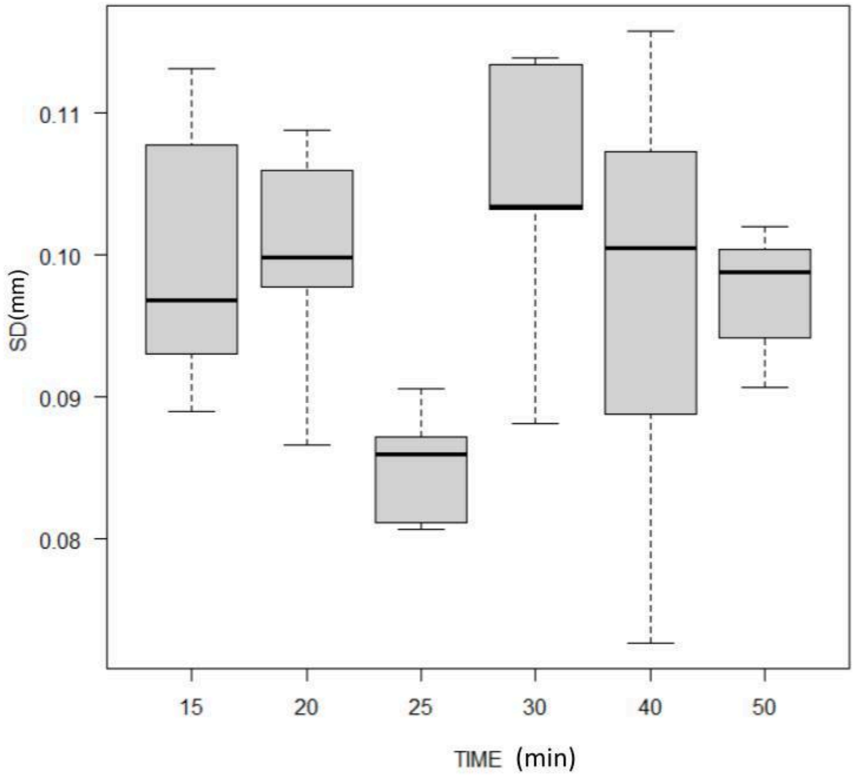

Figure 7-3 Boxplot showing the standard deviation of the respective thickness values representing the material homogeneity

7.3.5. 3D Images

For descriptive analyses, 3D-rendered images were generated using the uct_3d software. They provide a visualisation of 3D deviations in the thickness of the aligners within different groups and locations (Figures 7.4–7.9). The results show a similar colour distribution and generally yield positive deviations in the areas of central and lateral incisors, in the posterior interproximal septa, and in some isolated punctiform sites located on the cusps. Also, increased thickness values at the facial surfaces of incisors were noted in all groups.

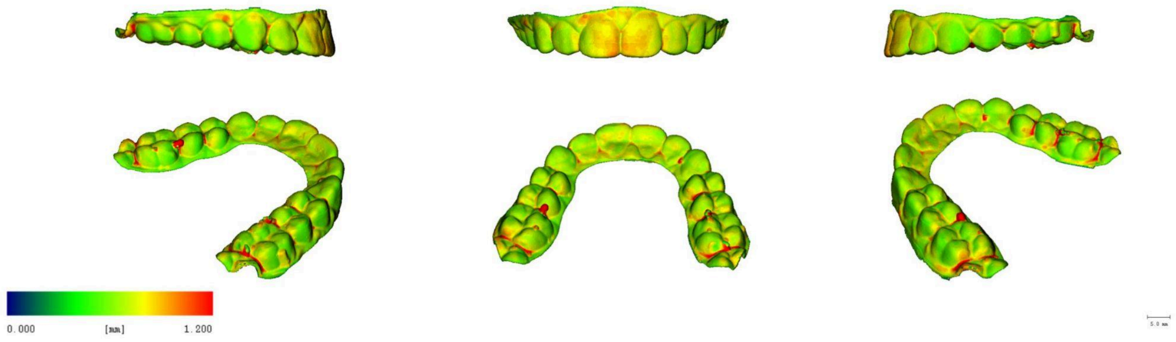

Figure 7-4 Representative renderings visualising the local material thickness of micro-CT scanned direct-printed aligners with a 15 min curing time (blue: 0.00 mm, red: 1.20 mm)

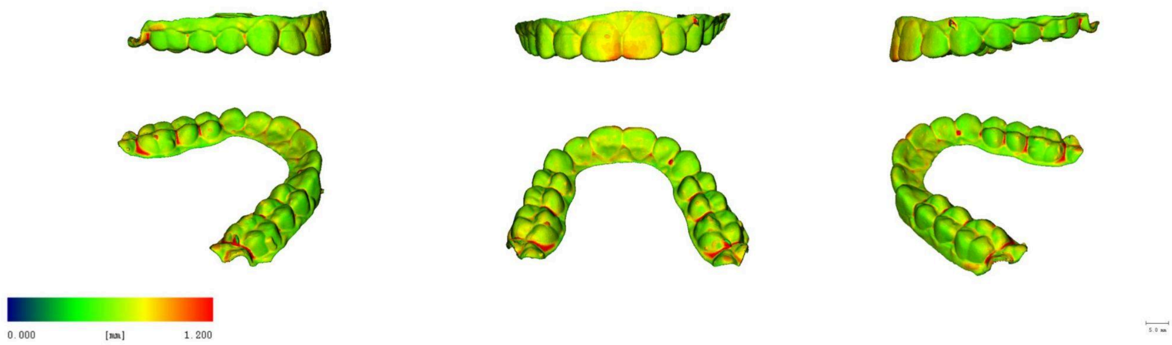

Figure 7-5 Representative renderings visualising the local material thickness of micro-CT scanned direct-printed aligners with a 20 min curing time (blue: 0.00 mm, red: 1.20 mm)

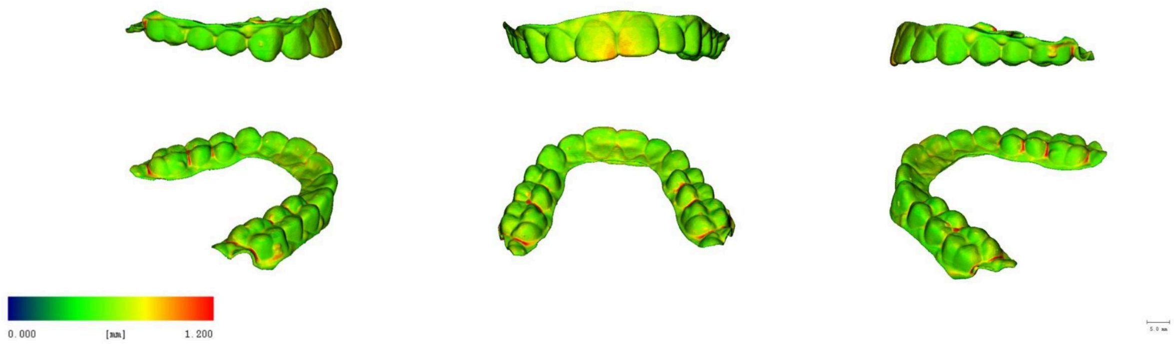

Figure 7-6 Representative renderings visualising the local material thickness of micro-CT scanned direct-printed aligners with a 25 min curing time (blue: 0.00 mm, red: 1.20 mm)

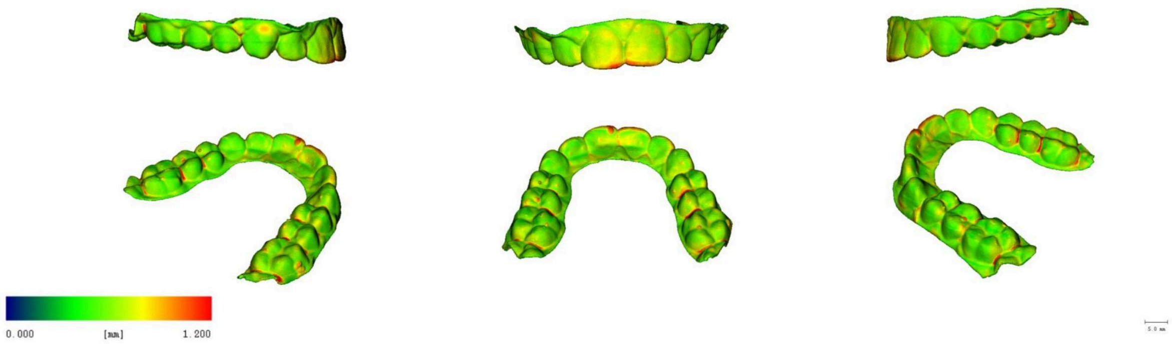

Figure 7-7 Representative renderings visualising the local material thickness of micro-CT scanned direct-printed aligners with a 30 min curing time (blue: 0.00 mm, red: 1.20 mm)

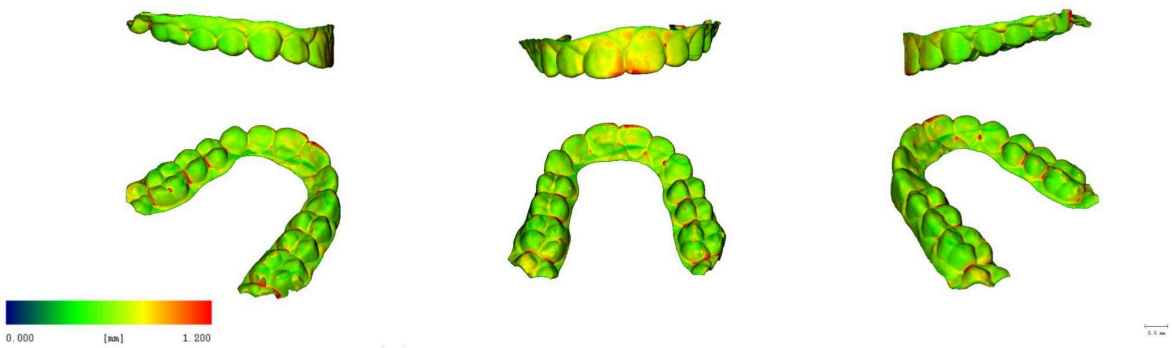

Figure 7-8 Representative renderings visualising the local material thickness of micro-CT scanned direct-printed aligners with a 40 min curing time (blue: 0.00 mm, red: 1.20 mm)

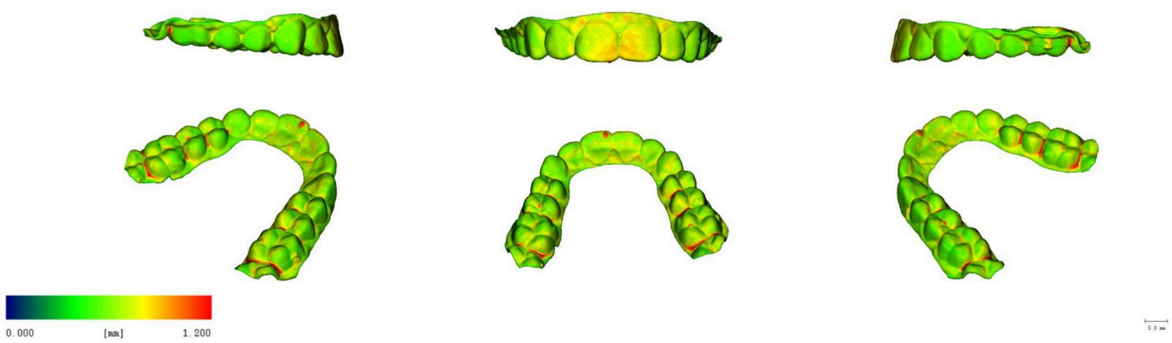

Figure 7-9 Representative renderings visualising the local material thickness of micro-CT scanned direct-printed aligners with a 50 min curing time (blue: 0.00 mm, red: 1.20 mm)

7.4. DISCUSSION

Previous studies on conventional aligners have shown that the final thickness of the device may depend on the thermoforming process and might be related to the geometry of the 3D-printed dental cast used for the production, which can vary according to different clinical conditions such as tooth shape and size, arch length, palatal vault depth, and alveolar bone height. Particularly, it was emphasised that within a single thermoformed aligner, different regions of the arch may present different thicknesses [11].

In the present study, no significant association was found between thickness values and curing time/conditions. Moreover, no differences in material heterogeneity were noticed among the groups. Despite this, and in line with previous studies, significantly higher thickness values were found at specific locations, i.e., central incisors and the mesiodistal centre of the central fissure. These observations confirm that direct 3D-printed aligners achieve a quite homogeneous output of the set initial thickness whereby they might present isolated locations of increased thicknesses.

Grassia et al. assessed the accuracy (trueness and precision) of orthodontic models and used four different 3D printers obtained from crowded and spaced dentition for the thermoforming of clear aligners. They concluded that accuracy was affected by the 3D printer employed as well as by the anatomical characteristics of the dental arches [12]. Interestingly, also in the present study, constant variation in thickness values was noted. Hence, also in the direct printing case, different thicknesses were found within single aligners, and further observations are needed to understand to what extent the thickness patterns remain the same for more irregular dentitions.

According to another study based on micro-CT scanning, aligners thermoformed over a higher model exhibited lower material thickness values, especially at facial and palatal surfaces [13]. In the cited study, differences in thicknesses between teeth ranged from 0.001 to 0.011 mm, whereas differences between locations ranged from 0.005 to 0.184 mm. In the present study, inter-reference point differences showed higher values, with a maximum of 0.27 mm (estimated difference between the central incisor and the canine). However, when related to the mean aligner thickness, in the worst case this difference shows a smaller weight than in the case of the thermoformed aligners (32.8% of the mean thickness rather than 57.5%), which were overall chosen to be much thinner.

Importantly, the aligner thickness can affect not only optical and aesthetical properties, but also the forces and moments expressed by the device, and exert an important influence on the orthodontic force applied to the teeth [6]. Particularly, the lack of homogeneity in thickness at different locations of the arch may lead to a reduced predictability of tooth movements. On the other hand, the homogeneity of thicknesses of 3D-direct-printed aligners has not yet been investigated and, in the present study, no biomechanical testing was performed to assess the clinical impact. Additionally, the intra-aligner heterogeneity may be less pronounced compared to the thermoformed ones, and with adequate 3D planning, it would be possible to modify the local thickness at specific sites for treatment purposes.

Coloured dimensional deviation maps (Figures 6–11) were generated in the present study to visualise positive and negative deviations from the planned thickness. The colours on the deviation maps resulted to be quite uniformly distributed among the different groups, with no differences regarding curing time. Therefore, the curing time did not seem to affect dimensional deviation, so we may infer that differences in resin shrinkage, according to the curing time, would not be observed over the minimal curing time suggested by the manufacturer, according to the first released protocol (15 min). The deviation maps provide instead a quick interface for recognising specific locations at which deviations were observed: these were particularly evident at the front teeth, at the interproximal level of posterior teeth, and at some isolated punctiform sites located on the cusps. We suppose that the positive deviation at the front teeth location was due to residual resin that, because of the 60° printing inclination and in spite of the centrifugation process, may have been incorporated into the area before post-curing, contributing to the local thickness increase. On the other hand, the joining of different surfaces may produce the thickness augmentation at the interproximal level of posterior teeth, while the different punctiform accumulation points correspond to some support insertion point.

According to Lee et al., the average thickness of the TC-85 specimens manufactured by 3D printing and photocured twice for 25 min under N2 was 0.56 mm, which was 12% higher than the set thickness of 0.5 mm (5). In the present study, the median vestibular thickness in the 25 min cured group was equal to the same value (0.56 mm), confirming the repeatability of the average thickness when the same printing and post-printing procedures are applied.

A very recent work took into account the thicknesses of thermoformed and 3D-printed clear aligners using micro-CT and reported that the median thicknesses of direct-printed aligners with a set-up thickness of 0.5 mm were 614.24 μm and 687.53 μm, respectively, according to the used cleaning procedure [8]. In fact, in the cited study, the first group was cleaned for 1 min with 99.5% IPA, the second one for 6 min and at 500 rpm using a centrifuge. Particularly, when considering buccal locations, the reported median [IR] thickness values are 579.34 μm, IR = [538.33–629.07] and 645.65 μm, IR = [614.24–676.19], which appear in the same range of our most similar subgroup: 560 μm IR = [510, 750], for the 25 min cured group which was, however, centrifuged twice for 5 min. Other differences with the cited study are that aligners were positioned at 30° as a print angulation with minimum supports, and a different 3D printer was used with a layer thickness of 50 μm.

However, in both our study and the cited one, a thicker output was observed in the anterior teeth compartment compared to the posterior teeth. We agree with the colleagues in suggesting that the augmented thickness of the anterior teeth in the 3D-printed aligners might have resulted from the fact that it is more difficult to remove any uncured resin remaining on the inner surface of anterior teeth.

Future studies are required to assess if specific resin from this site may be associated with increased cytotoxicity or allergenic risks.

7.5. CONCLUSIONS

In the present study on six groups of 3D-direct-printed aligners post-cured with a nitrogen generator for, respectively, 15 min, 20 min, 25 min, 30 min, 40 min, and 50 min, and one group cured for 30 min without the nitrogen generator, and taking into consideration 20 reference points, the local aligner thickness was assessed with a micro-CT scanner. No direct association was found between curing time and thicknesses. Nitrogen generator usage showed a significant effect on thickness. With a 60° printing inclination, and following the prescribed centrifugation process, a local thickness increase at the front teeth (with a median value of +0.15 mm at the central point of the incisal edge of +0.25 mm at the central point of the facial surface) was observed. Limitations of the present study include the following: First, the nitrogen effect was not investigated for all curing times as it was not our primary goal; in order to consider this factor, a much larger sample size would be required (two groups per curing time). Secondly, no biomechanical analysis was taken into account, and the impact of increased thickness in the front still needs to be studied. Eventually, the study was limited to a single printer/resin combination and future studies are needed to validate if the same patterns will be observed.

References

1. Boyer, R.A.; Kasper, F.K.; English, J.D.; Jacob, H.B. Effect of print orientation on the dimensional accuracy of orthodontic aligners printed 3-dimensionally. Am. J. Orthod. Dentofac. Orthop. 2021, 160, 732–742.e1.
2. Edelmann, A.; English, J.D.; Chen, S.J.; Kasper, F.K. Analysis of the thickness of 3-dimensional-printed orthodontic aligners. Am. J. Orthod. Dentofac. Orthop. 2020, 158, e91–e98.
3. Cole, D.; Bencharit, S.; Carrico, C.K.; Arias, A.; Tufekci, E. Evaluation of fit for 3D-printed retainers compared with thermoform retainers. Am. J. Orthod. Dentofac. Orthop. 2019, 155, 592–599.
4. McCarty, M.C.; Chen, S.J.; English, J.D.; Kasper, F. Effect of print orientation and duration of ultraviolet curing on the dimensional accuracy of a 3-dimensionally printed orthodontic clear aligner design. Am. J. Orthod. Dentofac. Orthop. 2020, 158, 889–897.

5. Mantovani, E.; Parrini, S.; Coda, E.; Cugliari, G.; Scotti, N.; Pasqualini, D.; Deregibus, A.; Castroflorio, T. Micro computed tomography evaluation of Invisalign aligner thickness homogeneity. Angle Orthod. 2021, 91, 343–348.
6. Lombardo, L.; Palone, M.; Longo, M.; Arveda, N.; Nacucchi, M.; De Pascalis, F.; Spedicato, G.A.; Siciliani, G. MicroCT X-ray comparison of aligner gap and thickness of six brands of aligners: An in-vitro study. Prog. Orthod. 2020, 21, 12.
7. Palone, M.; Longo, M.; Arveda, N.; Nacucchi, M.; De Pascalis, F.; Spedicato, G.A.; Siciliani, G.; Lombardo, L. Micro-computed tomography evaluation of general trends in aligner thickness and gap width after thermoforming procedures in-volving six commercial clear aligners: An in vitro study. Korean J. Orthod. 2021, 51, 135–141.
8. Park, S.Y.; Choi, S.H.; Yu, H.S.; Kim, S.J.; Kim, H.; Kim, K.B.; Cha, J.Y. Comparison of translucency, thickness, and gap width of thermoformed and 3D-printed clear aligners using micro-CT and spectrophotometer. Sci Rep. 2023, 13, 10921.
9. Hildebrand, T.; Rüegsegger, P. A new method for the model-independent assessment of thickness in three-dimensional images. J. Microsc. 1997, 185, 67–75.
10. R Core Team. R: A Language and Environment for Statistical Computing. R Foundation for Statistical Computing, Vienna, Austria. 2018. Available online: http://www.R-project.org/ (accessed on 19 August 2023).
11. Ammann, R.; Tanner, C.; Schulz, G.; Osmani, B.; Nalabothu, P.; Töpper, T.; Müller, B. Three-dimensional analysis of aligner gaps and thickness distributions, using hard x-ray tomography with micrometer resolution. J. Med. Imaging 2022, 9, 031509.
12. Grassia, V.; Ronsivalle, V.; Isola, G.; Nucci, L.; Leonardi, R.; Lo Giudice, A. Accuracy (trueness and precision) of 3D printed orthodontic models finalized to clear aligners production, testing crowded and spaced dentition. BMC Oral Health. 2023, 23, 352.
13. Ihssen, B.A.; Kerberger, R.; Rauch, N.; Drescher, D.; Becker, K. Impact of Dental Model Height on Thermoformed PET-G Aligner Thickness—An In Vitro Micro-CT Study. Appl. Sci. 2021, 11, 6674.

SWELLING ASSESSMENT AND LEACHING INSIDE ARTIFICIAL SALIVA

8.1. INTRODUCTION

A polymeric material which is immersed in a liquid medium undergoes a microstructural transformation, which depends on how the polymer chains interact with the medium and how much liquid phase enters into the polymer matrix, in a way that is related to the cross-linking degree of the polymer itself. Furthermore, this liquid flow may be reversible but it can determine a monomeric release into the liquid phase, and considering that the materials used are considered as toxic before the printing process, due to the large amount of people interested in using orthodontic aligners it becomes essential to assess the leaching of hazardous compounds, in order to guarantee patient safety [1]. Furthermore, the characteristics of aligner materials in a wet environment can affect their dimensional stability and clinical effectiveness, and therefore should be taken into account when choosing materials.

The purpose of this study was to assess the differences in weight variations over time between samples printed with the two above-mentioned different resins when they are immersed in a liquid medium (artificial saliva). This simplified environment was preferred to exclude subject-dependent variables, and was chosen to focus on what may happen when the main variable in sample preparation is the operator's compliance with the manufacturer's 3D printing and post-printing guidelines. Secondarily, differences between samples printed at different successive layers thicknesses (100µm and 50µm in the Z direction) were taken into account. The null hypothesis is that there is no difference in the swelling of samples printed with different resins, nor in the release of monomers in the liquid phase.

8.2. MATERIALS AND METHODS

8.2.1. Samples

The samples have been created from an STL file, using a CAD modeling software (UltiMaker Cura) and were designed in a dog-bone shape. The dog-bone had the following measures: overall width 10 mm, gauge width 5 mm and overall length 40 mm; thickness: 2 mm. The Tera Harz TC-85 resin (Graphy Inc., Seoul, Korea) and the Clear-A Senertek resin (Senertek, Karatas, Turkey) were used for sample production and samples were directly 3D printed using the instructions provided from the manufacturer. Hereby, the Phrozen Sonic XL 4k 2022 printer (Phrozen Technology, Hsinchu, Taiwan) was employed for the printing. Printing was conducted in successive layers of 100 µm (TC-85 resin, Group A0S), or 50 µm (TC-85 resin, Group B0S and Clear-A, Group E0S), with a down speed of 200 and a delay of 1000 ms. The first 6 layers were cured for 30 seconds. The height was 8 mm and the up speed was 100. The following layers were cured for 4 seconds with a 7 mm height and an up speed of 100. Supports were designed and planned using the Uniz software (Uniz, San Diego, California) to ensure the correct position on the printer plate. When the printing process terminated, the samples were removed from the plate and the supports were manually removed.

The resin excesses were accurately removed using a centrifuge spinning at 1000 revolutions per minute, which was used for 5 minutes two times. Thereafter, the samples were post cured for 20 minutes in a post curing unit (Cure M, Graphy, Seoul, Korea). The TC-85 samples were post-cured with a nitrogen generator, the Clear-A samples were cured without the nitrogen generator, according to the manufacturer’s instructions.

Each specimen was labeled and numbered with specific tags based on its group and type.
Inside the test tubes, 10 ml of artificial saliva (composed of 99% H_2O, and 1% electrolytes and proteins) were inserted, and the name of the sample contained (e.g., "A01S") was written on the outside.

8.2.2. Swelling Test

Five samples were chosen for each group. Therefore, a total of 15 samples were selected. To continue the project's development, all samples were weighed dry using a precision balance (Exacta P3, Munich, Germany) and subsequently placed inside the test tubes with artificial saliva in a thermostatic bath at 37℃ (Figure 8.1).

Figure 8-1 Set-up of the thermostatic bath

The swelling tests conducted consist of evaluating the weight increase of the sample after it has been immersed for 5', 10', 15', 30', 1h, 2h, 4h from the initial time and over a time frame of 11 days, which is even over the duration for which these dental aligners are installed. The samples were weighed at different frequencies. On the first day they were immersed, they were weighed according to the aforementioned time sequence. In the following days of the first week, they were weighed twice a day, in the morning and in the afternoon. In the second week, the samples were weighed once every two days. After the desired immersion time, the sample was removed from the test tube and any excess artificial saliva on the surface was dried using damp absorbent paper. The sample was then placed on the precision scale plate and the weight was recorded. Intraclass correlation coefficients (ICC) were calculated for 7 randomly selected samples. The weight of the dry sample was recorded by the same operator one time after a 10 days interval. The mean ICC value was greater than 0.98.

8.2.3. FTIR-ATR Spectroscopy

A FTIR-ATR spectrophotometer (Fourier Transform Infrared Attenuated Total Reflectance) was used (Thermonicolet 380, DTGS detector, OMNICTM software, v. 7.2, 100 scans) equipped with

ATR accessory (diamond crystal, ThermoFisher Scientific, Waltham, MA, USA) which utilizes the ATR technique to analyze solid or liquid samples directly on the surface of a high refractive diamond. ATR exploits the phenomenon of total internal reflection, where infrared light incident on the diamond surface is reflected inside the diamond itself, allowing for interaction with the sample in close proximity to the surface.

Results are reported as Absorbance versus wavenumbers, ν, with units of cm-1.
In our study, the possible release of materials into artificial saliva that came into contact with the samples was evaluated using FTIR analysis, and we used a control test tube of artificial saliva where no sample had been introduced as a reference. Four saliva samples were taken for group A0S, two for groups B0S and E0S and a small amount of control saliva were extracted and placed on the diamond using a micropipette. The FTIR-ATR operator was blind with respect to the tubes' labeling.

8.2.4. Statistical Analysis

To verify the normality of data, the Shapiro–Wilk test was used. Continuous variables are reported as means ± standard deviations (SD) or medians with interquartile range [IR] (whenever not normally distributed). Categorical variables are reported as a number and/or percentage. Additionally, when the data results were normally distributed, Levene's test for homogeneity of variances and the normality of residuals were validated.

A repeated measures ANOVA with group and time as factors was performed to assess the effects of time and group of samples and any relative interaction of the factors in weight variations over time . Differences with a p-value <0.05 were selected as significant. Data were acquired and analysed in the R v3.4.4in R v3.4.4 software environment [http://www.R-project.org/].

8.3. RESULTS

The results of the repeated measures ANOVA with time and group as factors are shown in Table 8.1

Table 8-1 Descriptive statistics and output of the repeated measures ANOVA for the relative weight increase of the samples (percentage). N, number of observations; Mean, mean difference; 95% Lower CI, 95% lower confidence interval of the difference; 95% Upper CI, 95% upper confidence interval of the difference; P value, repeated measures ANOVA Pr(F) value of the univariate effect for time and group respectively; Interaction, repeated measures ANOVA Pr(F) value of the group:time interaction. *: significant difference

	N	**Mean**	**95%Lower CI**	**95% Upper CI**	***P*-value**	**Interaction**
Time						
0’	15	0	-	-	<0.001*	<0.001*
5’	15	0.015	0.010	0.020		
10’	15	0.021	0.014	0.028		
15’	15	0.019	0.013	0.025		
30’	15	0.021	0.015	0.027		
60’	15	0.024	0.017	0.031		
120’	15	0.024	0.017	0.031		
240’	15	0.022	0.017	0.027		
Group					0.059	
A0S	5	0.80 (0.01)	0.792	0.808		
B0S	5	0.81 (0.02)	0.785	0.835		
E0S	5	0.77 (0.01)	0.758	0.782		

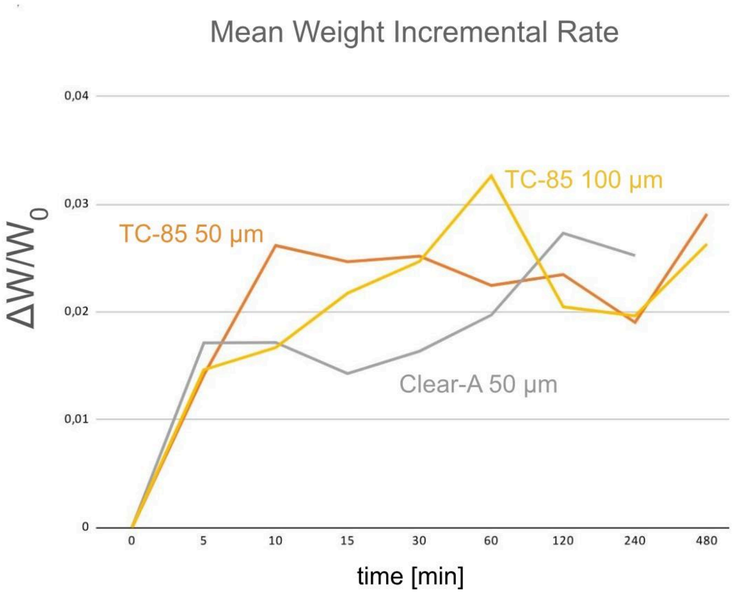

Figure 8-2 The mean value of the samples’ weight increases in the first 4 hours

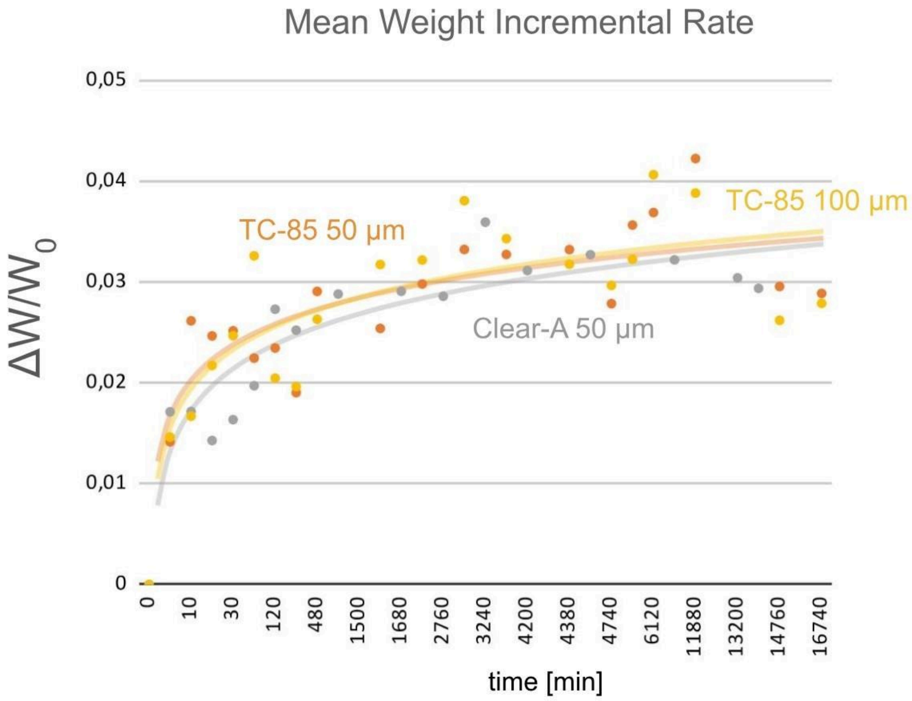

Figure 8-3 Mean value trend curves of the samples' weight in the first 11 days

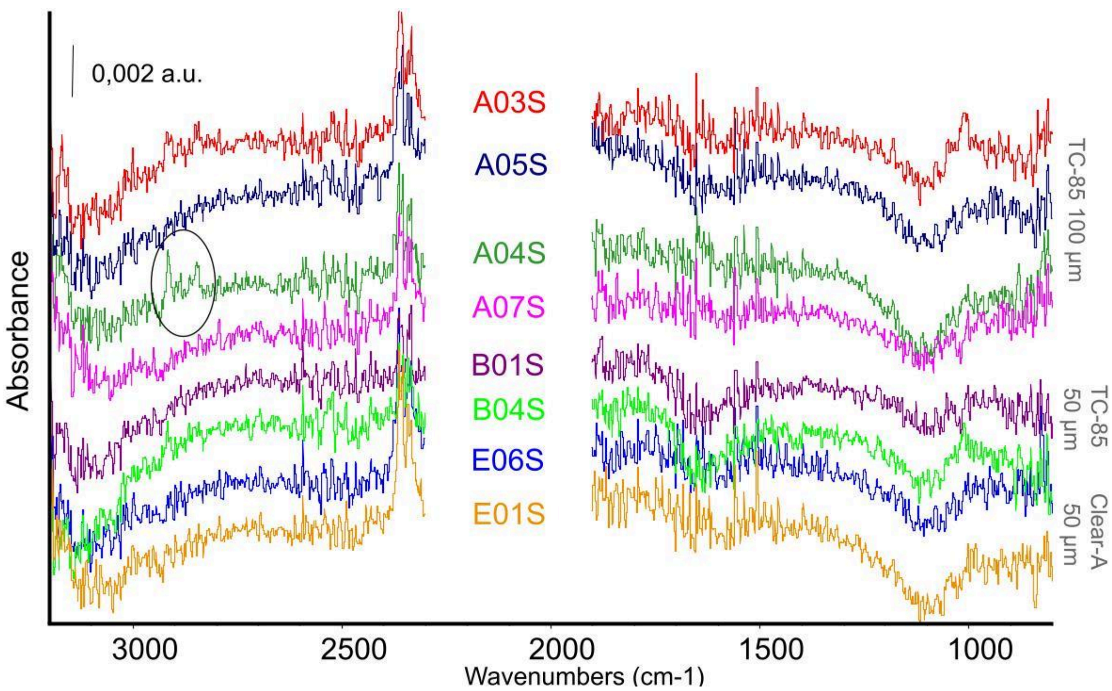

Figure 8-4 Frequency spectrum of the surnatant (artificial saliva). In the circle: spikes due to the stretching of the C-H bond

A significant longitudinal difference was found in the relative weight increase of the samples ($p<0.001$).

No significant differences were observed among groups ($p=0.059$). A significant group-time interaction was found ($p<0.001$).

The maximum weight increase in the first 4h was 3.6 %. The weight increase of the samples belonging to the A0S, B0S, and E0S groups shows a growing trend, with some "infinitesimal" oscillations that fall within an acceptable experimental uncertainty of 0.005. Trend curves of mean weight variations in the first 11 days are depicted in Figure 8.3.

The maximum weight increase in the 11 days period was 5.4% and it was reached after 54h in group E0S.

In Figure 8.4, the IR spectra obtained as the difference [spectrum obtained from the saliva sample under examination] – [spectrum of control saliva] are reported, magnified, in the spectral region of interest.

All the spectra show features due to residual, unsubtracted, water vapor and CO2 as background noise. Only in the IR spectrum of the saliva in which sample A04S was immersed, we can observe two very weak bands within the frequency range of 3000-2800 cm-1. Possibly, also the spectrum of sample A03S shows a similar signal. These bands relate to C-H stretching modes, which could be associated to the presence of organic species in the surnatant, that may be due to the dissolution of some polymeric resin components in the solution. However, an unambiguous assignment of these signals is limited by their very low intensity.

8.4. DISCUSSION

The problem of aging of orthodontic aligners has been addressed by the literature through different methodologies. The study of Condò at al. took into consideration Scanning Electron Microscopy before and after aging tests in different solutions of aligners made of multilayer aromatic thermoplastic polyurethane/copolyester polymers. The authors calculated a percentage weight relative variation of the samples as well and they found that no one of the samples, after the aging procedure, released any compound in terms of weight loss. Conversely, one of the polymers was subjected to a small increase in weight (about 2%) at the first contact with Phosphate Buffered Saline solution and a higher increment (almost 20%) when subjected to largely acid solution (10 M Orthophosphoric acid) [2].

In the present study on artificial saliva the mean weight increase in the first hour was estimated between 1.5% and 3%, with local variations depending on the considered type of resin/resolution.

This weight increase is an important indicator of sensitivity to liquid substances, because the absorption capacity, in addition to an increase in weight, will also determine an expansive volumetric change which can affect the adhesion of the aligner to the dental arches: often only a few hours after the first fitting, the patient experiences a looser and less tenacious adhesion of the aligner to the dental arch, which could induce a less effective mechanic reply. Moreover, water sorption could alter the application of orthodontic forces. In fact, a first insight on the changes in mechanical properties induced by the wet environment, even though the temperature may have played a role as well, comes from a previous experiment of ours, where dogbones samples of Tera Harz TC-85 resin underwent tensile tests at room temperature as they were kept dry, or after receiving a 1 min bath at 80°C (which is the action currently performed before giving the aligner to the patient). This experiment (not yet published) showed that the median tensile modulus was 454.42 MPa (Interquartile Range = [394.59, 471.89]) in the case of dry samples and 111.82 MPa (Interquartile Range = [86.75, 129.58]) in the case of wet samples and the difference by applying a Mann-Whitney U test was significant ($p = 0.002$).

The literature reports studies that have performed FTIR spectroscopy on dental aligners as well, such the one by Memé et al., which took into consideration the changes occurring in a particular type of thermoformed aligners exposed in vitro to coffee, tea, Coca Cola® and UV radiation for 24 and 48 h.

ATR-FTIR suggested that the chemical properties of the analyzed aligners were not affected by the exposure to the tested beverages and that the chemical characteristics were mostly preserved [3].
In another study, bright-field optical reflection microscopy on samples of thermoformed aligners before and after intraoral placement revealed abrasion at the cusp tips, adsorption of integuments, and localized calcification of the precipitated biofilm at stagnation sites, while FTIR microscopic analysis of the samples appliances revealed no release of traceable monomers or byproducts after immersion in an ethanol-water solvent [4].

In the present study ATR-FTIR spectroscopy was utilized to characterize, at the molecular level, any possible chemical modifications in the surnatant. The weight loss of the samples belonging to group A0S, as we can see in Figure 2, could be related to the appearance of bands due to C-H stretching modes, diagnostic of the presence of organic compounds.

Some other studies described the problem of aging in terms of mechanical interactions and wear. Elshazly et al. investigated the effects of artificial aging by thermocycling and mechanical loading on force/torque delivery by thermoplastic orthodontic aligners and they found a significant decrease in force/torque generation where mechanical loading had a greater impact than pure thermocycling [5], so that a complete picture on the problem of aging should take into consideration Flexural modulus, hardness, glass transition temperature (Tg), elastic and stress decay through a period of several days, viscous modulus, and loss factor [6,7].

Limitations of this study include the fact that the main factor that distinguishes the oral cavity from in vitro media is the presence of complex oral flora and their byproducts, as well as the accumulation of plaque on the material [8,9]. In fact, during the treatment period, bacteria, salivary enzymes, moisture and heat changes too may affect the characteristics of aligners [10]. Also pH changes, enzymatic activity, and mechanical stress from insertion and removal may influence aging effects. FTIR analysis was carried out only qualitatively, in order to obtain a direct comparison among all the samples in the chosen diagnostic spectral regions. Finally, to detect trace amounts of potentially critical leachables (e.g., residual monomers) and to enhance the sensitivity of the analytical methods, High-Performance Liquid Chromatography (HPLC) or GC-MS may be employed, to provide a more robust and quantitative assessment of material biocompatibility.

In this study, FTIR spectroscopy evidenced only in some samples very weak signals due to C-H stretching modes, which could be associated to the presence of organic species in the surnatant. However, no calibration curves have been created in this experimental setup and conclusions on which amount of leaching is clinically relevant cannot be drawn.

The weight increase of the samples belonging to the different groups showed a growing trend, with no significant difference between resins or layer thicknesses. The E0S group recorded a lower weight increase that, while not significant, may open the hypothesis that a different curing procedure (the E0S group was the only one cured without nitrogen generator) interferes with liquid sorption;, even though this was not an outcome for the present study, nitrogen-assisted post-curing may be a critical parameter in understanding the behaviour of the resins in the liquid medium, and it could deserve a systematic investigation. Another recent study stated that 3D-printed aligners Tera Harz TC85 and Clear A showed distinct absorption profiles [11], but the parameters chosen to describe the phenomenon are not comparable.

8.5. CONCLUSIONS

In the present study on 3D printed dog-bone samples with different resolutions (100μm and 50μm) or resins when they are immersed in artificial saliva, the maximum weight increase recorded in the first 4h was 3.6 %. The maximum weight increase in the 11 days period was 5.4% The release of organic compounds by polymer resins during the artificial aging process, monitored by FTIR of the liquid medium, appeared to be minimal under these simplified experimental conditions. Further studies, including the oral flora, their byproducts, pH changes, enzymatic activity, and mechanical stresses from insertion and removal of aligners are needed in order to fully understand the clinical eventuality and implications of leaching.

References

1. Willi A, Patcas R, Zervou SK, Panayi N, Schätzle M, Eliades G et al. (2023) Leaching from a 3D-printed aligner resin. Eur J Orthod 45, 244-249.
2. Condò R, Mampieri G, Giancotti A, Cerroni L, Pasquantonio G, Divizia A et al. (2021) SEM characterization and ageing analysis on two generation of invisible aligners. BMC Oral Health, 21, 316.
3. Memè L, Notarstefano V, Sampalmieri F, Orilisi G, Quinzi V (2021) ATR-FTIR Analysis of Orthodontic Invisalign® Aligners Subjected to Various In Vitro Aging Treatments. Materials 14, 818.
4. Schuster S, Eliades G, Zinelis S, Eliades T, Bradley TG (2004) Structural conformation and leaching from in vitro aged and retrieved Invisalign appliances. Am J Orthod Dentofacial Orthop, 126, 725-728.
5. Elshazly TM, Nang D, Golkhani B, Elattar H, Keilig L, Bourauel C (2023) Effect of thermomechanical aging of orthodontic aligners on force and torque generation: An in vitro study. J Mech Behav Biomed Mater 143, 105911.
6. Dalaie K, Fatemi SM, Ghaffari S (2021) Dynamic mechanical and thermal properties of clear aligners after thermoforming and aging. Prog Orthod 22, 15.
7. Albertini P, Mazzanti V, Mollica F, Pellitteri F, Palone M, Lombardo L (2022) Stress Relaxation Properties of Five Orthodontic Aligner Materials: A 14-Day In-Vitro Study. Bioengineering 9, 349.
8. Eliades T, Bourauel C (2005) Intraoral aging of orthodontic materials: the picture we miss and its clinical relevance. Am J Orthod Dentofacial Orthop 127, 403-12.
9. Selvaraj M, Mohaideen K, Sennimalai K, Gothankar GS, Arora G (2023) Effect of oral environment on contemporary orthodontic materials and its clinical implications. J Orthod Sci 12, 1.
10. Yazdi M, Daryanavard H, Ashtiani AH, Moradinejad M, Rakhshan V (2023) A systematic review of biocompatibility and safety of orthodontic clear aligners and transparent vacuum-formed thermoplastic retainers: Bisphenol-A release, adverse effects, cytotoxicity, and estrogenic effects. Dent Res J 20, 41.
11. Šimunović L, Miličević AM, Brenko L, Haramina T, Meštrović S (2025). Absorption and desorption dynamics of thermoformed and 3-dimensional-printed orthodontic aligners. Am J Orthod Dentofacial Orthop :S 0889-5406(25)00170-2.

EVALUATION OF THE WETTABILITY OF NOVEL AND CONVENTIONAL MATERIALS FOR THE PRODUCTION OF ORTHODONTIC ALIGNERS

9.1 INTRODUCTION

Wettability, along with other factors such as surface composition and roughness, plays a crucial role in bacterial adhesion. In fact, materials with a low contact angle, such as hydrophilic surfaces, tend to promote bacterial adhesion and biofilm formation, while those with a high contact angle (hydrophobic surfaces) are less prone to this type of adhesion. The aim of the present study is to evaluate the wettability of materials used for the production of conventional and 3D direct printing orthodontic aligners.

9.2 MATERIALS AND METHODS

Tera Harz TC-85 resin samples printed at a 100 µm resolution from three different printers (Phrozen Sonic XL 4K, Accufab L4D and Uniz NBee), Tera Harz TA-28 resin samples printed at a 100 µm resolution (Uniz NBee printer), Tera Harz TC-85 resin samples printed at a 50 µm resolution (Phrozen Sonic XL 4K, and Accufab L4D), Senartek Clear-A (Phrozen Sonic XL) printed at a 50 µm resolution, PETG, thermoformed PETG and Align material were examined, for a total of 19 samples. Each sample was tested three times. To extract the liquid, a sterile syringe was used to withdraw a quantity of physiological saline solution from a beaker, which was then placed as drops onto the sample. For the experiment, a Dino-Lite digital microscope was employed, allowing for the correct positioning of the sample and the application of the liquid drops. The microscope was connected to a PC; using the Dino-Capture 2.0 software, which displayed an enlarged image of the profile of the drops on the screen. The images were taken right after the droplet positioning.

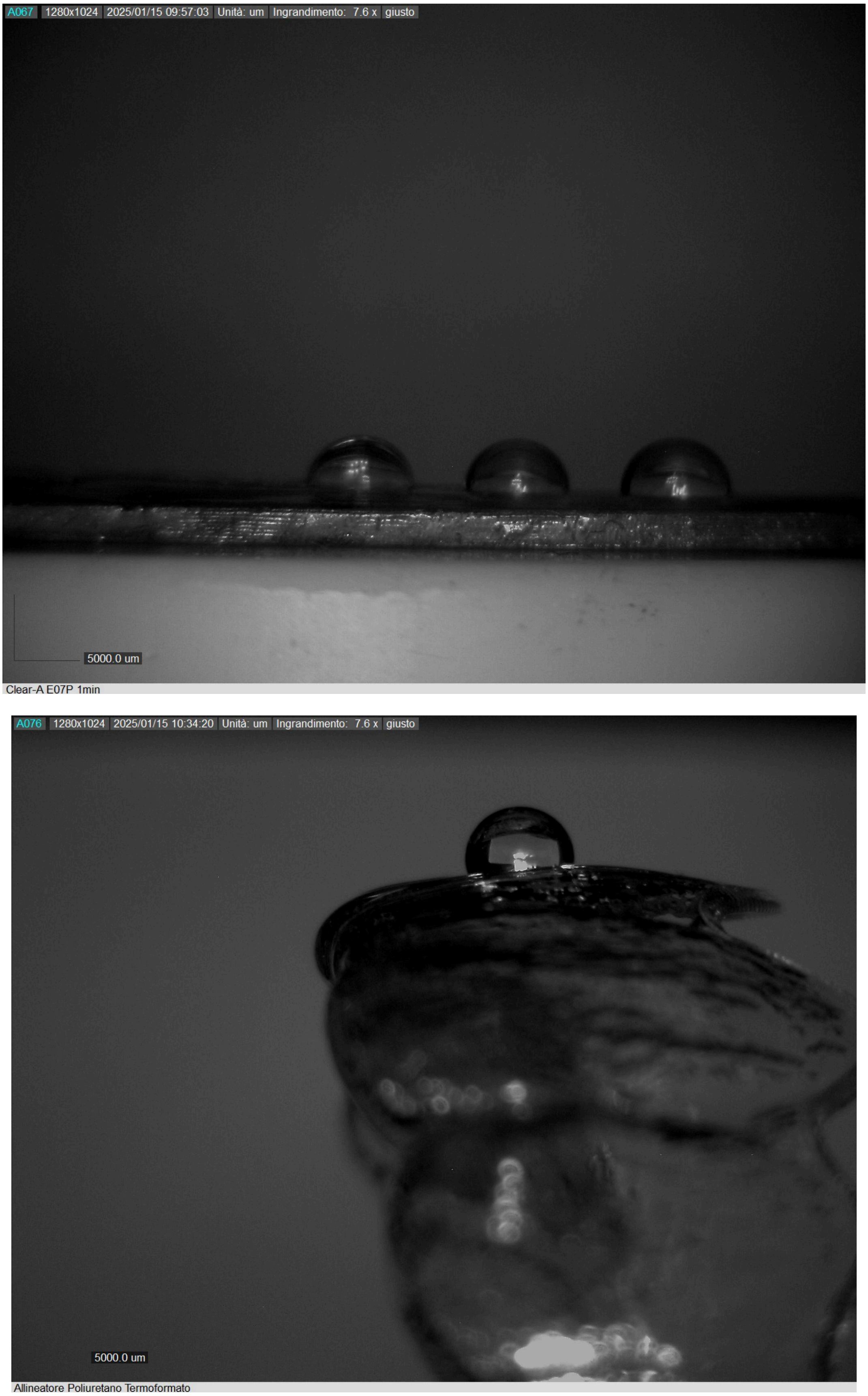

Figure 9-1 Direct printing samples and polyurethane aligner (thermoformed), with a drop of physiological saline solution

Using AutoCAD software, the profiles of droplets placed on material samples were analyzed, determining wettability (i.e. contact angle) values.

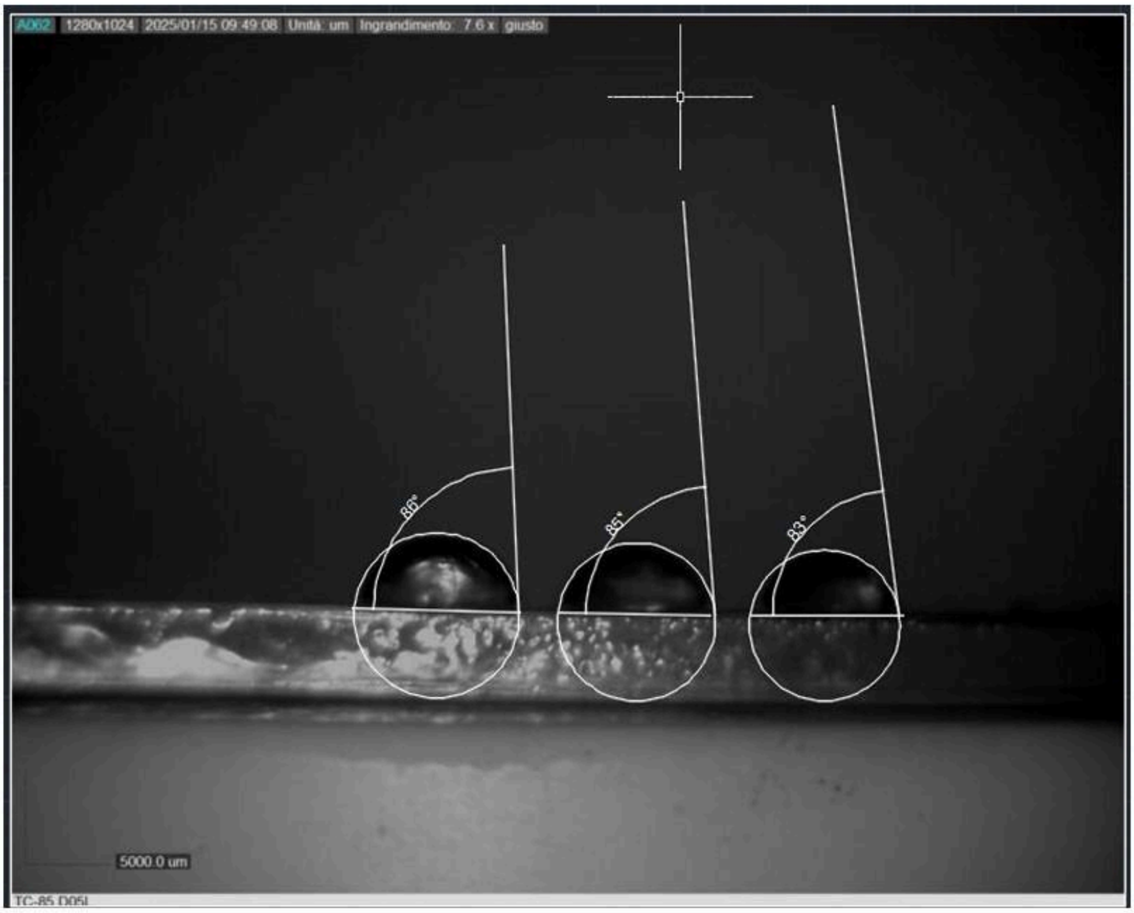

Figure 9-2 Direct printing sample, with 3 drops of physiological saline solution and respective contact angles

The collected data were organized into Excel tables to compare the behavior of the materials.To verify the normality of data, the Shapiro–Wilk test was used. Continuous variables are reported as medians and interquartile range. To evaluate differences among groups, the Kruskall-Wallis test was used, followed by a post hoc multiple comparison Bonferroni test. Differences with a p-value <0.05 were selected as significant. Data were acquired and analyzed in the R v3.4.4 software environment.

Table 9-1 Contact angle at T0.
PETGTF: thermoformed PETG samples;
PETG: PETG samples;
A: Tera Harz TC-85 resin samples printed at a 100 µm resolution (Phrozen Sonic XL 4K printer);
B: Tera Harz TC-85 resin samples printed at a 50 µm resolution (Phrozen Sonic XL 4K printer);
C: Tera Harz TC-85 resin samples printed at a 100 µm resolution (Accufab L4D printer);
D: Tera Harz TC-85 resin samples printed at a 50 µm resolution (Accufab L4D printer);
E: Senertek Clear - A resin samples printed at a 50 µm resolution (Phrozen Sonic XL 4K printer);
X: Tera Harz TC-85 resin samples printed at a 100 µm resolution (Uniz NBee printer);
Y: Tera Harz TA-28 resin samples printed at a 100 µm resolution (Uniz NBee printer);
Results are expressed as Median [Interquartile Range]; p-value**:** Kruskall–Wallis test *p*-value

Gruppo	Contact Angle (°)
PETGTF	76.50 [74.58, 78.83]
PETG	77.75 [77.25, 79.50]
A	69.33 [68.17, 69.83]
B	66.67 [64.83, 68.83]
C	71.17 [70.08, 72.33]
D	79.33 [76.67, 82.17]
E	78.67 [68.08, 89.33]
X	63.00 [53.12, 74.25]
Y	64.50 [63.62, 66.25]
Align material	102.50 [101.75, 103.25]
p-value	0.010*

9.3 RESULTS

The highest angle was recorded on the conventional material (102.50°, IR= [101.75, 103.25]), while the lowest was on the TC-85 samples printed at a 100 µm resolution (63.00° IR = [53.12, 74.25]). Overall, the differences between materials resulted as significant (p=0.010), the differences between printers did not.

9.4 CONCLUSIONS

3D direct printing materials resulted as less hydrophobic than traditional materials. Provided that wettability refers to the ability of a liquid (saliva) to maintain contact with a solid surface, this information suggests that patients may experience a greater friction between the aligner and the soft tissues (cheeks and lips) with this type of material.

Moreover, this property may give us information on how the aligner interacts with the oral biofilm: varying on the surface roughness, a higher wettability may enhance the bacterial adhesion.

BIOCOMPATIBILITY

10.1 INTRODUCTION

Dental aligners are indeed in direct contact with the oral mucosa for extended periods, which necessitates rigorous testing for cytotoxicity and cellular responses. The interaction of the resins with human cells is therefore critical to their safety and effectiveness. For example, it has been reported that the release of potentially harmful substances, such as bisphenol A (BPA), from 3D printed aligners can lead to adverse effects, including cytotoxicity and genotoxicity [1]. Given the increasing use of these materials in orthodontics, it is essential to conduct comprehensive biocompatibility and mechanical assessments to ensure that these devices do not pose risks to patients.

Cell proliferation and cell adhesion assays were performed on two cell lines to evaluate the biological safety of the proposed materials.

10.2 MATERIALS AND METHODS

10.2.1 Cell assays with human osteosarcoma cells

The test samples were prepared with three different resins in a disk geometry with a thickness of 0.5 mm and a diameter of 0.6 mm. TC-85 (Graphy Inc., Seoul, Korea) and Clear A resin (Senertek, Karatas, Izmir, Turkey) samples were prepared with the Phrozen Sonic XL 4K printer set with a 100 μm resolution. DCA (LuxCreo, Chicago, IL, U.S.A) samples were fabricated through direct 3D printing using an iLux Pro Dental 3D printer (LuxCreo, Chicago, IL, U.S.A.). Following printing, residual resin of TC-85 and Clear A samples was removed by centrifugation at 1000 rpm for two cycles of 5 minutes each and supports were removed. Post-curing was performed under controlled conditions; in particular, the samples were post-cured for 20 minutes using the Tera Harz Cure unit (Graphy Inc., Seoul, Korea).

To remove any residual resin from the DCA samples after printing, a two-stage ultrasonic washing in IPA (>99%) was performed at room temperature (iLuxWash Dental) for 8 minutes (4 minutes for each stage). Post-curing was carried out using a iLuxCure Pro curing unit (LuxCreo, Chicago, IL, U.S.A.) for 20 minutes, no nitrogen, as per the manufacturer’s instructions. The supports were subsequently manually eliminated.

Samples from each set were maintained under sterile conditions to evaluate the adhesion of human osteosarcoma cells (MG-63), previously obtained from the Cell Bank and Cell Factory (Istituto Nazionale per la Ricerca sul Cancro, Genova, Italy). Cells were maintained at 37°C in a humidified atmosphere at 5% CO2. F12-medium (Biochrom AG, Berlin, Germany) and Dulbecco's modified Eagle's Medium (DMEM, high glucose, EuroClone S.p.A., Milan, Italy) were used for the growth of cells under standard culture conditions. The final DMEM/F12 medium (50:50) was supplemented with 2 mM L-glutamine and 10% fetal bovine serum (FBS). To prevent cell adhesion to the well plate, the 12-well plates were pre-coated with 1% agarose.

To assess cell adhesion on the material samples, 15,000 cells were seeded within each well onto the material samples (one per well) and allowed to adhere by gravity for 48 hours. The plates were incubated at 37°C under standard humidity conditions in 2 mL of complete medium per well. Following incubation, samples were gently washed twice with PBS to remove non-adherent cells. The adhered cells were fixed using 4% paraformaldehyde (PFA) for 10 minutes at room temperature. Subsequently, samples were stained with a methylene blue solution for 5 minutes at room temperature to visualize adherent cells. The excess stain was removed by rinsing the samples five times with PBS. The samples were then imaged using a Nikon SMZ1000 stereomicroscope (Nikon Instruments, Tokyo, Japan) equipped with a Nikon DS5 camera and accompanying imaging software.

Cell viability and metabolic activity were assessed using the Presto BlueTM assay (Invitrogen Presto Blue TM Cell Viability Reagent, cat. n. A13262, ThermoFisher, Monza, Italy), as already reported in the literature [2,3]. The analysis was conducted on both samples in direct contact with the cells seeded in the wells and on cultures set up in transwell systems. In the transwell setup, the materials were placed on supports equipped with perforated membranes with 0.4 µm pores, allowing them to be suspended in the culture medium without direct contact with the cells. Control samples refer to cell growth in contact with the plastic well.

At different time points the Presto Blue dye was added at 10% v/v to the culture medium and incubated for 4 hours. At the end of the incubation period, the supernatant was collected, briefly decanted and centrifuged gently (approximately 400 × g for 5 minutes) to recover any cells remaining in suspension. The supernatant was then analyzed spectrophotometrically using a Spectra MR multiplate reader spectrophotometer (Dynex Technologies; Chantilly, VA, USA) by measuring absorbance at 570 nm and 600 nm. Spectrophotometric analyses of Presto Blue metabolism products were performed at 0-, 2-, 4-, and 7-days post-seeding to monitor cell viability and metabolic activity over time. The results were calculated as the average of treatment replicas normalizing each 570 nm reading to its corresponding value at 600 nm, subtracting the average blank value, and normalizing the results at each time point to the initial reading at T0, as already reported in the literature [4].

10.2.2 Cell assays with lymphoblastoid cells

To further assess the biocompatibility of TC-85 and Clear A materials, a human lymphoblastoid cell line immortalized with Epstein-Barr virus (designated D430B) was employed. These cells are particularly relevant for understanding scenarios such as a ruptured vessel or oral bleeding, where circulating white blood cells are present. Samples from both sets were sterilized as described earlier and utilized for cell culture experiments under direct contact or by employing a set-up with transwells. D430B cells, which proliferate in suspension and do not adhere to culture plates, were previously expanded under standard culture conditions (RPMI medium supplemented with 2 mM glutamine and 10% FBS). Experiments were conducted in 12-well plates, maintaining the cells at 37°C with standard humidity and 1 mL of medium per well. Cell viability and metabolic activity were assessed as reported in the previous paragraph..

10.3 RESULTS

The results from both direct contact tests and the transwell systems (Figure 10.1 (a)) provide a comprehensive evaluation of the materials' effects on cell viability and metabolic activity, highlighting the impact of both direct and indirect interactions between the cells and the tested materials.

In the cell adhesion experiments using MG-63 osteoblast-like cells, neither material supported cell attachment. Instead, cell aggregates were observed, as is typical when cells cannot find a suitable substrate for adhesion. In some instances, these aggregates remained on the material surfaces, as indicated by the red arrows in Figure 10.1 (b). Additionally, cultures of MG-63 cells were maintained in contact with the materials to assess cell proliferation and viability via the Presto Blue assay. After 4 and 7 days, no significant differences in cell proliferation or viability were observed between the two materials, as shown in Figure 10.1 (c). However, both materials exhibited reduced cell growth compared to the control, where cells adhered to plastic. This decrease in growth is likely attributed to a mechanical effect, where the physical interaction with the materials may cause detachment of some cells during the experimental procedure.

Figure 10.1 (d) shows the proliferation rate of MG-63 cells cultured in transwell systems with TC-85 and Clear A resins over seven days, compared to a control. Over time, the control showed steady growth, reaching a proliferation rate of 3.21-fold -fold by day 7. Similarly, Clear A demonstrated consistent cell growth, achieving a comparable final rate of 3.13-fold by day 7. However, TC-85 exhibited a significantly reduced proliferation rate at day 7, with a final value of 2.74-fold, showing a statistically significant difference (**$p < 0.01$) compared to both the control and Clear A. A similar trend was observed for the DCA resin, which was tested with the same method in a different moment (Figure 10.2).

The proliferation analysis of D430B cells on the two resins, TC-85 and Clear A, reveals slightly distinct behaviors (Figure 10.1 (e)). In the first 48 hours, cells grown on Clear A exhibit a faster initial proliferation rate (similar to the behavior on MG-63 (Figure 10.1 (c)), increasing to approximately 1.3-fold, while cells on TC-85 resin show a slightly slower rate, reaching approximately 1.2-fold. However, after day 2, the proliferation rate on Clear A appears to plateau at around 1.5-fold, suggesting potential limitations in sustaining long-term cell growth. In contrast, cells on TC-85 exhibit a more consistent and sustained proliferation rate, reaching approximately 1.5-fold by day 4 and 1.7-fold by day 7 without, however, having a statistically significant difference after 7 days of culture (Figure 10.1 (e)).

In the Transwell setup (Figure 10.1 (f)), where cells are cultured indirectly with the materials, a similar trend is observed. Initially, Clear A supports slightly faster cell proliferation (1.8-fold by day 2 vs. 1.6-fold on TC-85). However, Clear A once again reaches a plateau (approximately 1.9-fold by day 4), while TC-85 sustains a more progressive proliferation rate, achieving 2.1-fold by day 4 and approximately 2.2-fold by day 7.

10.4 DISCUSSION

As recently reported in the literature, very few studies have been conducted to study the cytotoxicity of 3D printing resins and their products. The results presented here indicate that both TC-85 and Clear A materials, when tested under direct and indirect contact conditions, do not exhibit cytotoxic effects that would impair cell viability or proliferation. The observed lack of cell attachment on both materials in the direct contact tests is noteworthy, as it suggests that neither material promotes favorable conditions for cell adhesion. This is particularly relevant in applications such as dental aligners, where preventing cell growth on the surface of the device can be advantageous. The inability of the cells to adhere to these surfaces may be beneficial, as it can prevent cell growth originating from minor lesions in the buccal epithelium on the mobile surfaces of the device. The reduced growth compared to the control group, where cells were adhered to plastic, can likely be attributed to mechanical effects. The physical interaction between the cells and the materials during the experimental procedure may cause detachment of some cells, potentially affecting the proliferation rate.

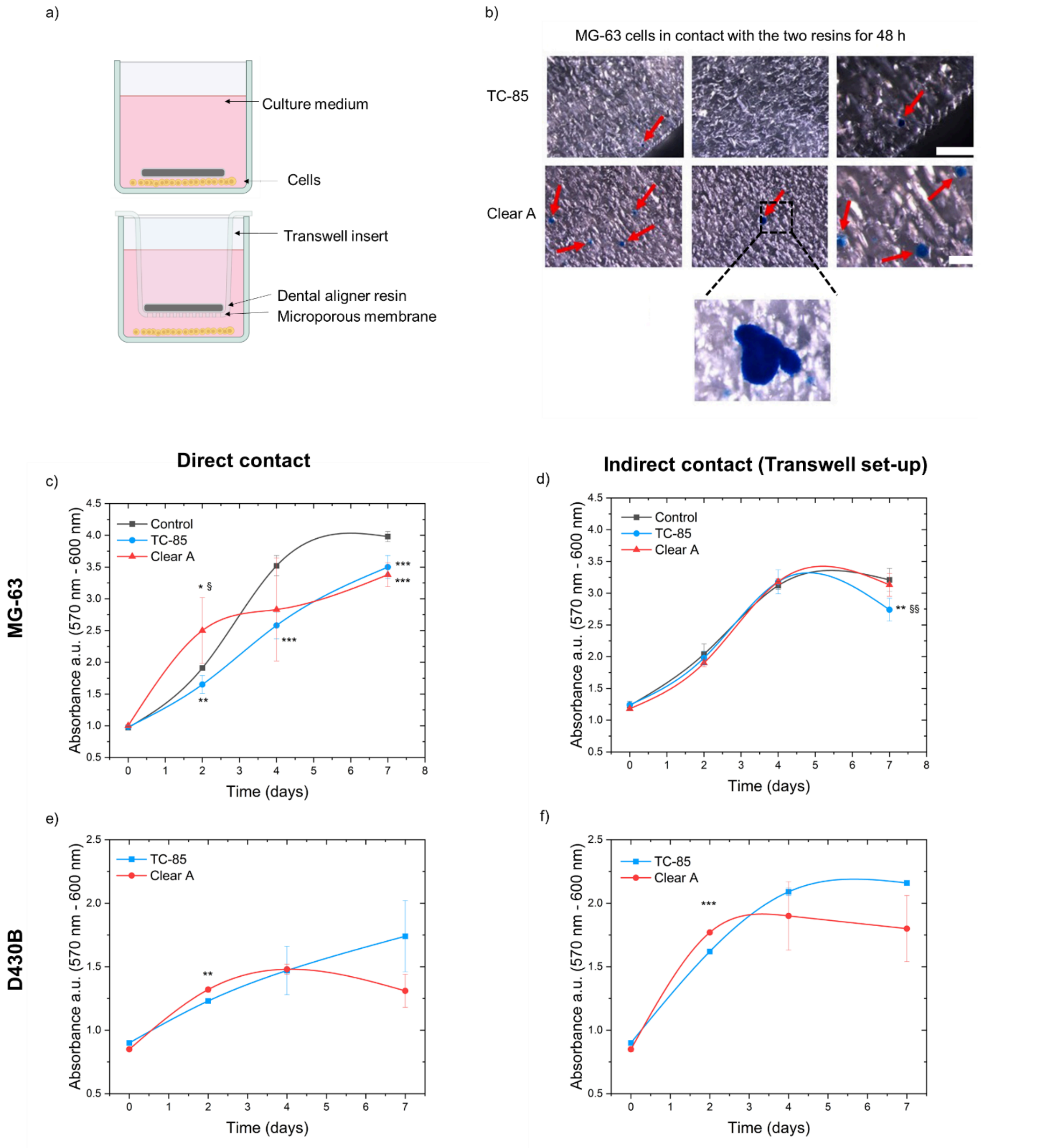

Figure 10-1 Evaluation of MG-63 and D430B cell proliferation in direct and indirect contact with two resins (TC-85 and Clear A) over 7 days. (a) Schematic of the experimental setups for direct contact and indirect contact using a transwell system. (b) Optical microscopy images of MG-63 cells after 48 hours of direct contact with the resins, with red arrows indicating cellular aggregates stained with methylene blue. Proliferation of MG-63 cells under direct (c) and indirect (d) contact. Proliferation of D430B cells under direct (e) and indirect (f) contact. Data points depict mean values ± SD of 5 independent determinations. Scale bar = 0.5 mm. * $p < 0.05$, ** $p < 0.01$, *** $p < 0.001$ (TC-85 or Clear A vs control), § $p < 0.05$, §§ $p < 0.01$ (Clear A vs TC-85)

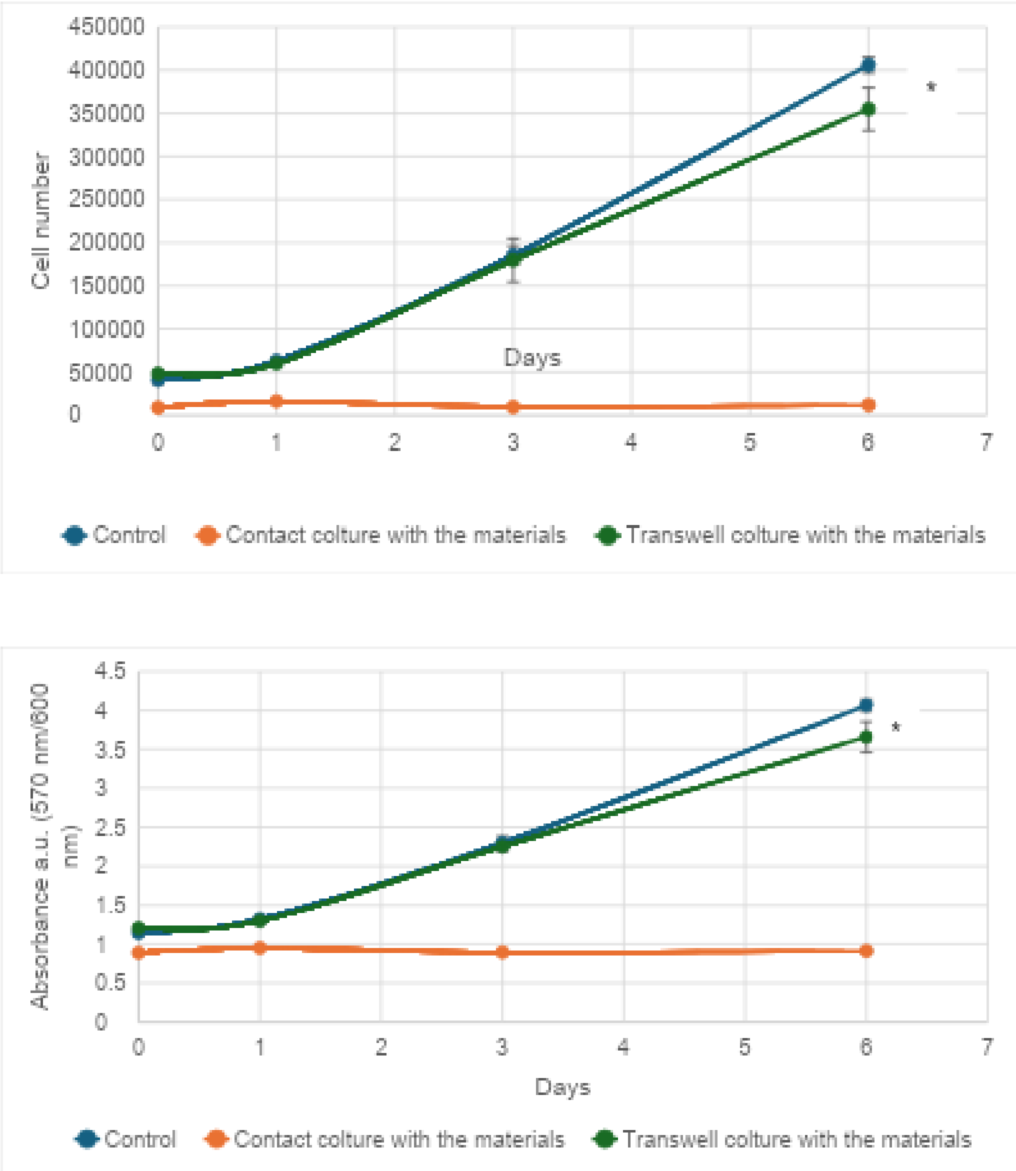

Figure 10-2 Evaluation of MG-63 cell proliferation in direct and indirect contact with the DCA resin over 7 days

This observation suggests that the materials themselves do not release any cytotoxic or inhibitory substances under the conditions tested, as evidenced by the similar proliferation trends observed in the transwell experiments, where cell growth was sustained but at a slower rate than the control. The comparison of D430B cell proliferation on TC-85 and Clear A reveals slightly different growth patterns, with Clear A initially promoting a faster proliferation rate but plateauing after day 2. Therefore, based on the results of both direct and indirect contact experiments, neither material appears to have any cytotoxic or cytostatic properties, and they both support cell viability, albeit at slower rates than cells grown on plastic controls.

10.5 CONCLUSIONS

The tested resins did not elicit cytotoxic responses in MG-63 or D430B cells, either through direct or indirect exposure. While they do not promote cell adhesion or proliferation in direct contact, they appear biologically inert and safe for applications involving transient or indirect tissue contact.

References

1. Francisco I, Paula AB, Ribeiro M, Marques F, Travassos R, Nunes C, Pereira F, Marto CM, Carrilho E, Vale F. The biological effects of 3D resins used in orthodontics: a systematic review. Bioengineering 2022;9.
2. Marrella A, Dondero A, Aiello M, Casu B, Olive D, Regis S, Bottino C, Pende D, Meazza R, Caluori G, Castriconi R, Scaglione S. Cell-laden hydrogel as a clinical relevant 3D model for analyzing neuroblastoma growth, immunophenotype, and susceptibility to therapies. Front Immunol 2019;10.
3. Marrella A, Tedeschi G, Giannoni P, Lagazzo A, Sbrana F, Barberis F, Quarto R, Puglisi F, Scaglione S. “Green-reduced” graphene oxide induces in vitro an enhanced biomimetic mineralization of polycaprolactone electrospun meshes. Mater Sci Eng C 2018;93:1044–53.
4. Alfei S, Giannoni P, Signorello MG, Torazza C, Zuccari G, Athanassopoulos CM, Domenicotti C, Marengo B. The remarkable and selective in vitro cytotoxicity of synthesized bola-amphiphilic nanovesicles on etoposide-sensitive and-resistant neuroblastoma cells. Nanomaterials 2024;14.

THERMALLY EXCITED GEOMETRIC RESTORATION OF DIRECT-PRINT ORTHODONTIC ALIGNERS AGAINST CREEP DEFORMATION: A QUANTITATIVE STUDY

11.1 INTRODUCTION

Limitations in the predictability of clear aligner orthodontics [1,2] stems from multiple factors, with the inevitable viscoelastic creep of clear aligner materials being an important contributor [3,4]. Clear aligners operate predominantly *via* a displacement-driven mechanism [5,6], which critically depends on maintaining the aligner's geometric integrity throughout treatment. However, while applying force to the teeth, the aligner’s polymeric material itself experiences an equal reaction force. Prolonged static force loading, induced by molecular chain mobility, results in decayed elastic properties, progressive stress relaxation, and permanent deformation [7,8]. This loss of geometric integrity compromises the aligner's ability to deliver precise tooth movement to the target positions, thereby reducing therapeutic efficacy [9].

3D direct-print clear aligners have recently gained significant attention, partly due to the shape-memory properties of 3D printable resins [10,11]. These stimuli-responsive materials can undergo a phase transition upon external stimuli (*e.g.*, thermal excitation) and recover their initial geometry. Nevertheless, prior studies have primarily demonstrated shape recovery using standardized test specimens (*e.g.*, bent bars returning to a flat state at different temperatures) rather than actual aligner geometries [10,12].

This study presents the first quantitative assessment of the three-dimensional geometric recovery precision of 3D direct-print aligners under thermal excitation. Three materials were comparatively evaluated: : Erkodur (thermoformed), Zendura FLX (thermoformed), and LuxCreo DCA (directly printed), under simulated intraoral conditions (37°C water bath, aligners worn on dental models, 7 days) with and without thermal excitation.

11.2 MATERIALS AND METHODS

For this in vitro study, two different setups were created based on a digital orthodontic treatment plan, which a written informed consent was obtained for (no further approval by a local ethics committee was needed). In the first setup, the major tooth movement was molar distalization, while the second setup mainly involved retraction of upper incisors (LinkedSmile, Wuxi, China). The amount of prescribed movement for each setup is described in Table 11.1. For each setup, four different groups were included. For each setup-group combination, 10 identical aligners were produced to obtain statistically meaningful data.

Table 11-1 Amount of prescribed movement for the two different setups

<table>
<tr><td rowspan="8">Posterior sector setup</td><td>Planned movement</td><td colspan="3">Tooth 16</td></tr>
<tr><td>Extrusion (E)/Intrusion (I), mm</td><td colspan="3">0.07I</td></tr>
<tr><td>Bodily Movement, Buccal (B)/Lingual (L), mm</td><td colspan="3">0.02B</td></tr>
<tr><td>Bodily Movement, Mesial (M)/Distal (D), mm</td><td colspan="3">0.21D</td></tr>
<tr><td>Rotation, Mesial (M)/Distal (D), °</td><td colspan="3">1.09D</td></tr>
<tr><td>Rotation, Mesial (M)/Distal (D), °</td><td colspan="3">1.09D</td></tr>
<tr><td>Torque, Mesial (M)/Distal (D), °</td><td colspan="3">0.67D</td></tr>
<tr><td>Tipping, Buccal (B)/Lingual (L), °</td><td colspan="3">0.03L</td></tr>
<tr><td rowspan="6">Anterior sector setup</td><td></td><td>Tooth 12</td><td>Tooth 11</td><td>Tooth 21</td></tr>
<tr><td>Extrusion (E)/Intrusion (I), mm</td><td>0.1I</td><td>0.14I</td><td>0.19I</td></tr>
<tr><td>Bodily Movement, Buccal (B)/Lingual (L), mm</td><td>0.18L</td><td>0.28L</td><td>0.27L</td></tr>
<tr><td>Bodily Movement, Mesial (M)/Distal (D), mm</td><td>0.19D</td><td>0</td><td>0.05M</td></tr>
<tr><td>Rotation, Mesial (M)/Distal (D), °</td><td>0.15M</td><td>0.33D</td><td>0.07D</td></tr>
<tr><td>Torque, Mesial (M)/Distal (D), °</td><td>0.56M</td><td>0.03D</td><td>0.12D</td></tr>
</table>

	Tipping, Buccal (B)/Lingual (L), °	0.22B	0.94B	0.13B

11.2.1 Directly printed aligners

For each tooth movement setup, twenty aligners (forty in total) were fabricated using a 3D printing process that followed the manufacturer's guidelines. Twenty aligners were used without thermal excitation (denoted as Group DCA), while another twenty were treated with hot water daily (denoted as Group DCAT). An iLux Pro Dental 3D printer (LuxCreo, Chicago, IL, U.S.A) was used along with DCA resin (LuxCreo, Chicago, IL, U.S.A). The aligners were designed with a thickness of 0.6 mm. Printing was carried out with a layer height of 100µm. Support structures were automatically added and adjusted using the LuxFlow Dental software (LuxCreo, Chicago, IL, U.S.A), with an angulation of 70° relative to the build plate, in accordance with manufacturer recommendations. To remove any residual resin trapped inside the aligners after printing, a two-stage ultrasonic washing in IPA (>99%) was performed at room temperature (iLuxWash Dental) for 8 minutes (4 minutes per stage).

Post-curing was carried out using a iLuxCure Pro curing unit (LuxCreo, Chicago, IL, U.S.A.) for 20 minutes without nitrogen, as per the manufacturer's instructions. The supports were subsequently manually removed, and the aligners were examined for surface imperfections and adjusted using a polishing wheel.

11.2.2 Thermoformed aligners

For each setup and material, ten dental models for thermoformed aligner production were 3D printed using an iLux Pro Dental 3D printer (LuxCreo, Chicago, IL, U.S.A). The thermoforming process was carried out utilizing 0.8 mm Erkodur PETG sheets (Erkodent Erich Kopp GmbH, Pfalzgrafenweiler, Germany, denoted as Group E) and Zendura FLX polyurethane sheets (Bay Materials LLC, Fremont, CA, U.S.A, denoted as Group Z).

To ensure dimensional accuracy, all printed dental models underwent a consistent post-processing protocol. Immediately after printing, the models were cleaned in 99% isopropyl alcohol (IPA) using the iLuxWash Dental (LuxCreo, Chicago, IL, U.S.A), which employs mechanical agitation to effectively remove resin from all surfaces, including detailed anatomical areas.

After cleaning, the models were air-dried and then post-cured using the iLuxCure Pro curing unit (LuxCreo, Chicago, IL, U.S.A.). The curing process lasted five minutes, in accordance with the resin manufacturer's guidelines, to complete polymerization and enhance the models' structural integrity.
Following thermoforming, the aligners were trimmed along the gingival margins using a rotary cutting tool and polished with a Lisko-B disc (Erkodent) to smooth and refine the edges. Each aligner underwent a thorough inspection for defects and its fit and retention were checked before testing.

11.2. 3 Scan acquisition

A thin layer of scan powder (Snow Scan Powder, Snow Rock, Norcross, Georgia, United States) was applied on the intaglio surface of all aligners in their original state The aligners were then positioned on the sample platform of the stationary optical scanner (Shining 3D DS-EX Pro, Hangzhou, China). The STL files generated from the scans (Scan A, original state as reference) were imported into Geomagic Control X-64 metrology software (Build version 2017.0.1; 3D Systems, Rock Hill, SC) as original reference files. The aligners were then worn on dental models and immersed in a water bath at 37°C water for 7 days. Note that the aligner and the dental model were from different steps in a single digital treatment plan, creating a mismatch and continuous stress between them, mimicking force loading conditions in real orthodontic treatment.

After each day, the aligners were removed from the dental models. A thin layer of scan powder was reapplied, and scanning procedure was conducted on Groups Z, E, and DCA (Scan B, deformed state). For Group DCAT, twenty directly printed aligners (ten with molar distalization and ten with incisors retraction) were immersed in a water bath at 100 °C for 60 seconds, and scanning was conducted afterwards with the powder reapplied (Scan C, restored state). Note that thermal excitation was not applied to thermoformed aligners, as heat treatment could permanently and irreversibly distort them.

Subsequently, profiles from Scan B were superimposed onto reference profiles from Scan A to assess 3D profile deformation due to material creep, while Scan C underwent the same procedure to assess geometric restoration after thermal excitation. Digital superimposition was performed using an automated iterative closest point algorithm to achieve the best match between profiles. The software's 3D comparison tool was used to compute deviations at all points between the compared profiles, and heatmaps were created to visually display these 3D profile differences (Figure 11.1 and 11.2). A ±100 μm tolerance level was used as the upper and lower bounds of clinical acceptance, consistent with previous studies [13-15]. Green indicates areas within the deviation tolerance. Yellow denotes areas exceeding the upper limit (with examined profile above the reference), while blue indicates regions below the lower limit.

11.2.4 Error Analysis

As control tests, aligners made of the three materials, without being worn on dental models (free-standing, no stress, no creep), were immersed in a 37°C water bath to assess methodology consistency. 3D scans were conducted at 24-hour intervals over 7 days. Additionally, scanning electron microscope (SEM) analysis of the scan powder was performed to evaluate potential methodology errors.

11.2.5 Statistical Analysis

The Shapiro–Wilk test was used to verify data normality. Continuous variables are reported as means ± standard deviations (SD) or medians with interquartile range [IR] (if not normally distributed). Categorical variables are reported as numbers and/or percentages. For each group, the percentage of points within the deviation tolerance (In.Tolerance percentage) were analyzed using the Friedman test. The Kruskall-Wallis test followed by the Mann–Whitney U-test with Bonferroni's correction for multiple comparisons was used to compare In.Tolerance percentages among groups for different tooth movement setups (molar distalization and incisors retraction). The Kruskal–Wallis test was also used to compare standard deviations to evaluate the scattering of In.Tolerance percentages among groups.

Differences with p-value <0.05 were considered significant. Data were acquired and analyzed in the R v4.2.2 software environment.

11.3 RESULTS

Data recorded of 80 aligners were included in the final analysis. A crack, possibly due to removal stress, was observed on Sample 5 of Group Z on day 7 (molar distalization); this sample was excluded from analysis. According to error analysis from control tests, all materials exhibited a 0.05 mm accuracy loss due to water absorption and/or operational error after 7 days. A 1% margin of error was attributable to operational variability. The error ascribed to powder layer thickness was 1μm, with a particle size distribution of 100-120 nm.

As shown in the evolution of heatmaps (Figures 11.1 and 11.2), the progressive creep deformation was visualized over the 7-day duration. For thermoformed aligners (Groups Z and E), areas outside the ±0.1 mm tolerance were evident after the first day, regardless of tooth movement type. Increasingly out-of-spec areas emerged progressively over time, peaking after the seventh day. The same trend was observed for direct-print aligners without thermal excitation.

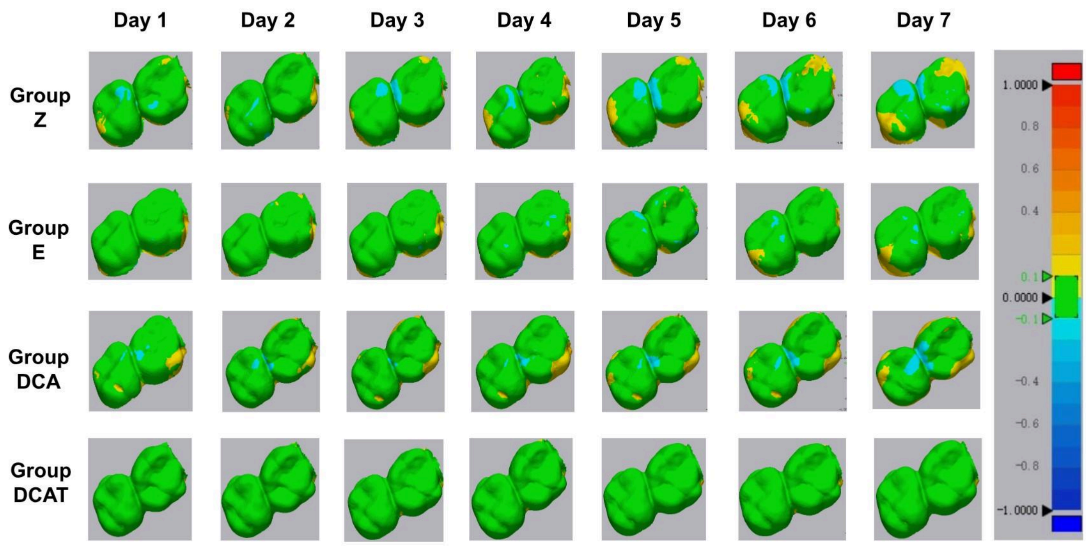

Figure 11-1 Representative renderings visualising the local material deviation of Scan B (deformed state) from Scan A (original state) for molar distalization setup in Groups E, Z and DCA respectively and deviation of Scan C (recovered state after thermal activation) from Scan A (original state) for Group DCAT over the considered period (7 days). The legend indicates the magnitude of positive and negative deviations in warm and cool colors, respectively (scale in mm)

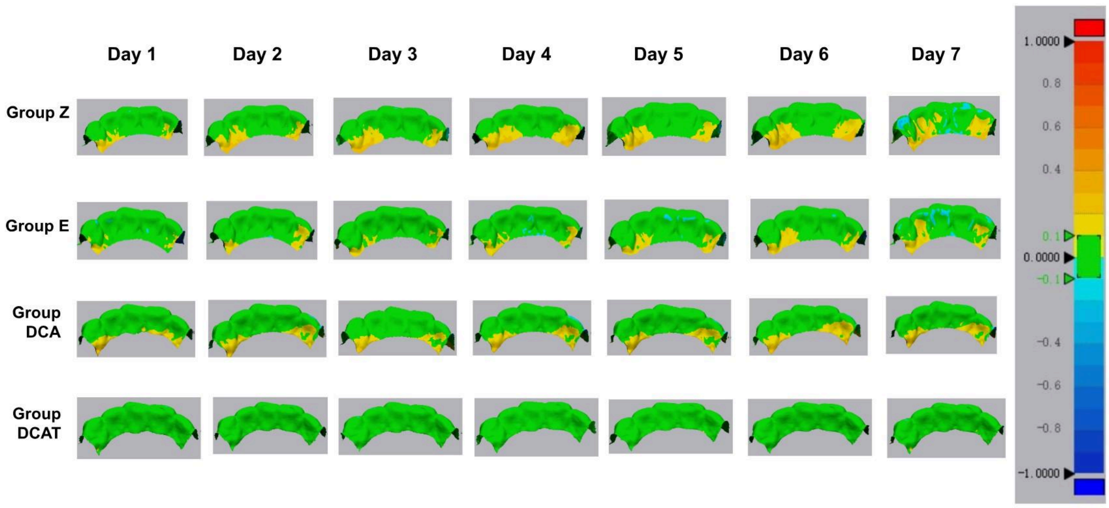

Figure 11-2 Representative renderings visualising the local material deviation of Scan B (deformed state) from Scan A (original state) for the incisors retraction setup in Groups E, Z and DCA respectively and deviation of Scan C (recovered state after thermal activation) from Scan A (original state) for Group DCAT over the considered period (7 days). The legend indicates the magnitude of positive and negative deviations in warm and cool colors, respectively (scale in mm)

Statistical data presented in Table 11.2 and Figures 11.3 and 11.4, quantitatively outlined the In.Tolerance percentages for different groups. For molar distalization, the In.Tolerance percentages of Groups E, Z, and DCA dropped to 82.58%, 62.40%, and 61.97% after 7 days, respectively. For incisor retraction, the In.Tolerance percentages showed similar progressive trajectories, becoming 79.91% (Group E), 80.69% (Group E), and 83.28% (Group DCA). In contrast, Group DCAT exhibited the most stable In.Tolerance percentage throughout the 7-day period, remaining >99% after the first 24 hours and maintaining high values of 96.04% (molar distalization) and 98.25% (incisor retraction) after 7 days. A significant effect of time was observed for Groups E, Z, and DCAT ($p < 0.001$, $p = 0.005$, and $p < 0.001$, respectively).

Table 11-2 In.Tolerance percentage for each group and over time. P-value: Friedman test p-value

	Overall	**DAY 1**	**DAY 2**	**DAY 3**	**DAY 4**	**DAY 5**	**DAY 6**	**DAY 7**	**p-value**
N	**559**	**80**	**80**	**80**	**80**	**79**	**80**	**80**	
Erkodur	84.50 [82.27, 86.48]	85.28 [81.19, 90.34]	86.08 [83.13, 90.56]	84.48 [79.29, 88.21]	85.23 [81.13, 90.57]	83.81 [77.43, 88.40]	83.19 [81.05, 91.05]	81.73 [74.45, 85.21]	<0.001
Zendura	82.02 [74.63, 86.13]	83.19 [78.19, 87.25]	84.59 [78.78, 87.23]	83.64 [77.97, 86.35]	83.16 [75.89, 88.28]	81.77 [72.38, 86.14]	82.54 [71.67, 85.50]	72.21 [67.16, 81.63]	0.005
DCA	78.20 [67.14, 85.66]	80.14 [69.34, 87.82]	79.55 [71.98, 87.30]	80.16 [72.02, 85.60]	78.78 [70.12, 85.72]	75.96 [65.14, 84.64]	75.66 [63.42, 85.21]	73.52 [60.67, 84.58]	0.273
DCA with Thermal Activation	98.43 [97.10, 99.40]	99.48 [99.23, 100.15]	99.38 [98.43, 100.00]	98.34 [97.85, 99.30]	97.77 [96.86, 99.06]	97.81 [96.25, 99.25]	97.21 [96.27, 99.21]	97.07 [96.21, 98.48]	<0.001
p-value	<0.001	<0.001	<0.001	<0.001	<0.001	<0.001	<0.001	<0.001	

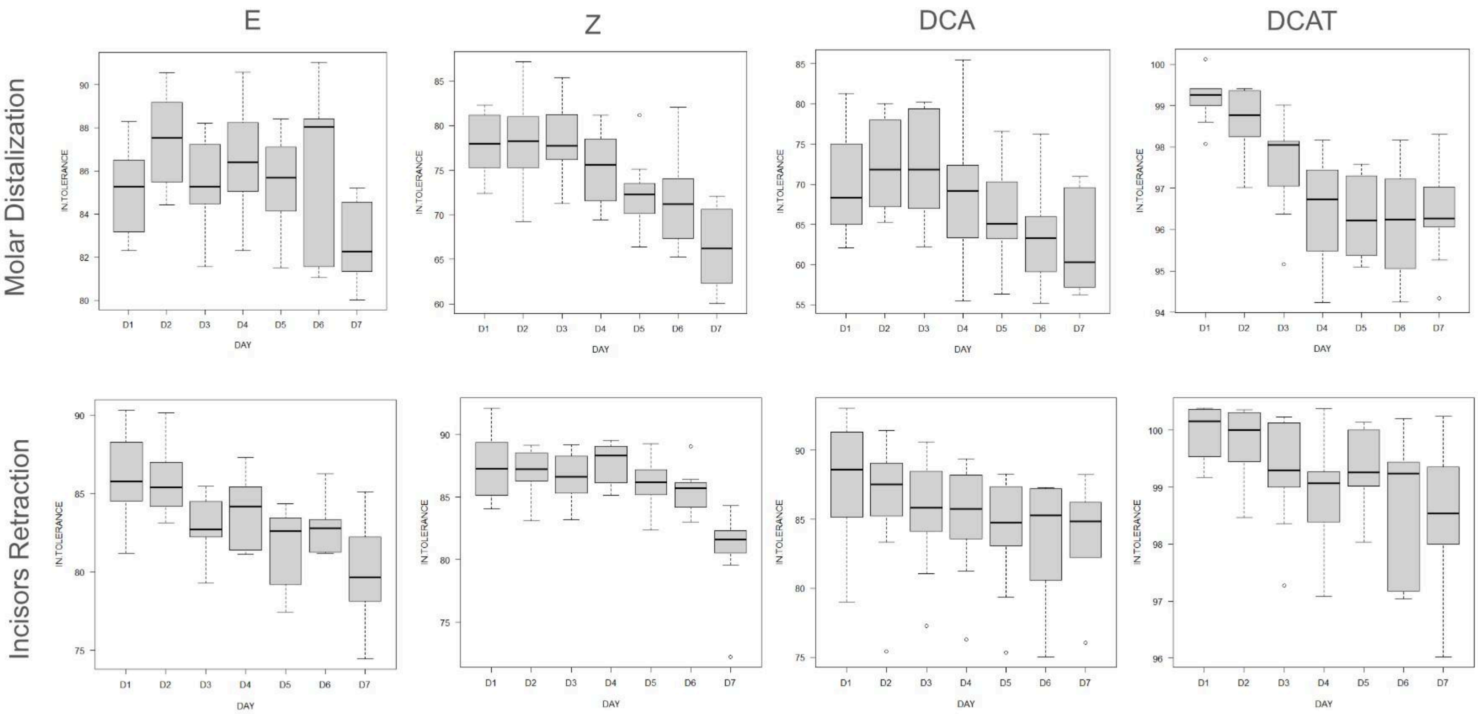

Figure 11-3 In.Tolerance percentage over time of the 3D profile superimposition of aligners from each group by movement type. Box and whisker plots indicate the range (whiskers), median (dark line), first and third quartiles (box ends), and outliers (dots)

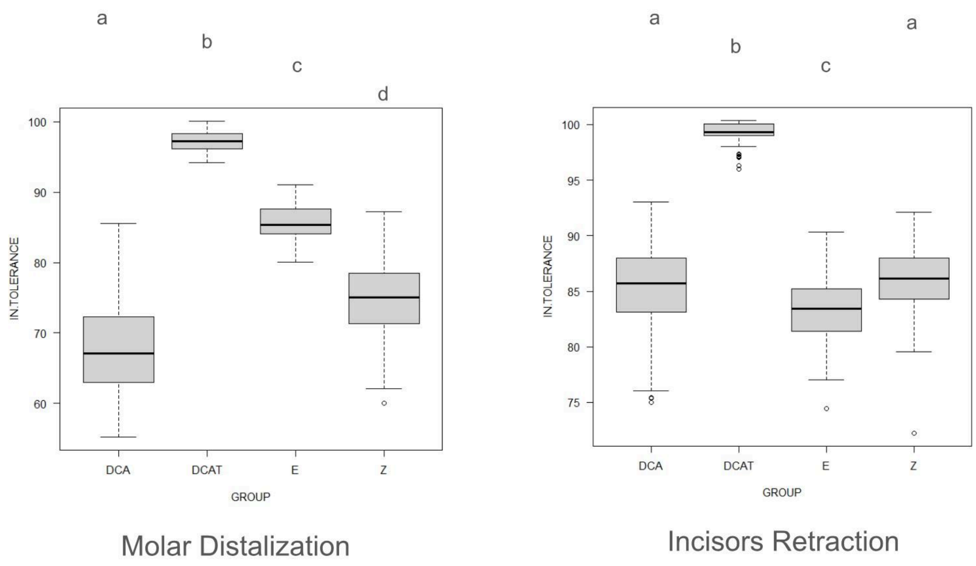

Figure 11-4 In.Tolerance percentage of the 3D profile superimposition of aligners from each group by movement type. Box and whisker plots indicate the range (whiskers), median (dark line), first and third quartiles (box ends), and outliers (dots). Groups not connected by the same letter in the above chart are significantly different (P <0.05)

11.4 DISCUSSION

For improved planning of orthodontic treatments with 3D direct-printed aligners, it is crucial to understand the new paradigm of shape memory materials and how their recovery behaviour may be clinically relevant in generating potential benefits. Shape recovery has been previously reported in the literature using resin samples subjected to bending tests, which allow direct visualization of the object returning to its original shape. A U-shaped specimen with clinically relevant thicknesses (0.5-0.7mm) was used to determine the initial bending angle and the bending angle at subsequent times, enabling computation of the shape recovery ratio upon exposure to a suitable thermal stimulus [10,16].

In the present study, a novel and clinically relevant method based on 3D geometry examination and digital superimposition was used to investigate the creep deformation of aligners after service and assess the geometric restoration of 3D direct-printing aligners.

Limitations of this study include the fact that simulated water batch conditions may not fully replicate real intraoral environments. Complex oral flora, their byproducts, and plaque accumulation on the material [17] were not considered. Moreover, during the treatment, aligners are continually exposed to heat fluctuations, moisture, respiration, bacteria, salivary enzymes, and UV radiation [18]. Force recovery, equally important as geometric restoration, requires systematic study in follow-up work. More importantly, clinical studies with statistical data are needed to establish how geometric restoration comparatively improves orthodontic efficacy in real cases, further solidifying its potential benefits.

11.5 CONCLUSIONS

The present study on the geometric evolution of aligners made from two conventional thermoformed materials and a recent 3D direct-print resin led to the following conclusions:

- Loading with continuous static force led to universal material creep of clear aligners, regardless of manufacturing method (thermoformed or direct-print). Deformation progressed with prolonged service time.
- Leveranging the material’s shape memory characteristic, direct-print aligners eliminated creep *via* precise and repeated restoration to their original geometry under daily thermal excitation (1 minute at 100℃), demonstrating an In.Tolerance percentage >96% after 7 days.
- Thermal-responsive geometric restoration has the potential to address the inevitable creep of clear aligners, possibly improving orthodontic efficacy. However, follow-up studies involving

real intraloral conditions, force recovery testing, and clinical data with statistically meaningful sample size are required to confirm these potential benefits.

REFERENCES

1. Oliveira P, Bugaighis I, Nunes Costa H, Mariano Pereira P. Perception of Need for Further Refinement in a Clear Aligner Treatment among Orthodontists, Dentists and Laypeople: A Retrospective Study. *Int J Environ Res Public Health*. 2022;19(23):15498.
2. Narongdej P, Hassanpour M, Alterman N, Rawlins-Buchanan F, Barjasteh E. Advancements in Clear Aligner Fabrication: A Comprehensive Review of Direct-3D Printing Technologies. *Polymers* (Basel). 2024;16(3):371.
3. Lombardo L, Martines E, Mazzanti V, Arreghini A, Mollica F, Siciliani G. Stress relaxation properties of four orthodontic aligner materials: A 24-hour in vitro study. *Angle Orthod.* 2017;87(1):11-18.
4. Olteanu ND, Szuhanek C, Rosu SN, Chitariu DF, Seghedin N, Panaite T, Casalean A, Zetu IN. An Assessment of the Mechanical Deformation Behavior of Three Different Clear Aligner Materials: A Digital Image Correlation Analysis. *Applied Sciences*. 2024; 14(17):7496.
5. Martínez-Lozano D, Castellanos-Andrés D, López-Jiménez A-J. Staging of Orthodontic Tooth Movement in Clear Aligner Treatment: Macro-Staging and Micro-Staging—A Narrative Review. *Applied Sciences*. 2024; 14(15):6690.
6. Wear T, Meade M. Optimising clear aligner therapy: What current evidence says about materials, attachments, and protocols. *Seminars in Orthod* 2025; Articles in press July 29
7. Jansen J. Understanding creep failure of plastics. *Plast Eng* 2022;78:34–38.
8. Aliotta L, Gigante V, Lazzeri A. Analytical modeling of stress relaxation and evaluation of the effect of plasticizer on polymer chain mobility. *ACS Omega* 2022;7:1234–1241.
9. Albertini P, Mazzanti V, Mollica F, Pellitteri F, Palone M, Lombardo L. Stress Relaxation Properties of Five Orthodontic Aligner Materials: A 14-Day In-Vitro Study. *Bioengineering* (Basel). 2022;9(8):349.
10. Lee SY, Kim H, Kim HJ, Chung CJ, Choi YJ, Kim SJ, Cha JY. Thermo-mechanical properties of 3D printed photocurable shape memory resin for clear aligners. *Sci Rep.* 2022 Apr 15;12(1):6246.
11. Alkhamees A. The new additive era of orthodontics: 3D-printed aligners and shape memory polymers-the latest trend-and their environmental implications. J Orthod Sci. 2024 Nov 25;13:55.

12. Choi JY, Kim H, Kim SH, Kim SJ, Cha JY, Lee SY, Lee J, Min J, Jang S, Khan TA, Kim HJ, Kim KB. Mechanical and viscoelastic properties of a temperature-responsive photocurable resin for 3D printed orthodontic clear aligners. *Sci Rep*. 2025 Jul 2;15(1):23530.
13. Favero CS, English JD, Cozad BE, Wirthlin JO, Short MM, Kasper FK. Effect of print layer height and printer type on the accuracy of 3-dimensional printed orthodontic models. *Am J Orthod Dentofacial Orthop.* 2017;152:557-65.
14. McCarty MC, Chen SJ, English JD, Kasper F. Effect of print orientation and duration of ultraviolet curing on the dimensional accuracy of a 3-dimensionally printed orthodontic clear aligner design. *Am J Orthod Dentofacial Orthop* 2020;158:889-97.
15. Boyer RA, Kasper FK, English JD, Jacob HB. Effect of print orientation on the dimensional accuracy of orthodontic aligners printed 3-dimensionally. *Am J Orthod Dentofacial Orthop.* 2021;160:732-742.e1.
16. Elshazly TM, Keilig L, Alkabani Y, Ghoneima A, Abuzayda M, Talaat S, Bourauel CP. Primary Evaluation of Shape Recovery of Orthodontic Aligners Fabricated from Shape Memory Polymer (A Typodont Study). *Dent J.* 2021;9:31.
17. Selvaraj M, Mohaideen K, Sennimalai K, Gothankar GS, Arora G. Effect of oral environment on contemporary orthodontic materials and its clinical implications. *J Orthod Sci.* 2023;12:1.
18. Yazdi M, Daryanavard H, Ashtiani AH, Moradinejad M, Rakhshan V. A systematic review of biocompatibility and safety of orthodontic clear aligners and transparent vacuum-formed thermoplastic retainers: Bisphenol-A release, adverse effects, cytotoxicity, and estrogenic effects. *Dent Res J.* 2023;20:41

PROTOTYPE PREPARATION OF A MAGNETIC NANOPARTICLES COATING FOR 3D PRINTABLE ORTHODONTIC RESINS

12.1 INTRODUCTION

Magnetic nanoparticles (MNPs) have garnered significant attention as nanocarriers in drug delivery, offering broad diagnostic and therapeutic potential. Their prominence stems from unique physicochemical properties, the ability to operate at both molecular and cellular levels, and their capacity for targeted cellular action, which minimizes systemic cytotoxicity. Consequently, dentistry has increasingly adopted nanoparticles and magnetic forces to administer medications for disease prevention and treatment. Therapies based on MNPs have proven highly effective against antibiotic-resistant bacteria and fungi. In aesthetic dentistry, MNPs enhance the translucency and wear resistance of materials. Furthermore, incorporating MNPs into dental composites, adhesives, and drug delivery systems inhibits biofilm formation, thereby reducing the incidence of caries, endodontic complications, and periodontal pathologies [1].In this context, Finite element modeling (FEM) has been proven as a relevant tool to characterize different ranges of magnetoelectric geometric arrangements and structures [2] and can provide a better understanding on how MENPs properties influence the magnetoelectric coupling.

The objective of this study was to test the feasibility of a surface coating for direct printed orthodontic devices loaded with nanoparticles sensitive to magnetic fields and to compute the magnetoelectric elicited effect in the case of a cell in direct contact with the appliance surface.

12.2 MATERIALS AND METHODS

Ten Tera Harz TC-85 samples were prepared in the form of parallelepipeds measuring 30 mm in length, 10 mm in width, and 2 mm in thickness, following the manufacturer's instructions (20 minutes of polymerization, print resolution of 100 microns). A 0.016% solution of magnetic CFO-BTO nanoparticles in isopropyl alcohol was prepared and mixed in a cup with the Tera Harz monomer. Five samples were immersed in the solution, then they received a 20 minutes curing in the dedicated unit.

A SEM–EDS (scanning electron microscopy (SEM) and energy dispersive X-ray spectroscopy(EDS)) pointwise analysis of the samples was performed through a Thermo Scientific

Phenom ProX G6 scanning electron microscope (Thermo Fischer Scientific Inc., Waltham, Massachusetts, USA), which features a light optical magnification of 27–160x, an electron optical magnification range of 160–350,000X, a 1-0.1% limit and a SED resolution of 80 nm.

A finite element method-based simulation tool, COMSOL Multiphysics, was used to characterize the magnetoelectric behavior of the obtained samples on a target cell put in direct contact with the material.

12.3 RESULTS

Phenom ProX images of the coated samples at 500 and 50000 magnifications revealed the presence of opaque spheroidal agglomerates in the range of 0.5-1 micron.

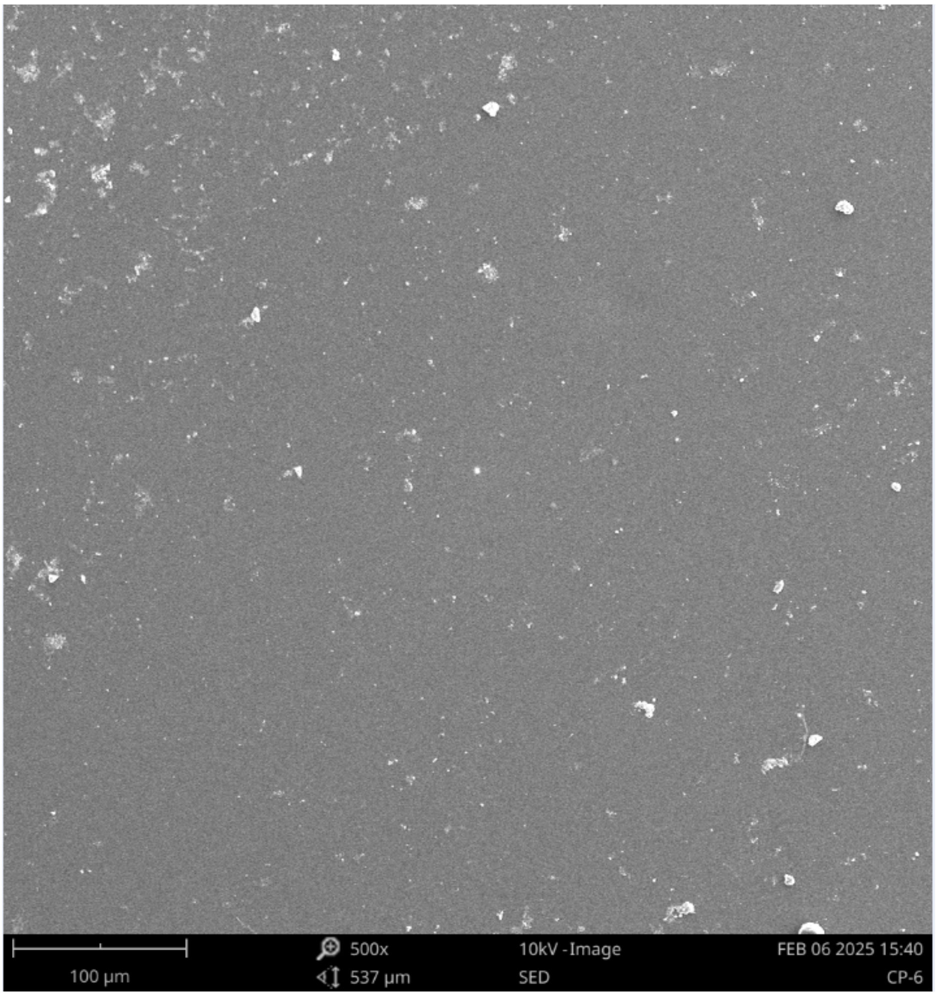

Figure 12-1 500X Phenom ProX image of the coated sample (max 150000X)

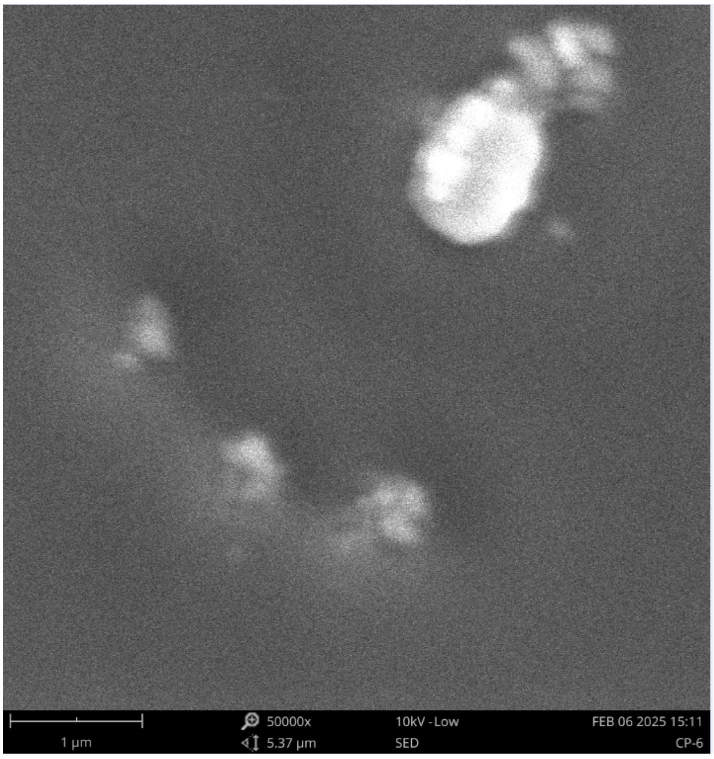

Figure 12-2 50000X Phenom ProX image of the coated sample (max 150000X)

The presence of Cobalt at a 2.88%, Barium at a 0.21% and Titanium at a 0.20% atomic concentration was confirmed by the EDs analysis.

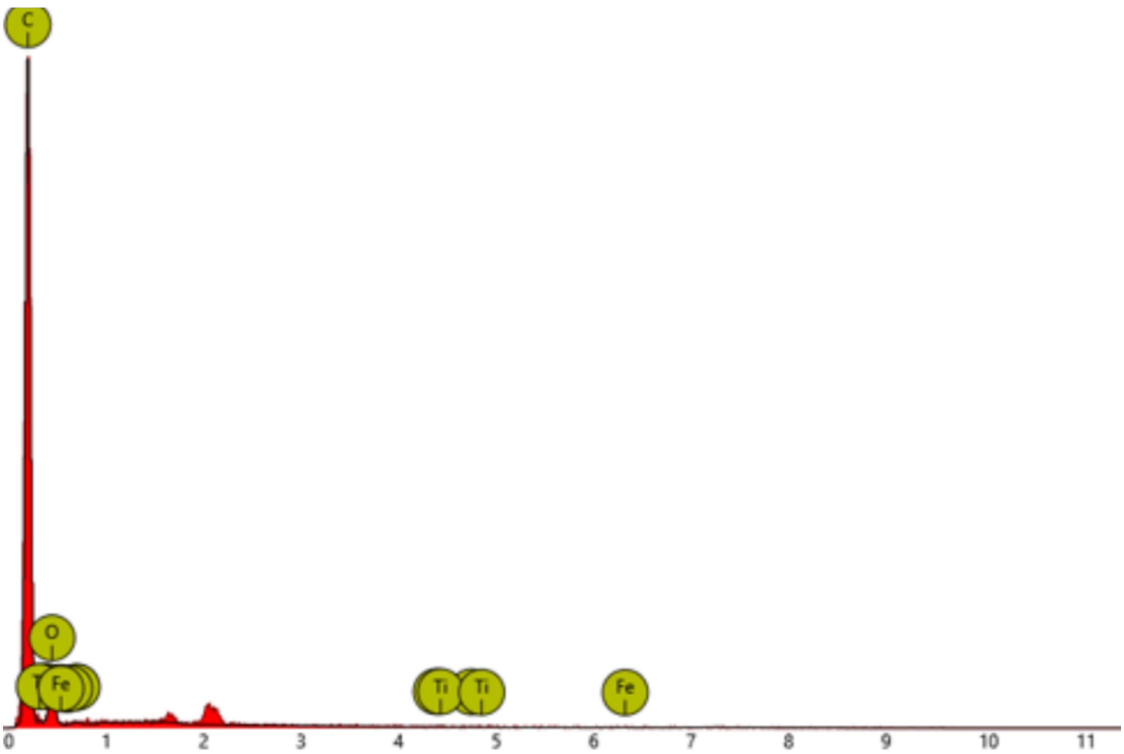

Figure 12-3 Spectroscopy graph

Table 12.1. Coating composition analysis

Element Symbol	Atomic Concentration (%)
C	53.72
O	43.00
Co	2.88
Ba	0.21
Ti	0.20
Fe	0.00

Based on these density characterisation, the finite element method-based simulation computed an electric field norm of 10 V/m in the proximity of the cellular membrane.

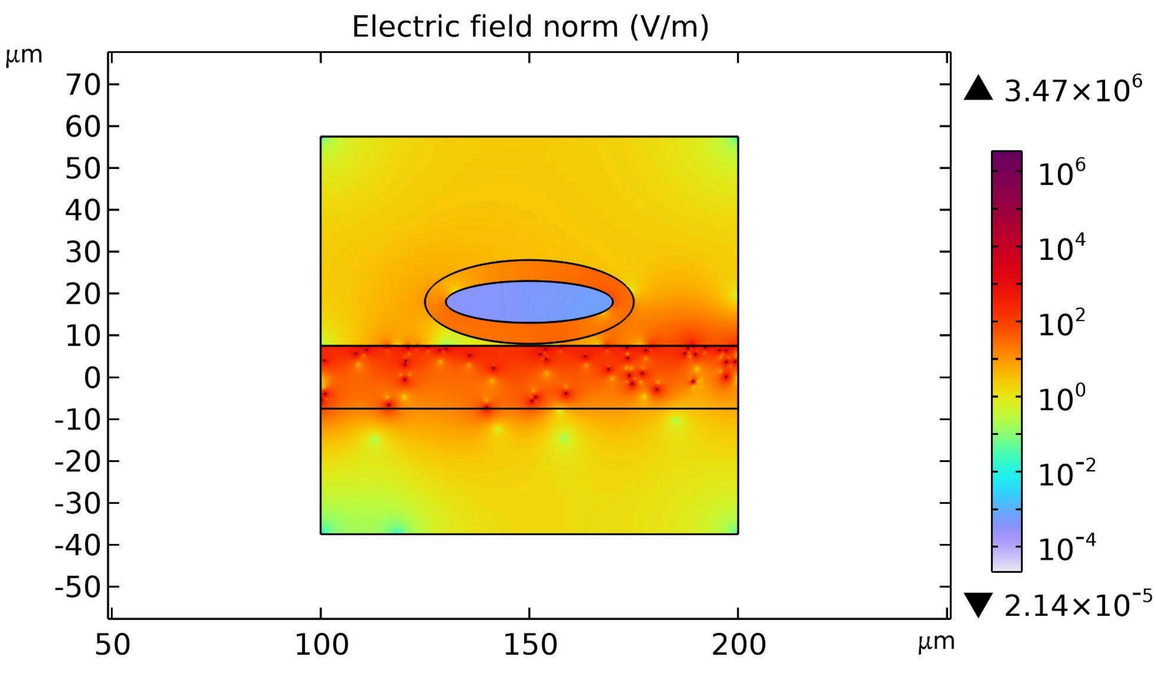

Figure 12-4 Colour map of the electric field norm computed by simulating a cell in direct contact with the coating of the sample

12.4 CONCLUSIONS

The surface coating of TC-85 samples with nanoparticles at a 0.016% concentration resulted as a procedure capable of conveying magnetoelectric nanoparticles on the surface of 3D printed orthodontic devices. While the elicited electric field appears to be far below any known threshold for cellular response, this experience opens to further refinements of the coating process as well as to biocompatibility and cellular stimulation tests.

REFERENCES

1. Mathew DM, Pushpalatha C, Anandakrishna L. Magnetic nanoparticles: A novel adjunct for dentistry. Materials Today: Proceedings 50 (2022) 173–180.
2. Fiocchi S, Chiaramello E, Marrella A, Suarato G, Bonato M, Parazzini M, et al. (2022) Modeling of core-shell magneto-electric nanoparticles for biomedical applications: Effect of composition, dimension, and magnetic field features on magnetoelectric response. PLoS ONE 17(9): e0274676.

CONCLUSIONS

The research conducted in this thesis highlights that direct 3D printing of orthodontic aligners represents a significant paradigm shift since the introduction of CAD/CAM technology in digital dentistry. While thermoforming remains a validated production technology for clear aligners, its inherent limitations, including material thinning, high labor costs, and significant environmental waste, have paved the way for the development of advanced biocompatible resins.

Based on the analysis of material properties and existing literature, the following conclusions can be drawn:

- Direct printing eliminates the drawbacks of the physical model and the thinning associated with stretching thermoplastic sheets. This allows for a more controlled thickness and complex geometries, potentially leading to more predictable and constant orthodontic force delivery.
- At room temperature, the choice of different printing resolutions on the Z-axis does not seem to influence the final properties of the Tera Herz TC-85DAC material.The use of different 3D printers (Phrozen Sonic and Accufab L4D) can result in variations in the thickness of the TC-85DAC resin samples and in terms of material ductility. The variation in printing thickness does not cause significant changes, except for the breaking load.
- The DCA mechanical behaviour is preserved at operating temperature and shows the same magnitude order of traditional materials. It displays a lower decay in mechanical properties than TA-28.
- Based on the results obtained from the tests on the materials, the TA-28 resin demonstrates superior performance in creep tests compared to the TC-85 resin.
- 3D direct printing materials are less hydrophobic. This remains a primary challenge for printed resins compared to the ultra-smooth surfaces of thermoformed PETG/TPU because it could directly correlate with increased plaque accumulation and potential gingival inflammation.
- A preliminary model of a dental arch and a passive aligner was correctly exported in Ansys, successfully starting the development of a computational mapping tool of the forces applied to the dental arch by 3D printed orthodontic aligners.
- The tested resins did not elicit cytotoxic responses in MG-63 or D430B cells, either through direct or indirect exposure. While they do not promote cell adhesion or proliferation in direct contact, they appear biologically inert and safe for applications involving transient or indirect tissue contact.

- Leveraging the material's shape memory characteristic, direct-print aligners eliminated creep via precise and repeated restoration to their original geometry under daily thermal excitation (1 minute at 100℃), demonstrating an In.Tolerance percentage >96% after 7 days
- The surface coating of TC-85 samples with nanoparticles resulted as a procedure capable of conveying magnetoelectric nanoparticles on the surface of 3D printed orthodontic devices. The elicitable electric field appeared to be far below any known threshold for cellular response.

In summary, direct-printed resins offered an adequate alternative to traditional methods by combining digital precision with material efficiency. While further research is needed to assess clinical efficiency, direct 3D printing is poised to become a promising tool in clear aligner therapy, offering a more customized, effective, and sustainable solution for both clinicians and patients.

APPENDIX

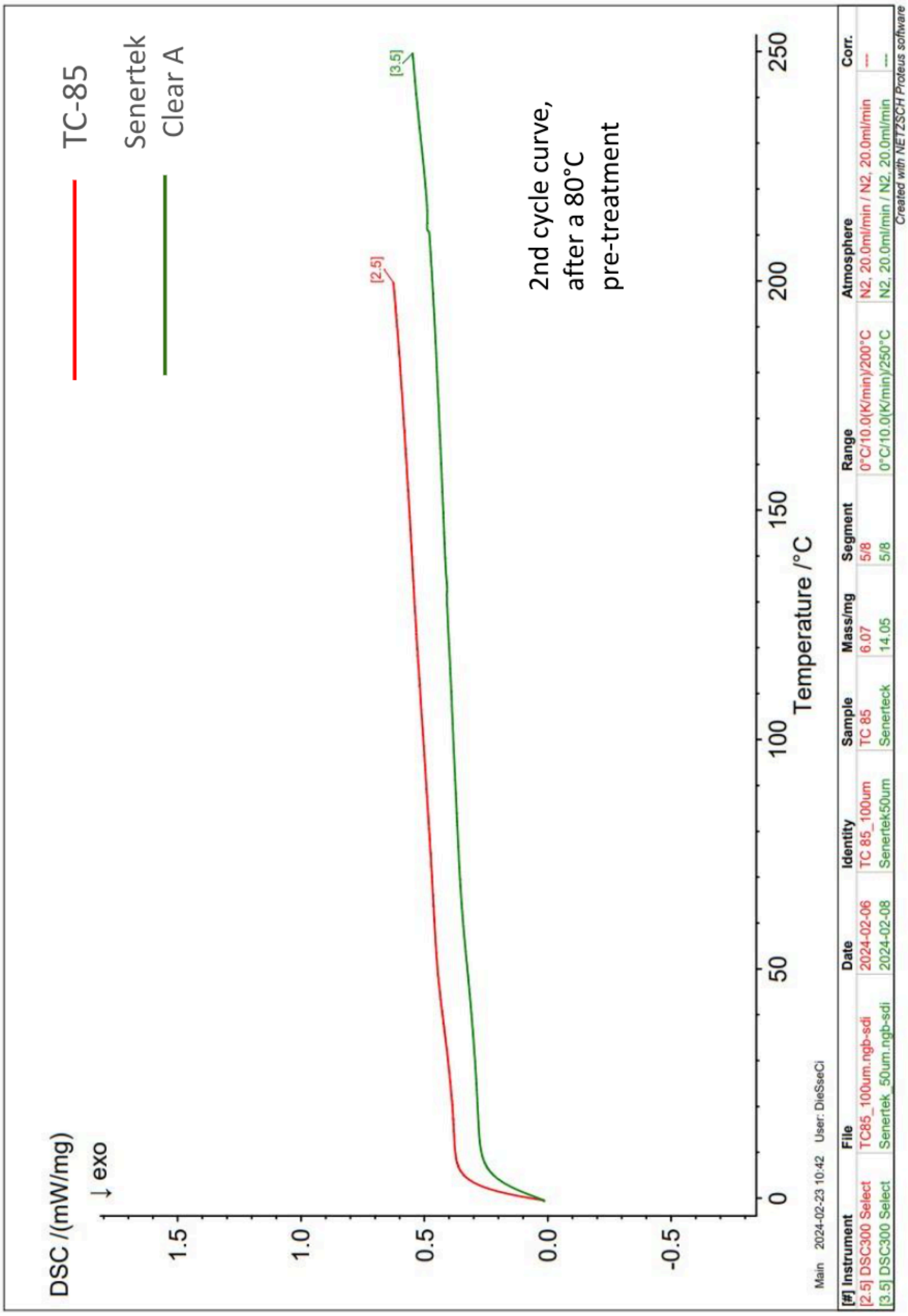

Figure A-1 DSC curve for the TC-85 and Clear A polymers

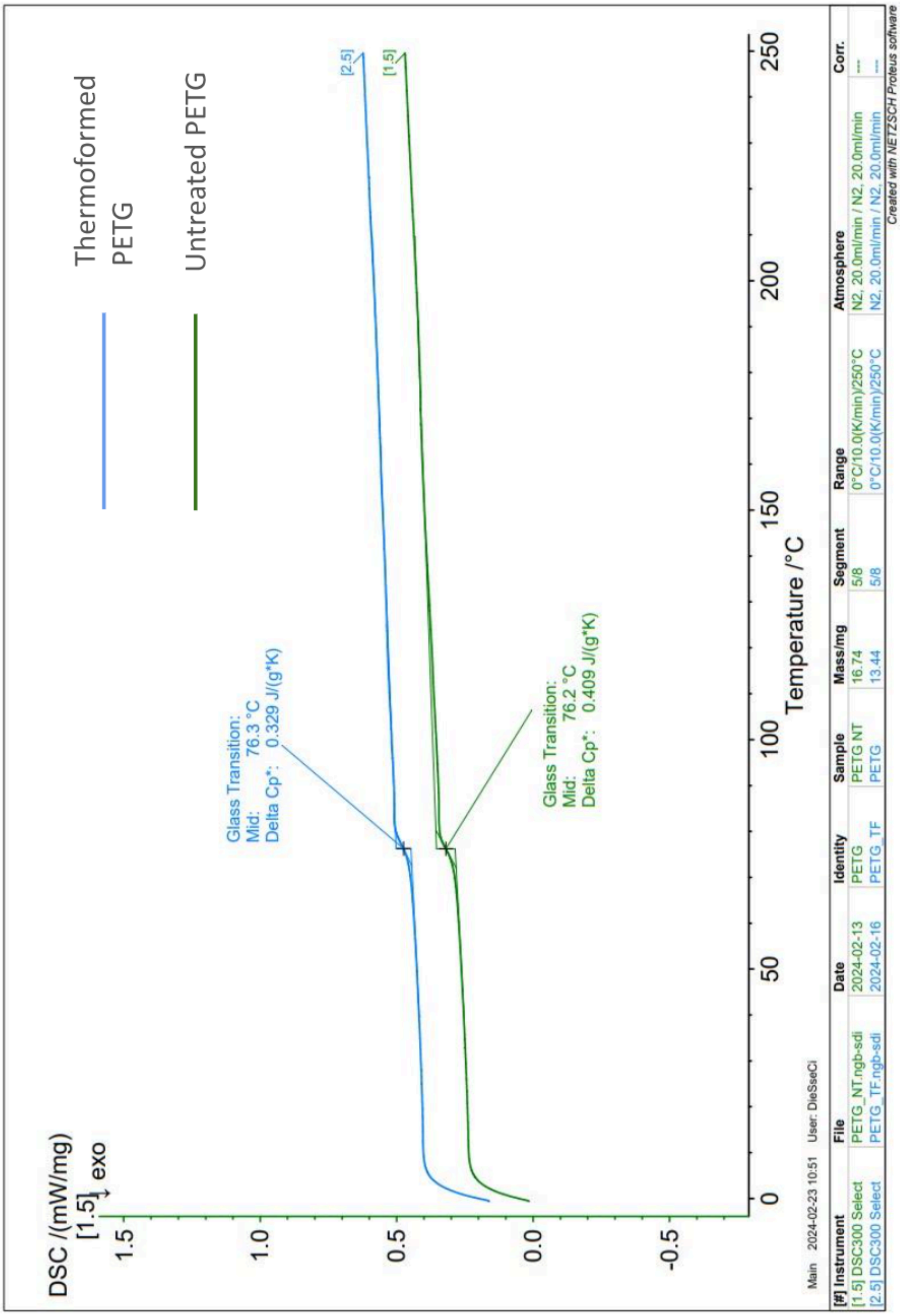

Figure A-2 DSC curve for thermoformed and untreated PETG

Material		Young Modulus (MPa)	Maximal Load (MPa)	Fracture Elongation (%)
DCA	Room temperature	1058.33	29.80	87
DCA	37°C	854.66 ✤	21.36	107
TA-28	Room temperature	787.15 ✻	26.16	-
TA-28	37°C	431.64 ✤	4.32	119
TC-85	Room temperature	1055.94 [479 ✻]	23.99	76
TC-85	37°C	483.10	14.12	48
Senertek	Room temperature	2028.68	41.30	15
PETG	Room temperature	2301.20	53.60	306
PETG	37°C	1671.70	49.14	263
PETG TF	Room temperature	2351.41	52.07	312
PETG TF	37°C	1161.57	46.34	259
PP	Room temperature	1400.00	30.00	70
PC	Room temperature	2300.00	70.00	100
TPU	Room temperature	2489.43	78.20	95

✻ dry-wet sample

✤ climatic chamber

Figure A-3 Resuming table of the measured mechanical properties for 3D printable polymers (the values for PP, PC and TPU were retrieved in the literature)